Pneumatic actuator for use in horticultural robots

Tillett, N. D.

Award date:
1998

Awarding institution:
University of Bath

Pneumatic Actuator for use in Horticultural Robots

Submitted by N D Tillett

for the degree of PhD of the University of Bath.

1998

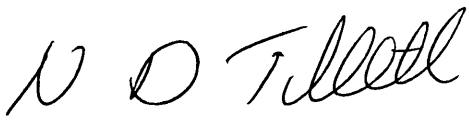

ProQuest LLC
789 East Eisenhower Parkway
P.O. Box 1346
Ann Arbor, MI 48106-1346

Summary

This thesis is concerned with the potential application of robotic technology to horticulture. It focuses on the development of jointed manipulators for applications in which horticultural products are handled directly. A review of applications and related robotics research has been conducted and contrasted with the requirements of traditional industrial robotic systems. It is concluded that there are substantial differences between the two areas and that whilst much can be learned from industrial robotics, there is a need for research aimed at specific problems posed by the horticultural environment.

The main part of the research concentrated on one example of an appropriate technology: servo pneumatics, and specifically on the development and control of a novel rotary joint incorporating flexible inflatable bladders. The kinematic characteristics of the joint have been examined through both theoretical and experimental means. This led to a new design which minimises hysteresis caused by the distortion of the inflatable bladders whilst maintaining a constant output torque throughout its stroke. Torque-to-weight ratio has been maximised in a robust device which requires little or no precision engineering in its fabrication. Two such joints have been constructed and linked to form a two-axis manipulator. A dynamic controller based on techniques identified from a short review of pneumatic system control strategies has been implemented. A dynamic model of the servo system has been developed. Simulation was used to assess the influence of design variables on performance, notably those affecting hysteresis and its effect on stability.

As an illustration of the potential of the technology a vision-guided tomato packing demonstration has been constructed. This task of packing eight tomatoes was conducted reliably in twenty seconds.

Acknowledgements

I would like to thank my supervisors, Drs Nick Vaughan and Adrian Bowyer for their help and advice in the course of this work. I am also grateful to my colleagues at Silsoe Research Institute who have helped in many ways but particularly to Nobby Grundon who provided most of the technician support and to Donna Litchfield who assisted with the compilation and presentation of this thesis.

I would also like to thank my wife Robin Tillett for her patience particularly during the latter stages of thesis writing.

This work has been part funded by the Ministry of Agriculture, Fisheries and Food. The flexible actuator, registered trade mark 'Flexator', has been used with the permission of Airmuscle Ltd.

Table of contents

Notation

a	controller array index indicating axes number
A	Area
c	thickness of a partially inflated bladder
C_L, C_H	capacitor values for low and high pass filters respectively
C_p	constant pressure specific heat
C_v	constant volume specific heat
C_1, C_2	valve coefficients
e	position error (linear)
F	webbing tension
F()	short term integration of error function
FL()	long term integration of error function
I	inertial payload
KV	flow coefficient
K_e	proportional to error gain
K_p	proportional to differential pressure gain
K_{tp}	proportional to transient pressure
K_v	proportional to velocity gain
L	arm link length
M	mass flow
M_c	moment about hose clamp
n	calibration look up table index
N	controller bias value
P_a, P_b	pressure in bladders
P_q	quiescent pressure
q	heat energy
Q	volumetric flow rate
r	inner roller radius
R	gas constant
R_a	arm radius (for given α_1)

R_b	radius of fully inflated bladder
R_L, R_H	resistor values for low and high pass filters respectively
R_o	outer cylinder radius
T	actuator output torque
T_s	air supply temperature
U_{out}	output voltage to valve
V	swept volume
V_a, V_b	volume of bladders
W	bladder contact width with outer cylinder
X	valve spool displacement
x,y	Cartesian position co-ordinates
α	first moment of area
α_0	joint 0 output angle
α_1	joint 1 output angle
β	angle from bladder clamp
γ	ratio of specific heats
δ	angle between arm link 0 and radius
θ_o	output angle
θ_d	demand angle
λ	sonic velocity
ρ	density of air
τ	system time constant
τ_f	high pass filter time constant
ϕ	angle from clamp to bladder break away point
σ	bladder wrap round angle when deflated
ν	fixed volume
ω	frequency
[ ]	indicates an array whose values vary with error and output velocity

Subscripts

i	initial value
a, b	clockwise and anti-clockwise bladders
0,1	axis 0 and 1

1 Introduction

Robots are an important and established part of industrial automation. They have resulted in improved productivity and product quality. Even in the UK, which has a relatively low robot population density compared to other industrialized nations, there were over 8000 robots installed by the end of 1993 [Wilson, 1995]. Despite the existence in horticulture of a large number of tasks requiring relatively simple repetitive actions, robot technology is almost completely absent. The reasons for this, which are examined in more detail in Chapter 2, relate to the availability of cheap labour, the small size of typical businesses making R&D difficult to justify, seasonal demand and most importantly, the variable nature of plants. It is, therefore, not surprising that the few examples of robotic technology already within commercial horticulture have involved less sophisticated industrial equipment handling plants in man-made containers, rather than handling the plants themselves. This thesis is primarily concerned with the use of robots to handle plant material directly.

If commercially available robotic technology costs were the only major barrier to exploitation in horticulture one might simply wait for current long term trends of increasing labour costs and reducing robot costs to balance the cost-benefit equation. However, the financial gap is large and the trends slow. Furthermore, fundamentally different requirements between manufacturing industry and horticulture with respect to precision and hygiene for example, will mean that there will always be technical problems. The way forward is to develop technologies especially for horticulture (which may have much in common with the food industry [Tillett, 1995]), borrowing from industry where appropriate, but taking different routes where it is not. Financial justification will be based on either doing the task more cheaply than a human operator or to a higher standard or a combination of both. This work has concentrated on cost reduction in general terms and has not focussed on specific applications except for the purposes of demonstration. The overall objective of this work was to develop low-cost robot technologies that are suited to horticultural applications. In particular, effort was directed at a major component of robotic systems: the manipulator or robot arm.

1.1 Definitions and Scope

Interpretations of what is meant by robotics can vary even among experts. It is useful to clarify the terms that are used in this thesis. An appropriate definition of a robot is that used by the Robot Institute of America [Ranky and Ho, 1985], namely "A programmable, multifunction manipulator designed to move material, parts, tools or specialised devices through variable programmed motions for the performance of a variety of tasks". The manipulator itself is that sub-system of the robot which facilitates physical movement. The scope of this thesis is limited to jointed manipulators that operate in a restricted working envelope. To obtain access over a wide area, they can be mounted on vehicles which may themselves form part of a robotic system. Such robotically operated vehicles, whilst a research interest of the author, [Hague and Tillett, 1996; Marchant et al., 1997] fall outside the scope of this thesis. A jointed manipulator of the type in question here consists of actuators, mechanical linkages, feedback transducers and a motion controller. Research relating to the design and application of such manipulators forms the central subject of this thesis.

A typical robotic system also includes a supervisory computer, and a tool or end effector mounted at the end of the manipulator which acts on the working material. Owing to the variable nature of biological objects and the unstructured environment in which they grow, sensors form an essential part of horticultural robot systems enabling them to respond with some intelligence to their environment. The integrated nature of robotic systems has meant that, whilst not the main thrust of this research, some work has been conducted on these other elements in order to demonstrate manipulator performance.

The thesis progresses from a general survey of robotics applied to horticulture, through to specific areas of novel engineering research. In Chapter 2, a wide range of potential horticultural applications are reviewed, along with previous horticultural robotics research. The industrial robotics and general engineering background is then discussed in Chapter 3. In Chapter 4, some of the problems highlighted in the previous Chapters

are discussed in the context of manipulator specifications. Pneumatic actuation in general and a novel rotary actuator incorporating flexible inflatable elements in particular, is identified as an appropriate basis for a horticultural manipulator. Research objectives related to the goal of developing a robust low-cost horticultural manipulator using this flexible actuator are then identified.

Chapter 5 onwards covers the engineering research which forms the core of this thesis. In Chapter 5 theoretical and experimental techniques are used in the analysis and design of the novel flexible joint. Particular attention is paid to understanding joint geometry, so that a constant output torque can be maintained, as well as identifying and minimising sources of hysteresis. Two such joints are then incorporated into a simple manipulator. Chapter 6 deals with the general problem of the control of servo-pneumatic systems and implementation applied to the manipulator. A linearized analysis of the dynamics of the pneumatic servo system is conducted in Chapter 7. This is used to develop a model, which is then extended to include non-linear elements such as friction and rubber-induced hysteresis. Verification is conducted and the model used to investigate some design parameters. High-level control and overall system performance are covered in Chapter 8. The construction of a tomato packing demonstration is covered in Chapter 9. Overall conclusions and suggestions for further work are given in the final two Chapters.

2 Horticultural Background

2.1 Potential applications and review of previous work

Over the past fifty years horticultural production has been transformed by mechanisation. Costs have dropped and the work has become less arduous for people. The techniques used involve growing the crop as bulk material to be handled by machines developed specifically for the purpose. There are, however, tasks, which for reasons of plant habit or susceptibility to damage have remained largely untouched by this revolution. They still rely on the dexterity and intelligence of manual labour to handle each object individually. It is for these applications, where traditional mechanisation has so far failed, that the robotic option may be appropriate. In this Chapter such potential applications are reviewed along with relevant horticultural robotics research. The list is not exhaustive but is representative of the horticultural sector. This Chapter is based on work described in reference [Tillett, 1993a].

2.1.1 Mushrooms

A major problem in developing robotic systems for horticultural applications is the identification of the biological target, its location and orientation. Computer vision is the most versatile and promising approach to this task, which is also capable of providing information to sort target produce into size or quality grades. It is the subject of much research both within and outside the agricultural sector [Tillett R. D., 1991]; its capabilities are likely to continue to increase. Used in conjunction with other sensors, computer vision will form an important part of many horticultural robot systems. The techniques of computer vision are much simplified if the lighting and background scene of the subject can be controlled. Much early research work has therefore concentrated on crops grown in protected environments.

Mushrooms are ideal in this respect, since they are grown within windowless buildings

in a compost substrate that contrasts well with the product. Furthermore, there is no foliage to obscure the mushrooms. Thus for growing systems in which the crop is grown on one level, in bags or in deep troughs, mushrooms are a relatively straightforward subject for robotic harvesting. While many mushrooms are grown in this way the larger European growers employ shelf or tray systems in which layers are stacked one above the other, leaving as little as 300 mm clearance for machinery. Where some damage is acceptable, in processing for example, the mushrooms can be harvested in bulk using cutter bars drawn across the growing medium. For fresh market produce this is unacceptable and a commercial project[1] has been conducted to robotically harvest individual mushrooms from trays [Woodcock, 1990; Wheeler, 1990]. The robot used an industrial, electrically driven, Cartesian co-ordinate manipulator with a suction-cup end effector to grasp the mushrooms. Computer vision was used to identify the target and guide the manipulator. The headroom problem was overcome by moving the trays to another building containing the robot. This was convenient for transporting the harvested produce but incurs cost in moving the trays and risk of cross contamination between growing areas. This option is not available with shelf systems, which are fixed. Operation of a robot between shelves is the subject of investigation [Tillett R.D. and Reed, 1990; Reed and Tillett R.D., 1994; Reed et al., 1995], but it provides severe limitations to the optical and mechanical systems.

2.1.2 Micro-propagation and ornamentals

Another labour intensive horticultural activity in which the environment is totally controlled is micro-propagation[2]. This sector of the industry has also been the subject of robotic research [Fujita, 1989; Billington and Grundon, 1990; Kozai et al., 1991; Deleplanque et al., 1985; Okamoto et al., 1993]. As with mushrooms, work has been

---

[1]This robot has not, to the author's knowledge, been commercially successful to date.

[2]A method of propagation in which very small cuttings are grown on in a nutrient medium in order to produce high replication rates of genetically identical material.

concentrated on end-effector design and image analysis techniques. Commercially available industrial manipulators have been used, which work well in the controlled environment. A particular advantage of eliminating manual labour from micro-propagation is a reduction in the risk of contamination. Thus systems have to be designed in such a way as to allow for adequate sterilization of end-effectors. The diverse nature of commercial micro-propagation is such that a robot would be required to tackle several different plant species. These may have a variety of habits, requiring different dissection and planting strategies. Whilst some respond well to dissection along arbitrary lines, most require accurate identification of dissection points in what is sometimes a complicated three-dimensional structure. Micro-propagation is atypical of horticulture in that the scale of operation is small, requiring accuracy of 1 mm or less depending on the techniques used. Robotic micro-propagation has been demonstrated to be practical for some species, though further research in the analysis of more complicated images is required to provide general solutions [Tillett R. D., 1991]. To date there has been no commercial uptake of this technology. In addition to the technical difficulties, one reason has been the shift in commercial production from western high-wage economies to countries with lower wage rates. The industry itself has also suffered from competing technologies such as embryogenesis[3] which offer cheaper methods of propagation for some species.

The pruning of container-grown ornamental plants is a similar, though scaled up, problem to that of the dissection of some more complicated micro-plants. Analysis of the image and decision making would be different in so far as the objective is to produce an aesthetically pleasing shape, as well as to prune at technically correct points. Standard industrial manipulators might be used, but as scale increases industrial equipment is likely to become disproportionately expensive and over-specified, particularly regarding accuracy. Except for research on transplanting bedding plant seedlings [Kutz et al., 1987] and geranium cuttings [Simonton, 1990; Simonton, 1991],

---

[3]A method of tissue culture in which individual cells are allowed to multiply to form new plants.

both of which used industrial manipulators, little work has been done on robotic ornamental plant production. The ornamental plant industry is, however, using increasingly sophisticated industrial automation techniques to handle and grade container grown plants [Tillett and Lane, 1992; Tillett et al., 1992] demonstrating a willingness to accept the technology if it can be shown to work.

2.1.3 Fruit

Non-robotic techniques are widely used to mechanically harvest fruit for processing. Most of these rely on vibrating branches of the tree or bush to dislodge fruit, which is collected below. The main disadvantages are damage to the harvested fruit, potential damage to the plant and, where fruit ripens unevenly, premature fruit removal. The first is usually the most serious problem and tends to get worse as fruit size increases. Consequently, almost all types of fruit for the fresh market are picked by hand and are possible subjects for robotic harvesting.

Apples:

Parrish and Goksel (1977) conducted an early laboratory robotic harvesting study on apples. A rudimentary manipulator was guided to the fruit using pattern recognition techniques from a video camera image. This has been developed further by Grand D'Esnon et al. (1987) who developed a robot called MAGALI illustrated in Figure 2.1. The French team used a three-degree-of-freedom hydraulically powered, spherical coordinate manipulator with joint position feedback and a suction-cup end-effector. The fixed camera was mounted at the centre of the two rotary joints at the base of the manipulator, so that vision coordinates coincided with robot coordinates. An advantage of this configuration was that when the target was not wholly or partially obscured, the end-effector could be guided along the line of sight without encountering obstructions. This principle, first proposed by Schertz and Brown (1968), reduced the problem of collision avoidance to one which could be solved without knowledge of the three dimensional structure of the plant and environment. To reach to the full height of the

trees, the manipulator was mounted at the end of an elevating arm, which incorporated a conveyor to take detached fruit to a bulk bin. The manipulator and conveyor assembly were mounted on an automatically guided vehicle to provide motion between trees. In reviewing French work on robotic fruit harvesting, Boorely et al (1990) reported a change from hydraulic to electrical power. This was said to improve manipulator control, allowing a maximum speed of 3 ms^{-1} and an accuracy of ±3 mm.

Further work by the French team [Rabatel et al., 1991] on robotic apple harvesting has shown that, depending on the tree shape, up to 85% of fruit was visible from outside the canopy. Using their image-processing algorithms as many as 95% of these could be detected. This level was dependent on apple variety and, in particular, colour contrast, as well as the proportion of mistaken detections tolerated.

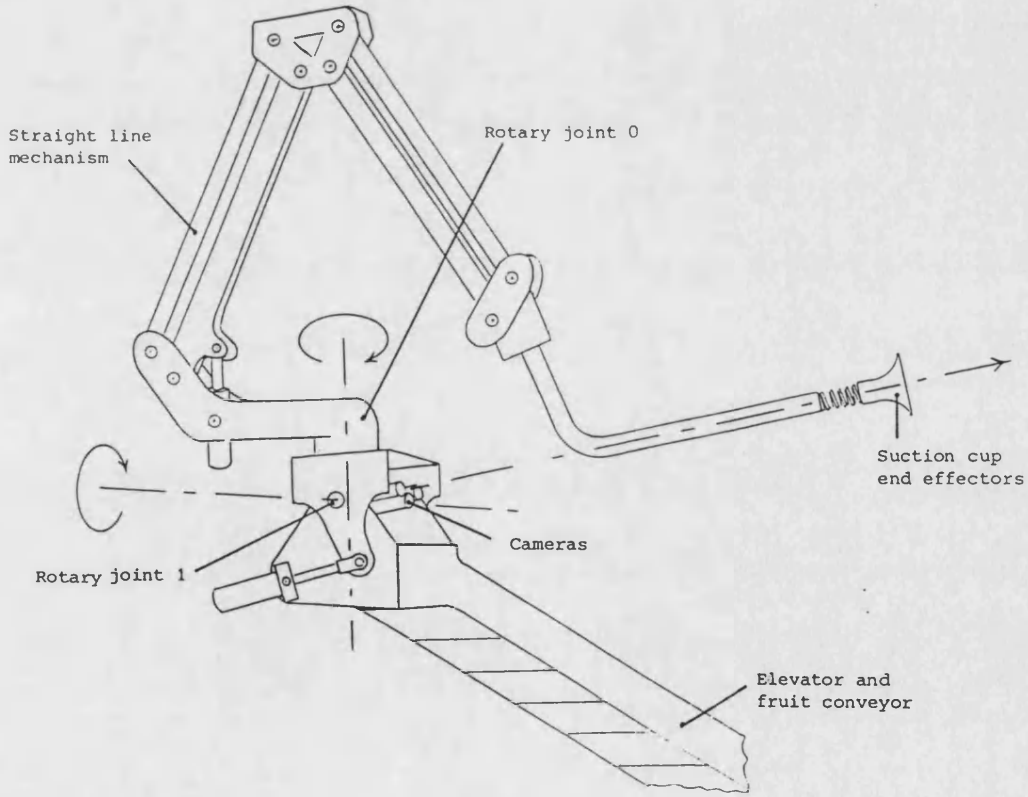

Figure 2.1 Apple harvesting robot [Grand D'Esnon et al., 1987] "MAGALI"

Oranges:

In a similar study Juste et al. (1990) assessed fruit visibility in Spanish orange orchards. They found fruit visibility to be only 40-50% in existing orchards, but that by pruning the trees as a continuous hedge this could be improved to 80-85%.

A consequence of the "line of sight" approach to guidance, is that the manipulator and/or end-effector obscure the target from the camera during the later stages of the picking cycle. Harrell et al. (1989) pointed out that this period of dead reckoning guidance could lead to inaccuracy if the fruit moved, owing to wind disturbance for example. They overcame this in an orange harvesting robot by mounting the camera at the end of the extending arm of a spherical coordinate manipulator within the end-effector (Figure 2.2). Actuation of the manipulator was achieved using hydraulic drives with joint position and velocity feedback. The manipulator moved so that the camera performed a vertical scan of the plant thus achieving relatively high resolution over a large area. When an orange was detected both rotary joints were adjusted to put the fruit at the centre of the field of view. The arm then extended along the third axis to pick the fruit. The "eye-in-hand" approach provided a clear view of the target, the position of which within the image can be used in closing the position feed back loop during extension and was independent of any flexibility in the manipulator. The vision system used the contrast between fruit and background colour to track fruit at a rate of sixty new images per second. If computationally more demanding techniques of image analysis were required, where for example there was no colour contrast, then additional motion sensors and sensor fusion techniques would be required to achieve real-time control by this means. Field trials gave picking cycle times of between 3 and 7s, 75% of which were successful when conditions were favourable. The proportion of fruit picked to those on the tree was not given. The economic viability of this result was not commented on, but in an earlier economic study, Harrell (1987) concluded that performance would have to be higher than that reported above in order to compete with traditional systems. Two principal technical problems were reported. Passage through the canopy produced large and rapid changes in light intensity, which could not be accommodated by the automatic exposure control. Secondly, typical vision feedback

signal sensitivity increased by two orders of magnitude as the camera approached the target fruit. This increased sensitivity to the vision data resulted in reduced stability. In order to compensate system gains were altered as range to the target decreased. The range information was provided by an ultrasonic proximity detector.

Levi et al. (1988) also investigated the feasibility of harvesting oranges robotically. They used a proprietary cylindrical coordinate manipulator with a camera mounted on and moving with the vertical and rotational axes. The camera scanned the tree and divided the view into a series of 20 windows in order to achieve adequate resolution. When fruit was identified, vertical and rotational axes motion aligned fruit with the centre of the field of view. An adjustment was then made for the slight offset of the camera from the arm that was extended to pick the fruit. In such a system it is important that the manipulator remains rigid during extension as any errors due to backlash, bearing wear etc, are not compensated for.

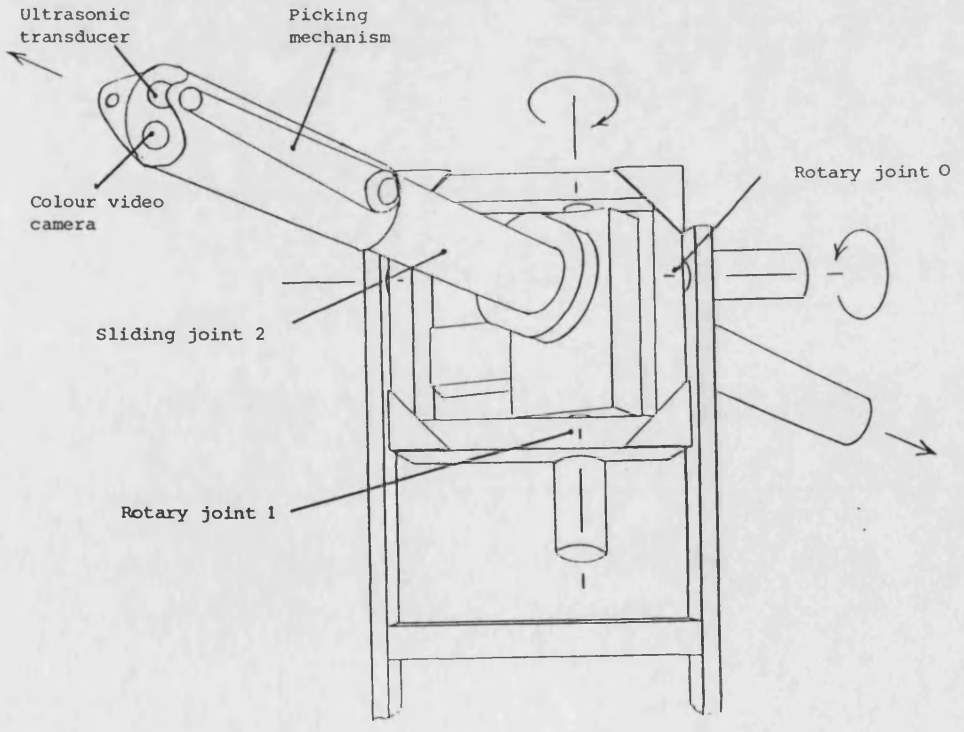

Figure 2.2 Citrus harvesting robot [Harrell et al., 1989] with "eye in hand"

Melons:

Wolf et al. (1990), in a joint American/Israeli project, have investigated the robotic harvesting of melon from a specialist vehicle. Their work, which might have application for other large field grown fruit or vegetables concentrated on end-effector design rather than deployment from a manipulator. Namikawa et al. (1992) also worked on robotic melon harvesting, though their work concentrated rather more on the hydraulic manipulator they developed for this purpose [Iida et al., 1993].

Tomatoes:

Tomatoes grown under glass exhibit most of the features already discussed for field grown fruit, and have been investigated from the point of view of robotic harvesting by Balerin et al. (1991) and Kondo et al. (1995). While they are subject to natural light variations, shading is often available, there is minimal wind to cause plant movement, and it does not rain. In addition, there are useful structural features for guidance and support as well as services such as mains electricity. The long (approximately six months) harvesting season would provide good utilisation easing economic justification. It is likely that tomatoes, in common with other crops, would be better grown under husbandry techniques modified to suit robotics. For tomatoes this may mean altering the practice of layering stems down as they grow in order to keep fruit within reach of people. By allowing greater vertical spread, visibility of fruit may be improved at the cost of taller glasshouses. Similarly, single rather than double rows might improve visibility and access at a cost of reduced yield per unit area. Kawamura et al. (1986) laboratory tested a dual purpose battery powered mobile robot for field tomato harvesting, as well as chemical thinning and weed control.

Many crops such as tomatoes do not mature uniformly and require frequent selective harvesting passes in order to maximize yield and quality. In some cases each pass may only yield one or two fruit per plant. Under these circumstances a robot that stops at each plant will be relatively slow. Sévila et al. (1992) investigated the possibility of deploying a robot manipulator from a continuously moving platform as a means of speeding this process. Their experimental system consisted of a spherical coordinate

manipulator mounted at the rear of a small mobile platform, both of which were electrically driven. A camera was mounted at the front of the vehicle so that fruit was detected some time before the manipulator reached its position. Manipulator extension was fast relative to vehicle forward motion and timed so that it only penetrated the crop within ± 5° of the angle seen to be unobstructed by the camera. The French research team developed a transformation between vision and manipulator coordinates, taking into account a number of potential misalignments. Laboratory testing demonstrated ±3 mm accuracy. Their work may be useful in a number of other applications, such as the precision placement of agrochemicals on fruit and other crops. In the author's opinion, whilst of long term interest, manoeuvring a manipulator from a moving platform is likely to add to the cost of operation and to detract from its reliability. The first successful commercial mobile applications of this type are most likely to be conducted on a stop-start basis so that there is no motion as the manipulator is guided to the target. Whilst work rate might be lower, reduced complexity and cost should offset this.

Grapes:

Winter vine pruning remains one of the few operations in grape production that must still be conducted, at least partly, by hand. This is largely due to the degree of intelligence required to make decisions on where to cut. Sévila et al. (1990) in France, Gunkel and Throop (1992) and Naugle et al. (1989) in the United States, have conducted research in the area of vision guided intelligent robotic pruning. Their research to date concentrated on image analysis and algorithms for decision making. Both teams used fairly conventional manipulators in their laboratory trials: the French one was electrically powered and the American hydraulic [Norman et al., 1991]. The feasibility of robotically harvesting complete bunches of grapes for the minority of vineyards in France that cannot accept conventional mechanisation techniques was investigated by Sittichareonchai et al. (1989). They concluded that the task was impractical with existing vine layouts, owing to the difficulty of locating the stem and avoiding obstructions while cutting and grasping the fruit. Monta et al. (1995) reported on the development of end-effectors for bagging bunches of grapes and spraying vines.

Their device was mounted on a multi-purpose mobile robot for vineyards. The five degree-of- freedom experimental manipulator was electrically driven and tested with some success in a laboratory environment.

2.1.4 Vegetables

Although a major part of horticulture, field vegetable production, with a few exceptions such as work by Humberg and Reid (1989) on asparagus harvesting, has not been an important area for robotics research. An exception might be very high-value vegetable crops such as cucumber, in which a high proportion of seedlings are grafted. This labour intensive task has been the subject of automation research [Kurata, 1994], though arguably the techniques applied are those of automation rather than robotics. There are, however, a few applications in field vegetable production where the robotic approach may be appropriate. These are tasks that require flexibility of response according to environmental factors. In particular the concept of reducing inputs, agrochemical or any other, to an absolute minimum by targeting plants (crop or weed) individually, would require a robotic approach. Working to this precision is unlikely to be carried out at rates comparable with current wide boomed sprayers and so the driver might have to be removed for economic operation. Autonomous robot crop protection vehicles, capable of being programmed to work in a variety of crops, might therefore be required. Such vehicles are a research interest of the author, although they are outside the scope of this thesis [Baylou, 1987; Hague and Tillett, 1996]. It has been suggested by Thompson et al. (1995) that to get very precise treatment on an individual plant scale the treatment device should be mounted on and move independently of the vehicle. They chose 'HEXA' a very fast 6 degree-of-freedom parallel manipulator with electrocution as the chosen method of treatment. Whilst of great interest in the longer term, the author regards the very much simpler and faster technique of turning on and off closely spaced arrays of independent spray nozzles to be much more practical in this application [Marchant et al., 1997].

2.1.5 Packhouse operations

Grading operations for fruit and vegetables have, to a large extent, been automated by applying modern sensing techniques including computer vision to traditional grading lines [Marchant and Moncaster, 1990]. Packhouse operations such as trimming and handling individual items for packaging or as part of pre-prepared meals are, however, an important area of potential application. In general, problems are simplified as the environment is controlled and there is no foliage to obstruct the view or manipulator. Usually the material to be packed is presented on a table or conveyor thus reducing the problem to a predominately two dimensional one. These operations, which have much in common with other food sectors [Wallin, 1993; Tillett, 1995] such as meat packaging [Khodabandehloo, 1993], have yet to be automated as they are subject to natural variation in the material. The processed food packaging industry has, on the other hand, been able to exploit industrial robotic techniques as the product is uniform, though even here robotics are not yet widely used [Cleary, 1995]. The factory like nature of the packhouse also has some financial advantages when trying to justify robotics, as the pack house can operate multiple shifts, and operate regardless of weather or light.

Regular changes in packhouse production lines, both in product and presentation, make flexibility of very great importance when packing fresh produce. It is this need for flexibility that has precluded automation in many areas and is why robotics offers an attractive alternative. One of the arguments used for not automating the final stage of the production process, packaging, is that people provide final inspection. Fortunately, modern automatic grading and inspection techniques now mean that these tasks too can be automated, though an element of manual inspection is likely to remain for some time.

Hygiene requirements for robots that handle products for direct consumption by the end customer are stringent. Robot manipulators for food handling must, therefore, be washable and be inherently leak proof against oil and other contaminants. The environment in many food packing halls is a compromise between the conflicting

requirements of human comfort and food storage. Robotic operations need not be so compromised and could for example be conducted at low temperatures thus improving product quality and shelf life.

2.2 Economic factors

For robotics to succeed in commercial horticulture, the benefits of their use must exceed the costs. In this Chapter an attempt has been made to quantify economic factors based on the situation in the United Kingdom. Although some assumptions have been made it is hoped the figures will help to identify those applications which are best suited to robotics and therefore most likely to fulfil the cost/benefit criterion. A major benefit of a robot is the direct replacement of semi or unskilled labour. The costs of recruiting and retaining such labour will be subject to some regional variation. Nix (1997) estimates the typical cost of employing a regular agricultural worker to be £6.17 per hour. Part time or casual workers are less expensive to employ but require costly supervision and are increasingly difficult to recruit for tedious repetitive tasks. Discussions with companies involved in meat packing put their labour cost at £7 per hour. This includes welfare and insurance costs which they claim are increasing as cases of injury through repetitive strain injury etc become more common. A labour cost of £6.50 per hour has been assumed throughout this Chapter.

The saving in labour costs is the product of the hourly rate, the difference in productivity relative to manual labour and the number of hours, assuming similar supervisory costs. Seasonal tasks such as harvesting apples are, therefore, likely to produce lower annual savings than those such as packing, which might run throughout the year. Similarly, tasks that robots perform at a favourable speed relative to manual workers are likely to be more attractive. If the limitation to robot speed is speed of computation for target identification, then robot systems will be better suited to the manipulation of larger higher value items requiring longer reaches such as top fruit than smaller products such as soft fruit.

In general industrial robot work rates are higher than a single person employed on the same task. Typical horticultural robotics research projects on the other hand rarely achieve manual rates, though we might expect speeds to improve as commercial development takes place. For this economic assessment, it is arbitrarily assumed that a single robot manipulator will perform at the same rate as a manual worker. Robots do not require meal breaks or sleep, enabling them to work longer hours, say 16 hours a day. To illustrate the potential quantifiable labour savings, two examples have been chosen:

First, a pack house operation running throughout the year, changing products with the seasons possibly packaging imported produce in the winter months.

Annual labour saving = £6.50/h x 16 h/day x 250 days/year
= £26,000

Secondly, top fruit harvesting with an eight week season, in which the robot is laid up for the remainder of the year.

Annual labour saving = £6.50/h x 16 h/day x 48 days/year
= £4,992

These simplistic figures clearly illustrate the need to keep the robot productively occupied for as long as possible. In terms of robot design, this might mean building in flexibility of role to encompass pruning, for example as well as fruit harvesting.

In practice the benefits would not be restricted to labour savings and might include higher accuracy, improved consistency, better hygiene and more reliable management information through linking computers. The latter may become particularly important as supermarkets, who dominate horticultural retailing, increasingly demand complete produce traceability from their suppliers. The effect of the robotic system on product quality may in some applications be an overriding economic factor, the importance of

which is likely to increase with the value of the product. Even small percentage increases in class one classification of a high-value product may well outweigh robot or labour costs. Similarly a reduction in quality is likely to make the system uneconomic. Whilst it is important to bear these factors in mind, they will be highly application dependant and so have been omitted here.

A consideration of robot costs shows that flexibility also becomes important to the manufacturer. If the same basic machine can be sold to cater for a variety of needs, then standardisation will reduce development and manufacturing costs. This is also likely to lead to improved reliability and lower maintenance charges. The cost of horticultural robots is difficult to judge, as the specification is not directly comparable with industrial machines, which vary in price from a few thousand to several hundreds of thousands of pounds. The important differences are firstly, the need to provide sophisticated sensing techniques to cope with natural variations in biological objects, which increase costs, and secondly, the probable ability to cope with millimetre rather that sub-millimetre accuracy as well as tolerance to various target orientations, which will keep costs down. Other costs associated with the implementation of robotics and not easily quantified include efficiency, in terms of percentage of task completed, possible product damage and the retention of suitably skilled labour for supervision and maintenance. Also from the business point of view, investment in capital equipment is less flexible than in labour, which can be laid off or redeployed in difficult times.

In the following an attempt is made to quantify specialist horticultural robot costs. Using proprietary controller and vision processing components in a system based on a personal computer, the cost of control hardware is estimated to be £10,000. The cost of mechanical components is even more difficult to estimate, but is thought to be £15,000 for the manipulator and end-effector. Thus, for pack house type operations, robot system costs might be about £25,000. Discussion with those running commercial organisations in agriculture and horticulture suggest that capital projects with paybacks greater than three years are very rarely considered except for low risk investments such as buildings and that two years might be regarded normal. If capital is written off over

two years at 15% and provision is made for an annual maintenance charge of 20% of capital, an annual cost of approximately £20,000 results. On these figures and those given above for labour saving, robotics in the packhouse look economically attractive. It is very clear however that cost effectiveness is fairly finely balanced and critically dependant on capital costs. If we recalculate using more typical industrial robot capital costs of say £40,000, the annual cost would increase to an uneconomic £30,000 indicating that cost reduction is an important objective.

In operations such as top fruit harvesting the manipulator has to be made mobile and provision made to transport the product. In order to reduce equipment costs whilst maintaining high production rates, it has been proposed by Harrell (1987) and others that each harvesting vehicle carries several manipulators. Nevertheless, since the cost per manipulator is likely to be higher due to the increased sophistication required for mobile outdoor operation and benefits lower as a result of a shorter season, the economics of robotic top fruit harvesting looks less attractive than those for packhouse operations. However, the difficulty of recruiting seasonal labour for physically demanding harvesting jobs makes fruit harvesting an application of great importance. For this reason much overseas government and industry funded research has been done in the area, the economics of which will undoubtably improve as robotic technology develops and becomes cheaper to implement.

2.3 Discussion

The wide variety of potential applications discussed above can be placed into two categories. In the first target orientation is not critical, allowing simple compliant end-effectors such as suction cups to be used from manipulators with only two or three degrees-of-freedom. In these cases it is normal to use a computer vision based line of sight approach to avoid the need for additional degrees-of-freedom to reach round obstructions. Examples of this type include the apple harvesting work of Rabatel et al (1991) in which the camera was placed at the geometric centre and remained static as the manipulator extended. Another example is the orange harvesting robot of Harrell

et al (1989) in which the camera was mounted within the end-effector.

The second category of application requires some alignment of the end-effector with the target. This requires a more sophisticated sensing, control and guidance system. It also requires a manipulator with more degrees of freedom and generally a more complex end-effector. There are fewer examples of this category. They include the work of Okamoto et al (1993) on micropropagation using a four degree-of-freedom manipulator and Monta et al (1995) who used a five degree-of-freedom manipulator and a sophisticated end-effector to bag bunches of grapes. In economic terms the former category of application using less complex equipment is likely to be considerably less expensive to implement.

To the authors knowledge none of the research projects described have yet found their way into commercial horticulture despite, in some cases, the involvement of manufacturing companies. There are likely to be many reasons for this, but there are two reasons which dominate. These are firstly the cost of implementing the technology and secondly the difficulty of maintaining quality. Product quality is absolutely critical to fresh produce production, the area of horticulture in which robotics are most needed. The latter highlights the need for an integrated approach to commercial systems in which minimising damage and automatic quality inspection form an integral part of the handling process. The former suggests that effort should initially be concentrated on the simplest applications in engineering terms which can also offer good equipment utilisation. In the context of UK horticulture one might select tomatoes and mushrooms as suitable subjects for robotic harvesting and packhouse operations for robotic handling. Of these packing probably has the most potential and has been chosen for the demonstration in Chapter 9.

3 Industrial Robotics Background

Industrial robotics have traditionally been led by the demands of the automotive industry, though other manufacturing areas (notably electronics) are increasingly important. Within this range of industries Ranky and Ho (1985) broke down applications into the following areas:

Pick-and-place, requiring point-to-point control for tasks such as machine loading/unloading, palletising and packaging.

Welding, which might require point-to-point control for spot welding or trajectory control for arc welding, flame or laser cutting etc.

Machining, which would generally require trajectory control and a rigid structure to maintain accuracy under offset loads during drilling or routing applications for example.

Cleaning/deburring, which may require force feedback in addition to position or trajectory control.

Spray painting, which is normally a trajectory control problem.

Assembly/inspection is a fast growing area which requires relatively high precision position control.

A feature of these applications within manufacturing industry is that they can and usually are conducted "blind", that is to say the robot does not sense object position and react accordingly, it assumes the object is located where it should be. Repeatability rather than accuracy is a key performance criterion and is related to component dimensional tolerances. It has been suggested [Wilson, 1995] that one of the positive impacts of the early robots in the automotive industry was that manufacturers were

forced to improve their manufacturing tolerances in order to make robots work! This, it is suggested, had an overall improvement in product quality and consistency. Having achieved a high standard of manufacturing tolerances there is little incentive for users to pay for more expensive robots with added intelligence to deal with variable components. Perhaps because of this, the main thrust of recent manufacturing industry robotics research has been aimed at improving performance in terms of speed, repeatability, payload and reduced costs. It has also been very important as their numbers grow to design robotic systems to be easier to use and programme by non-specialists. Integration with existing machine tools is also an area of great importance particularly with regard to information flow between computers and the synchronization of operations. Very few manufacturing robots work in isolation; they would normally form part of an integrated production line. The high cost of stopping many of the larger production lines has led to a lot of interest in off line programming techniques. This allows much of the system to be tested using computer-generated models of the product before any hardware is actually produced, so reducing down times.

Another group of specialist industrial applications cover tasks which cannot or at least are very difficult to conduct manually with safely. Examples are to be found in nuclear and offshore industries amongst others. In contrast with manufacturing industry, speed is not normally a priority, though the ability to deal with an uncertain or not precisely mapped environments is. The cheapest and simplest way of endowing a robot with intelligence is to use remote manual operation. In its simplest form this might involve placing a transparent screen between the operator and the robot. However, this is not always possible so, teleoperation using video images from a camera mounted on the robot is sometimes practised. The difficulty of performing complicated tasks using purely visual information from a single view has led researchers to investigate virtual reality techniques [Stone, 1992], both as an operator training aid and directly in conducting the task using tactile feedback for example. The progression from teleoperation to fully autonomous operation in unstructured or semi-structured environments requiring high levels of intelligence and flexibility is an active research area.

Robotics for the food processing industry is another group of potential applications, though in practice their commercial impact has been minimal and limited to the packing of processed items such as chocolates. It is however an area in which research is being conducted notably in butchery [Khodabandehloo, 1993]. Key issues are the detection and path following of meat cuts from the carcass, the accuracy of which has a critical impact on the economics. The provision of appropriate food-grade manipulators is also being pursued as standard industrial manipulators have been found not to be adequate [Taylor and Brooking, 1994].

Industrial robot requirements in general have been well served by the use of electrical drives, which in themselves have fairly linear characteristics. The non-linear effect of mechanical coupling between axes is to some extent reduced by the relatively high gear ratios used between drive motors and manipulator links. Typically, Proportional, Integral and Derivative (PID) dynamic control strategies are employed independently on each axis [Boddy and Taylor, 1992]. This approach has the virtue of simplicity, but a quest for increasing performance in terms of higher speeds and payloads means that more sophisticated control strategies which take axes interaction into account are being developed [Ranky and Ho, 1985; Boddy and Taylor, 1992]. This need is particularly acute for the minority of robots that use direct drives where the inertia of the robot arm is directly coupled to the motor. Fluid power is occasionally used in industrial robotics. Hydraulics power has advantages where high payloads are required or where the environment is unsuitable for electric drives. Pneumatics offer particular advantages in environments requiring hygiene, but are most commonly used in lightweight pick-and-place operations utilizing two mutually perpendicular linear drives. Non-proportional pneumatic actuators are widely used industrially in robot end-effectors and in ancillary fixtures due to their high force-to-weight ratio, robustness and low-cost.

A large number of alternative robot geometries exist using various combinations of revolute and prismatic joints. The predominance of rotary electrical motors, the compactness of revolute joints and the ease of accurately measuring rotary displacement, means that revolute robots are popular. In general three such joints and

their links form the arm which positions the end-effector, and three further joints form a wrist which orientates it. The solution of the resulting kinematic equations and techniques for dealing with singularities are now well understood [Ranky and Ho, 1985] and can be solved in real time. Prismatic joints are also fairly common. Electrical direct linear drive can be achieved with linear motors [McKay, 1996], but more commonly ball screws are used to convert from rotary to linear motion. The most common fluid power actuators, cylinders, are naturally linear though mechanisms can be used to provide limited stroke rotary motion. The best known non-robotic example being an excavators arm which, whilst effective, does suffer from geometric non-linearities. More commonly linear actuators especially pneumatic ones are used in Cartesian robot geometries, which have the advantage of having simple coordinates transformations. They can however be mechanically clumsy if overhangs are required. Cartesian geometry is best suited to gantry type applications in which the main axis straddles and is supported both sides of the working area. Parallel robot configurations using an inverted Stewart platform [Harris and Laurenson, 1992] (of which the most common application is aircraft simulators) or other mechanism [Thompson et al., 1995] are discussed in research papers but to the author's knowledge they have not found widespread industrial application despite the potential advantages of very high speed due to the low inertia of the moving parts.

As discussed above, industrial robotics is a very diverse area. Performance requirements range from high speed machines with an accent on repeatability and compatibility with other computer systems in manufacturing, through to robots for hazardous environments where the priority is for flexibility and intelligence. It is clear from the previous Chapter that horticulture offers yet another different set of performance criteria, though obviously much can be learned and borrowed from industrial robotics. In Table 3.1 an attempt has been made to summarize and compare typical industrial manufacturing robot specifications with those required for horticultural use. The contents of the table are based on the literature already discussed and the authors background knowledge. Due to the diverse nature of the potential applications the table includes a number of generalizations. However, it does provide a means of highlighting the key areas of difference, accuracy/guidance and environmental requirements.

Feature	Horticultural use	Industrial manufacturing use (Puma 562)
Speed	1.5 ms^{-1}	1.2 ms^{-1}
Acceleration	20 ms^{-2}	20 ms^{-2} (estimated)
Reach	0.7 m	0.864 m
Payload	1 kg	4 kg
Dynamic (trajectory) accuracy	± 20 mm	± 1 mm (estimated)
Static accuracy / repeatability	± 2 mm	± 0.1 mm
Typical (half stroke) point-to-point settling time	1 s	2 s (estimated)
Guidance / sensors	Vision and others	Proximity detectors
Actuator type	Pneumatic	Geared DC servo motors
Degrees of freedom	3	6
Geometrical configuration	Spherical with common vision and mechanical coordinates	Revolute
Robustness	Capable of withstanding collisions in a semi-structured environment	Not capable of withstanding collisions
Washability	Hose down	Not washable
Tolerant to dust and dirt	Yes	Not tolerant
Hygiene	Required for some applications	Not easily converted

Table 3.1 Typical manipulator specifications

4 Discussion and Identification of Key Research Areas

In this Chapter each of the major manipulator design issues is discussed with a view to identifying, as far as is possible, general specifications. The discussion is then focused down to specific candidate technologies that might meet the specifications. Finally areas of research are identified to develop these technologies to the point that they might provide practical solutions to horticultural robot problems.

4.1 General specification

4.1.1 Geometry

The probable reliance of horticultural robots on sensory information makes a desirable choice of geometry one that simplifies the relationship between sensory and mechanical coordinates. For non-planar tasks such as fruit harvesting, the technique described in Chapter 2.1.3 of mounting the camera at the physical centre of the base of two rotary joints (waist and shoulder) of a spherical coordinate robot is very attractive. This geometry allows movement along a `line of sight', avoiding the need to produce three dimensional maps of the work space to avoid obstructions. A slight variation on this theme using a rotary axes robot configuration is illustrated in Figure 4.1. A second sensor, possibly ultrasonic [Grand D'Esnon et al., 1987; Hall et al., 1994] or tactile [Foroughi et al., 1987], could be mounted at the end of the manipulator within the end-effector to provide sensory information in the third dimension along the 'line of sight'.

In simple planar applications such as packing or mushroom harvesting these requirements can be met by mounting a camera on a stiff frame vertically above a cylindrical coordinate robot or a Cartesian robot as illustrated in Figure 4.2. This approach has the virtue of simplicity and provides a high degree of freedom in the choice of optics and lighting where there are no obstructions. It is particularly appropriate for static operations in which it is easy to keep the camera steady and clear of obstructions.

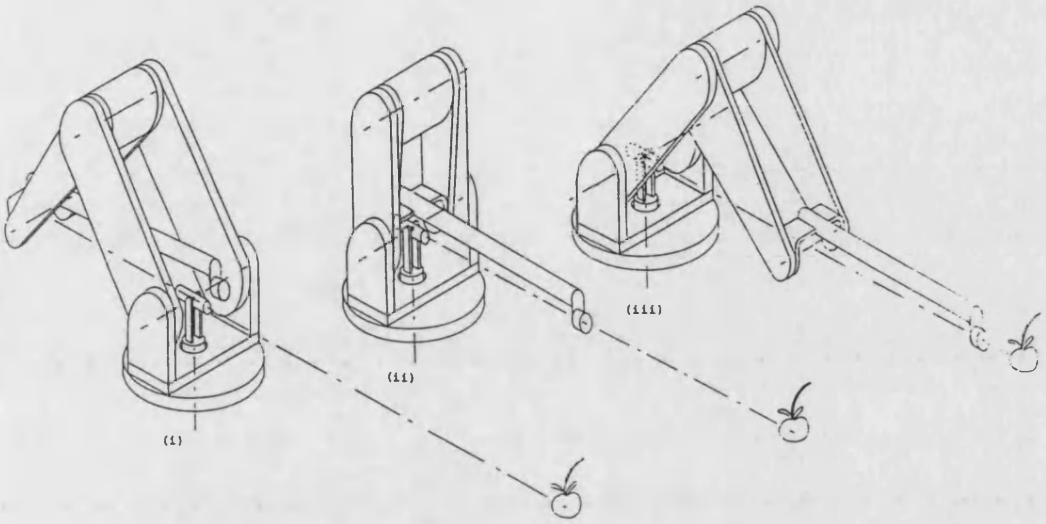

Figure 4.1 Rotary axes spherical co-ordinate robot with vision location of target and end-effector position

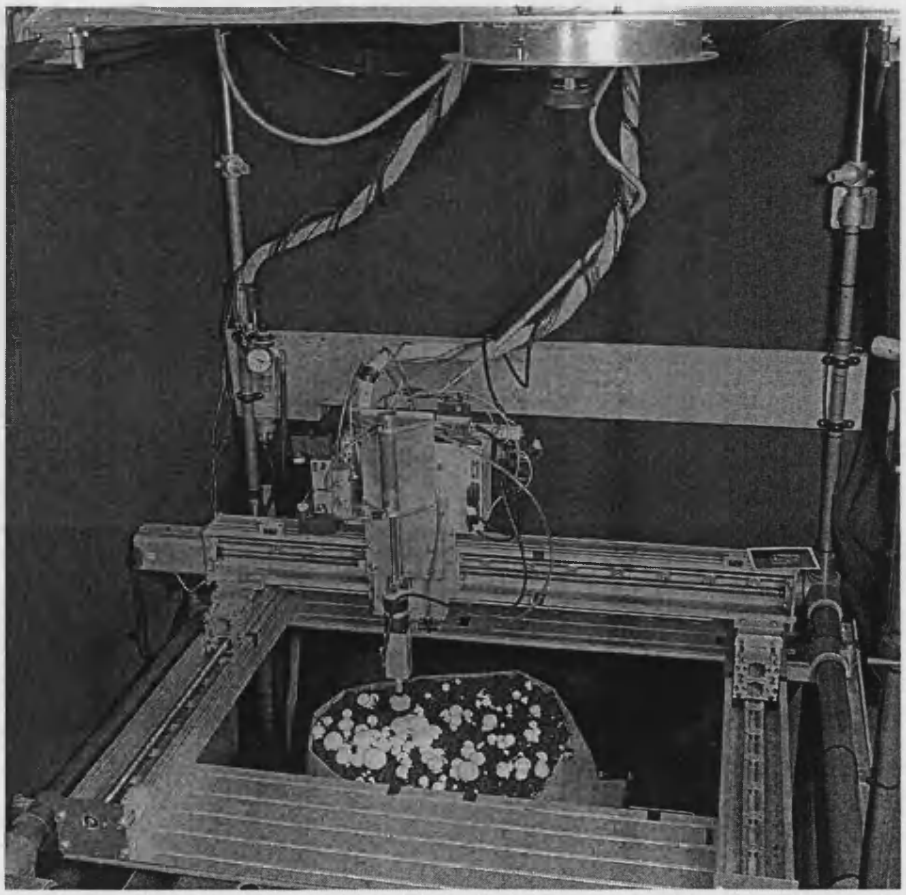

Figure 4.2 Vision-guided Cartesian co-ordinate robot harvesting mushrooms

In most cases end-effectors need a large degree of compliance to cope with the indeterminate orientation and natural variation of horticultural products. To some extent this compliance reduces the number of degrees-of-freedom required of the manipulator. Thus for many horticultural applications it might only be necessary for the manipulator to have three degrees-of-freedom. This allows complete freedom of end-effector position but at a fixed orientation in contrast to industrial manipulators which typically have six degrees-of-freedom providing a full range of orientation.

A number of alternative manipulator mechanisms and geometries exist, each with their own advantages and disadvantages. Cartesian geometries and linear mechanisms are conceptually easier to deal with than rotary systems when used in conjunction with vision guidance which is also Cartesian. However, coordinate transformations for all common robot configurations can readily be done by modern computers and so do not represent a real barrier. Linear mechanisms are particularly convenient in gantry type applications in which it is possible to support the major axis either side of the working area. Where it is necessary to cantilever beyond supports, linear mechanisms become clumsy. They are also difficult to seal against contamination. Another factor in favour of rotary joints is that rotary position transducers are generally less expensive and more robust than their linear counterparts.

Because most potential applications for robotic manipulators within horticulture are a direct replacement for manual labour, the maximum reach required from a manipulator is limited to an arm's length, say 0.7 m. For similar reasons perhaps, this is also typical for industrial robots though they do cover a broad range. Applications such as micro-propagation allow a lower limit, determined by the size of the growing containers, say 0.2 m. Whilst the introduction of robotics may change horticultural practices, as other forms of mechanisation have done, these limits provide a useful starting point, particularly as robots may work alongside people in the first instance.

4.1.2 Actuators

There is little reason to suppose that the speed and acceleration requirements of horticultural manipulators will be substantially different from the 1.5 m/s and 20 m/s^2 found in typical industrial machines. However, the delicate nature of many horticultural products means that these figures probably represent upper limits. Factors which dominate the choice of actuator for industrial robots are cost and ease of control to high levels of absolute accuracy and repeatability. Based on these criteria, servo electrical drives, usually through a minimum backlash precision gearbox, are often used. These drives are also energy efficient, making them attractive for mobile applications where power is limited. Where cost constraints outweigh speed and payload requirements, stepper motors are used to provide a fine, repeatable, stepwise movement. Providing the starting position is known and a count of pulses in each direction is made control can be open-loop, requiring no proportional feedback elements [Morgen, 1983].

Applications where electrical drives are inappropriate owing to moisture, heat, dust, etc. and particularly where payloads are high, sometimes use hydraulic drives which are relatively tolerant of such environments. Hydraulic drives are already widely used in agricultural field machinery [Iida et al., 1993] and forestry [Thollot and Bonicelli, 1992; Herman et al., 1992]. However, the valves required for robotic applications are relatively expensive and require good standards of filtration.

In much of horticulture payloads are modest at about 1 kg, but there are often two further requirements, namely the ability to be washed down or sterilised and the guarantee that oil or any other contaminant will not come into contact with the product. The former is difficult to satisfy with electrical drives and the latter with hydraulics. It might be possible, however, to minimise these problems by placing the actuators some distance from the end-effector and using `tendons' to transmit motion, though this has not been considered further here as the mechanical complexity and therefore cost are likely to be high [Jacobsen et al., 1984]. There are also a number of applications in which it is sufficient to ensure that the end-effector only is contamination free.

An alternative to electrical and hydraulic drives is pneumatics. Pneumatic actuators are washable, can operate with clean air and might be attractive in the food as well as horticultural industries. Drive can be direct without gearboxes simplifying design whilst minimising weight and costs. The compressibility of the medium also has safety advantages, both from the point of view of protecting the robot and any people who may accidentally come into contact with it. A further advantage of pneumatics is the ability to control compliance within the actuators by altering system parameters. On the negative side, compressibility is the cause of their greatest disadvantage, difficulty of control, and accounts for their poor energy efficiency. In comparison with hydraulic systems, which typically operate at 10-20 MPa, pneumatic actuators operating at 600 kPa are physically large and cumbersome at high loads and so might be less appropriate for larger machines with high payloads. However, at typical robotic payloads of the range being considered here, a pneumatic drive offers power-to-weight ratios exceeding those of common electrical drives. Until recently, the difficulties of control have meant that pneumatics have only been used to provide movement between fixed stops. Recent advances in pneumatic valve design have resulted in the availability of low-cost proportional control valves. This, coupled with the development of alternative control strategies designed to cope with non-linear systems that can be implemented using small computers, makes pneumatic powered robots an attractive option. Street et al. (1990) have already made progress in this direction in an agricultural context with the development of a pneumatic robot for teat cup attachment as part of a fully automatic milking unit.

Pneumatic actuators take several forms. The most common giving linear motion is the conventional ram consisting of a cylinder, rod and piston. To obtain rotary motion over a limited arc (less than 360°), vane type rotary actuators are available. Various pneumatic actuators [Levpolz and Lofmark, 1991; Winters, 1990; Immega, 1986; Baldur and Blach, 1985; Kawamura et al., 1987; Dils, 1992] also exist, which operate by inflating rubber `muscles', providing linear or rotary motion, the latter being particularly appropriate for a robot with rotary joints. An advantage of these devices is their high force/mass ratio and that there are no sliding joints to produce stiction,

though internal flexing of the reinforced rubber members results in hysteresis. To achieve double acting motion, two such rubber muscles can be arranged in opposing pairs. Unlike cylinders, flexible actuators do not always produce a constant force over their full stroke.

4.1.3 Feedback and control

The required static point-to-point accuracy of alignment between end-effector and target will be determined by the degree of compliance in the end-effector but is likely to be of the order of ± 2 mm. Provided trajectory control is adequate to avoid collisions, say ± 20 mm, dynamic accuracy will not be important except in special cases. The ability to cope with a target having constant velocity, such as that on a conveyor belt, might, however, be useful in packhouse applications. An important difference between horticultural and industrial robots is that as well as tolerating almost an order of magnitude more in positional error, the former requires accuracy to be relative to sensor system coordinates.

For closed-loop control a means of feeding back the position of each joint is required. The most common techniques are optical incremental encoders, inductive devices and potentiometers. They are available in a range of resolutions and accuracies and in linear and rotary forms. Potentiometers have the advantages of being inexpensive, light and compact as well as providing absolute position from start up though they do have small, typically 1%, non-linearities and are more prone to signal noise than encoders.

A feature common to encoders and potentiometers is that they are electrical devices that require protection against water, dust, etc. This is less difficult to achieve than in power components such as electric servo motors since heat dissipation is not a problem. However, it would be preferable to eliminate all electrical components from the manipulator. This might be achieved by using a remote measuring system to monitor manipulator and end-effector position and orientation. This would have the further

advantage of correcting for errors in position due to wear or flexibility in the structure. Such a system has been developed in a laboratory environment using lasers to track position for the purpose of performance evaluation. It is unlikely, however, to be appropriate as a means of providing feedback in horticulture, as it is expensive and is likely to suffer from foliage shielding the lasers. An alternative for vision guided robots might be to use the normal target identification system to also monitor manipulator position. The principle difficulty with such arrangements is that the data update rate would have to be high enough to provide good dynamic control, typically 200 Hz or better. In general this is not feasible, though data fusion techniques might alow vision data to be used in the dynamic feedback loop if combined with other appropriate data sources such as accelerometers. In practice the difficulty of correcting for interactions in accelerations between axes for more than the simplest problems is not likely to be practical and so some kind of position transducer would have to be retained.

Where the end-effector is in view of the vision system, it would be possible to re-calibrate feedback transducers regularly, to coincide with vision coordinates in which the target has been identified, thus compensating for some flexibility in the structure. This need not be carried out as frequently as required for vision feedback for dynamic control and can be simplified by providing a view easily interpreted by the vision system which might provide orientation as well as positional information.

The controller employed will depend largely on the choice of actuators and the mechanical design. As discussed in Chapter 3 common commercial industrial practice is to use independent PID controllers on each electrically driven axis neglecting geometrical non-linearities and dynamic interactions. Whilst capable of improvement such arrangements provide adequate performance for many industrial tasks. Where the drive components themselves are non-linear the controller is liable to become increasingly sophisticated. Performance criteria, such as the need for velocity as well as point-to-point control, will also increase demands placed on the controller. For example, the controller for a system utilising pneumatic actuators, and coordinated movement between axes might be expected to be fairly complicated and non-linear.

4.2 Key research areas

It is clear from the earlier discussion of actuators that pneumatic technology has much to offer in terms of low-cost drives which are tolerant to horticultural environments provided the control limitations can be overcome. It was therefore decided to concentrate on pneumatic actuation. Given that the manipulator was to be pneumatically actuated there remained considerable choice in the detailed implementation. It was intended that much of the work of this thesis should be generic to pneumatic servo systems and capable of application to a number of alternative systems. In order to provide focus to the work however, one specific actuator type was chosen.

Taking the view expressed above that rotary joints were preferred and accepting that converting linear to rotary motion was clumsy and complicated if torque was to be held constant over a normal working stroke, it was concluded that a rotary actuator was needed. Commercial limited stroke vane type actuators, whilst simple, have poor torque-to-weight ratios. Continuous rotation air motor/gear box combinations have a better performance in this respect, but are more complicated, less robust and consume a lot of air which makes them expensive to run. Commercially available rotary pneumatic actuators based on contracting "muscles" are very limited in torque and exhibit a varying output torque with position.

A novel alternative based on a patented actuator with the registered trade name 'Flexator' [Hennequin and Fluck, 1987], was chosen by the author for this application. In this design, motion is provided by the inflation of lay-flat hose folded back on itself and clamped to a cylinder as shown in Figure 4.3a. A length of webbing is wrapped over this inflatable bladder, round the cylinder and attached to a roller running concentrically within the cylinder. As the bladder inflates it pulls the webbing circumferentially causing the roller to rotate as illustrated in Figure 4.3b. Two such arrangements acting in opposite directions provide double acting motion. The advantage of this form of actuator lies in its simplicity, robustness and the potential for

a high torque-to-weight ratio. The principal disadvantages are that it exhibits approximately 20% hysteresis and that torque varies with position.

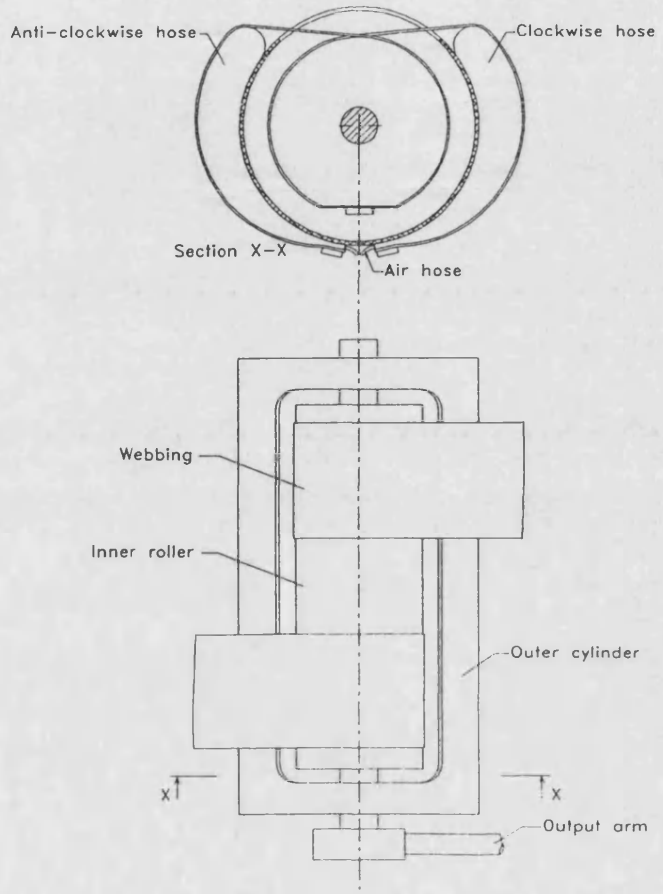

Figure 4.3a Basic flexible actuator representing an effective starting point for this work.

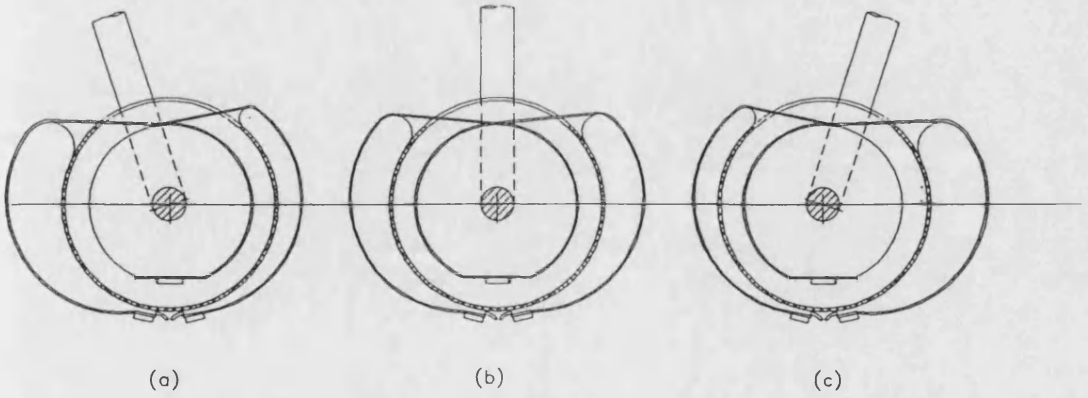

Figure 4.3b Clockwise output motion from (a) to (c) as air is supplied to the right hand bladder and exhausted from the left hand.

In this thesis the analytical and experimental process of turning the 'Flexator' into the relatively high performance rotary actuator illustrated in Figure 4.4 is described. The refined actuator has been used in the construction of a 2 degree-of-freedom manipulator which was integrated with vision guidance to perform a demonstration application of tomato packing.

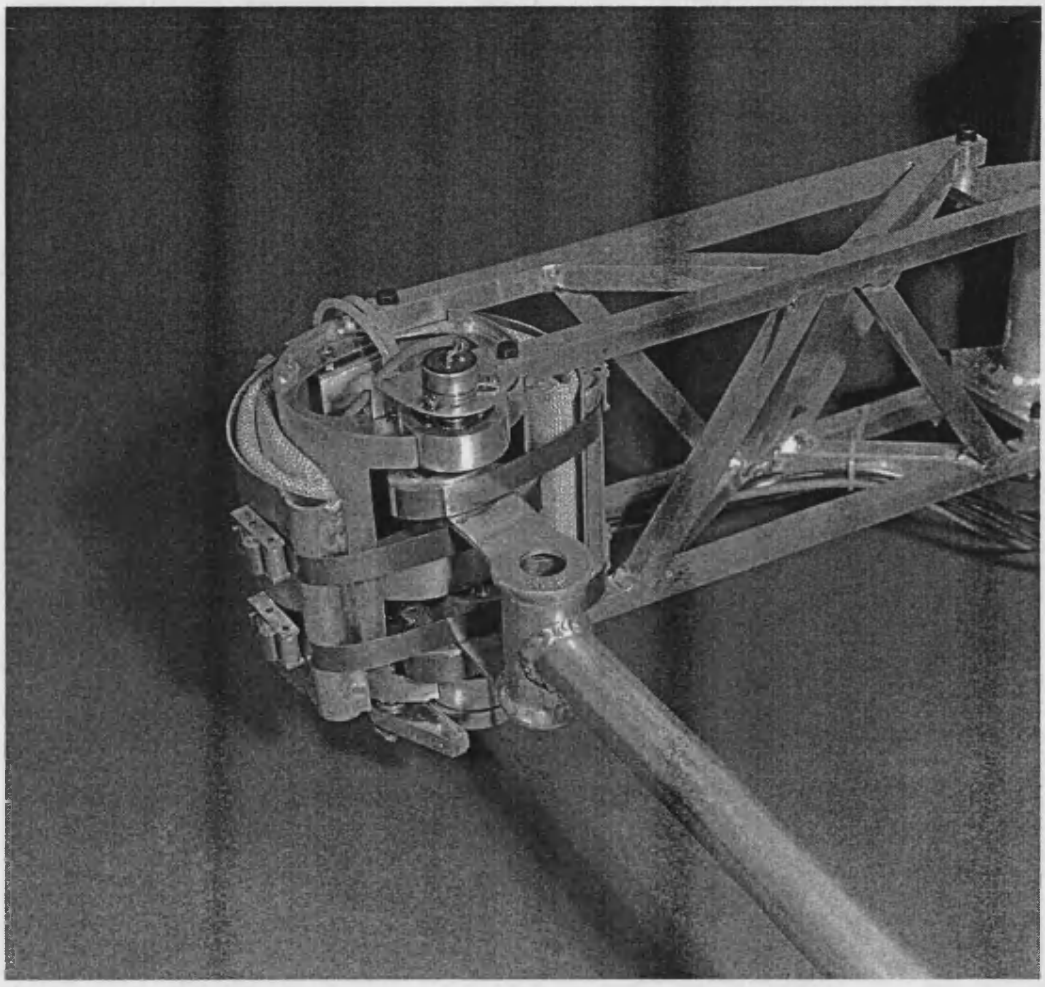

Figure 4.4 High performance rotary actuator.

Key research areas therefore related to the goal of developing a robust low-cost horticultural manipulator using the flexible actuator described above. The objectives can be summarized as follows:

- To understand the kinematic characteristics of the flexible actuator, including static stiffness, with respect to variations in output torque with stroke and sources of hysteresis.

- To devise novel mechanical designs for a pneumatic rotary robotic joint based on an understanding of its kinematic characteristics .

- To develop control strategies which meet adequate performance for horticultural applications.

- To understand the dynamic characteristics of pneumatic servo positioning systems in general and those utilizing the flexible actuator in particular through computer simulation with a view to providing a design tool.

- To demonstrate the effectiveness of the design and control strategies through the construction and evaluation of a demonstration system.

5 Mechanical Design

In this Chapter the kinematic characteristics of the pneumatic rotary actuator are analysed. The results of this analysis are then used to help develop a robot joint that meets the needs of the application. Two such joints are then linked to form a two degree of freedom manipulator.

To date the basic actuator, illustrated in Figure 4.3, has only been used in applications which demand relatively low dynamic performance and accuracy. These include puppetry animation for which position control was open-loop, and a wheelchair mounted manipulator. The latter was developed into two versions. The original version [Hennequin, 1990] was based on actuators of the type illustrated in Figure 4.3 and used open loop control. In the second version Prior et al (1993) developed a crude form of closed loop control for a similar manipulator, but did not report the performance achieved. The objectives of the work described in this Chapter were as follows:

- To modify actuator output characteristic to give a constant output torque throughout its stroke.

- To minimise bladder distortion induced hysteresis.

- To maximise power density in terms of both weight and bulk.

- To show how actuators can be linked to form a robot manipulator

These have been achieved through a combination of theoretical analysis, experimentation and innovative design. The work was also covered in references Tillett (1993b) and Tillett et al. (1994).

5.1 Actuator theoretical characteristics

The torque generated by the basic actuator as depicted in Figure 5.1 was the product of the tension in the webbing (F) and the radius of the inner roller (r). In the basic actuator the radius was constant, but the tension reduced with the degree of inflation. The mechanism for this was a reduction in the contact area between the bladder and the outer cylinder. As the bladder inflated, it attempted to straighten and form a circular cross-section tube. The reduction in contact area was therefore both along its length and across its width. Inspection showed that regardless of bladder hose length and over a limited stroke, webbing between the bladder and inner roller remained substantially parallel to the axis of symmetry, that is vertical as shown in Figure 5.1. Assuming that webbing tension acted in this direction over the normal working range of movement simplifies analysis and should not lead to large errors.

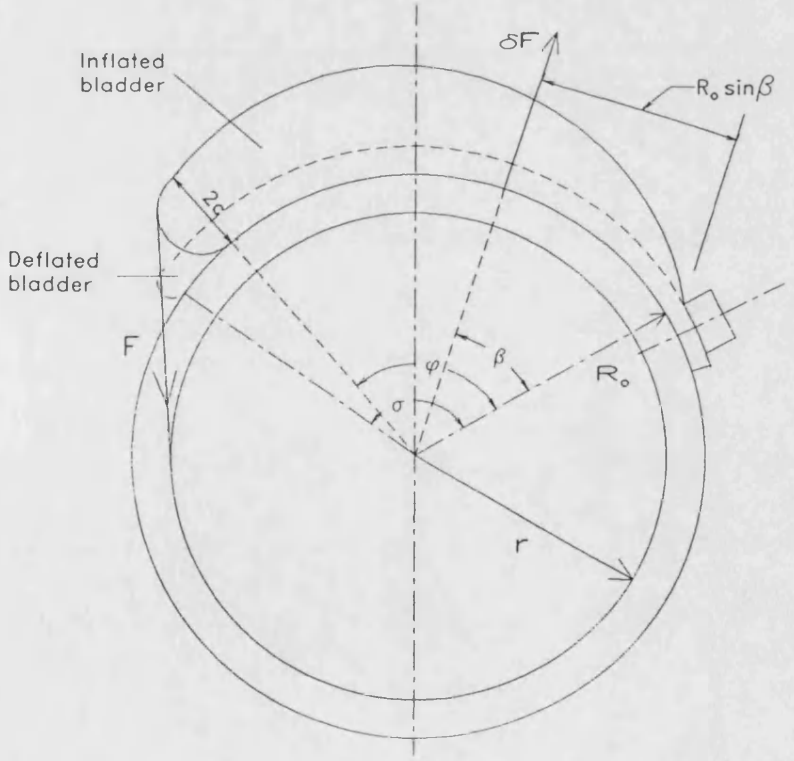

Figure 5.1 Forces on webbing and bladder

Considering the bladder and webbing as a free body and taking moments M_c about the clamp:

$$M_c = F\,2R_o \cos\left(\frac{\pi - \sigma}{2}\right) = \int_o^{\phi} R_o \sin\beta\ \delta f \qquad (5.1)$$

$$\text{Also}\quad \delta f = P W R_o\, \delta\beta \qquad (5.2)$$

where δf element of reaction force between bladder and cylinder.

F webbing tension

P pressure

R_o outer radius

W contact width

β angle from clamp

ϕ angle from clamp to break away point

σ wrap round angle when deflated

The bladder hose was fabricated in a braided synthetic material with a neoprene lining, and its wall was regarded as inextensible. It is shown later that the bladder wall does stretch under inflation, but the assumption made here is reasonable, since it does not have a significant effect on overall geometry.

$$\text{Hose perimeter} = 2\pi R_b = 2W + c\pi \qquad (5.3)$$

where R_b = radius of the fully inflated bladder

c = single thickness of a partially inflated bladder

It was assumed that c and therefore W were constant along the length of the bladder. Inspection of Figure 5.1 shows this not to be the case. Fortunately the largest variation in thickness occurs between the centre of the bladder and its clamp where the radius of action is small and so the assumption is thought not to incur large errors.

Considering the unclamped end of the bladder and regarding the mechanism of bladder straightening as being one of unrolling away from the outer tube then:

$$\text{Change in contact length} = c\pi = R_o(\sigma - \phi) \tag{5.4}$$

To convert webbing tension to actuator output torque T:

$$T = F.r \tag{5.5}$$

where r = inner roller radius

Rearranging and combining Equations (5.1) to (5.5) we obtain.

$$T = \frac{PR_o r}{2\cos\left(\frac{\pi - \sigma}{2}\right)} \left(\pi R_b - R_o\left(\frac{\sigma - \phi}{2}\right)\right) (1 - \cos\phi) \tag{5.6}$$

It has been determined experimentally that there is a constant ratio of $1:1.3R_o/r$ between contact angle ϕ and the actuator output angle for the geometry used in this experimental and theoretical work. The calculated variation of torque with actuator angle is presented graphically in Figure 5.2. It can be seen that as an approximation torque was expected to reduce linearly with rotation. Referring back to Equation (5.6) this reduction had two components. The first $(1 - \cos\phi)$ was due to a reduction of contact length. The second $(\pi R_b - R_o(\sigma - \phi)/2)$, was due to a reduction in contact width and can be minimized by increasing bladder radius or width in relation to outer radius. Comparison with experimentally derived data on the same graph reveal a generally good correlation but show that considerable hysteresis was present in practice. The experimental data was obtained using the basic actuator depicted in Figure 4.3 using only one of the two bladders to provide single acting motion.

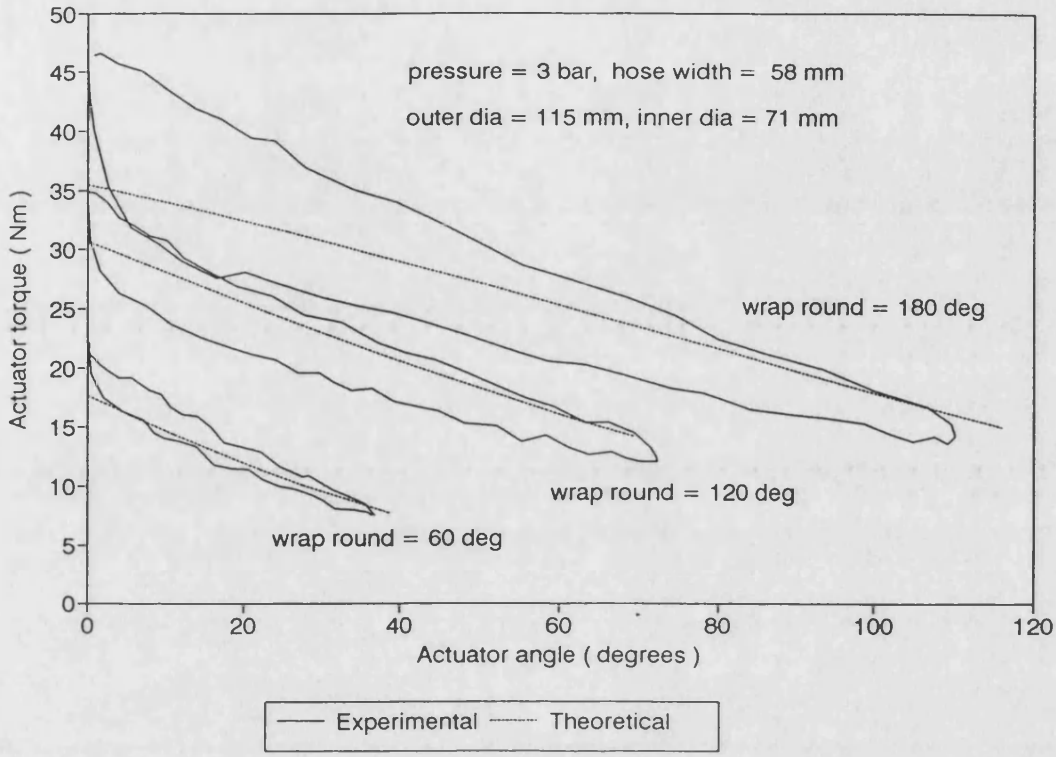

Figure 5.2 Experimental and theoretical torque vs displacement characteristics of basic single acting actuator of the type depicted in Figure 4.3

5.2 Experimental investigation of sources of hysteresis

5.2.1 Inflatable element

Experimental measurements described above have revealed that the basic flexible actuator exhibits considerable hysteresis which made dynamic control difficult. There were a number of factors contributing to the hysteresis. The first was sliding motion between the bladder and outer cylinder. For small bladder wrap round angles σ, typically less than 120°, the bladder stayed in direct contact with the cylinder over its full contact length. As the bladder inflated and straightened it rolled away from the

cylinder without sliding motion. For larger wrap round angles kinks developed in the bladder as it inflated causing sliding motion between bladder and cylinder as illustrated in Figure 5.3. The resulting friction absorbs energy leading to hysteresis and wear. With cos $((\pi-\sigma)/2)$ as a denominator in Equation (5.6) increasing wrap round angle clearly increases the available torque for a given actuator size. However, as discussed above and illustrated by the experimental results in Figure 5.2, hysteresis increases disproportionately with wrap round angle and so some compromise must be sought. It has been shown that sliding between bladder and outer tube can be minimised by restricting the angle that the fully collapsed bladder subtends when wrapped around the outer tube to less than 120° [Tillett, 1993b].

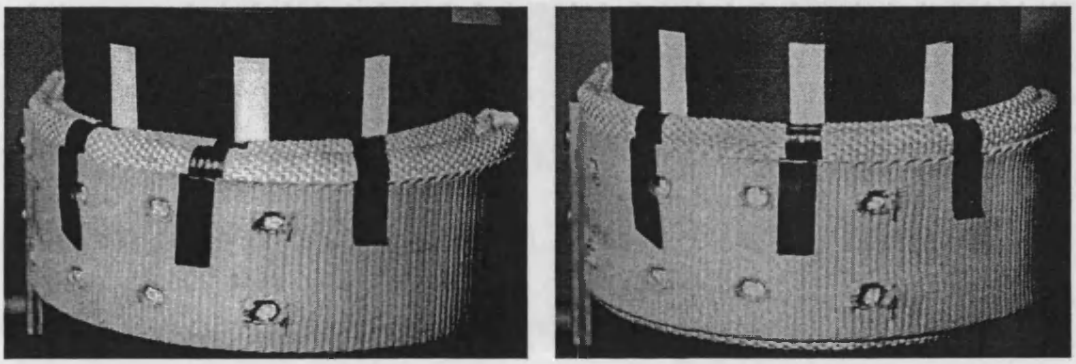

Figure 5.3 Illustration using tape markers of slip between webbing, bladder and cylinder during the inflation of an actuator with an 180° wrap round angle when deflated

In order to investigate further sources of hysteresis and to develop techniques for minimising them, the single-acting experimental rig illustrated by Figure 5.4 was constructed. This rig used a deflecting roller to prevent the webbing fouling the outer cylinder over a range of inner roller diameters and strokes. A further advantage of the deflecting roller was that the webbing angle as it left the bladder remained constant, so that the earlier analysis remains valid. Angular displacement was monitored by a rotary potentiometer connected directly to the output shaft, and torque was measured by a load cell connected to the output arm and held perpendicular to it. A constant supply pressure was maintained during rotation by connecting the hose to a pressure vessel of very much larger volume.

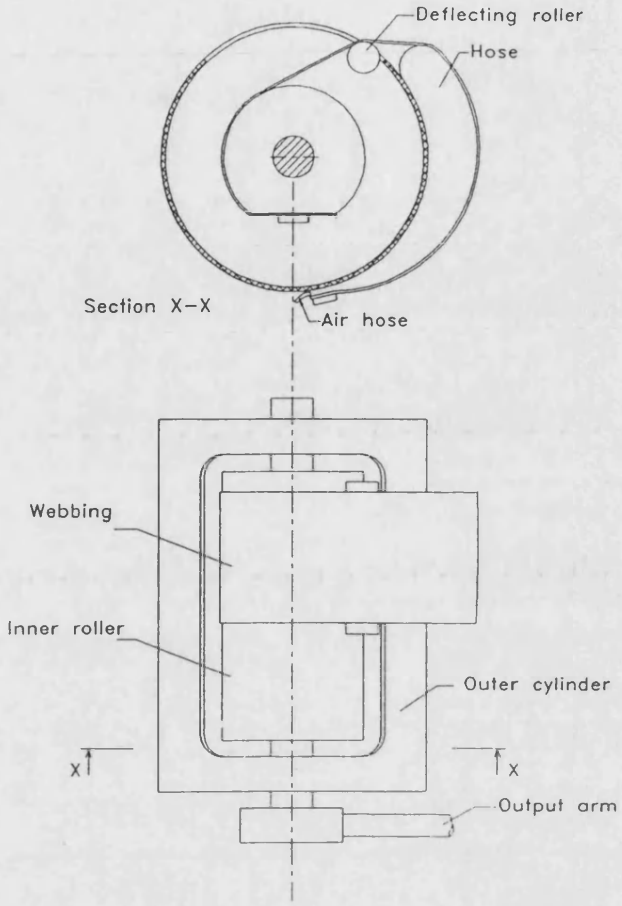

Figure 5.4 Single acting experimental rig with deflecting roller

An important contributor to hysteresis was the woven synthetic hose material with its neoprene lining from which the bladder was constructed. Tension tests on a sample of hose material gave an elastic modulus of approximately 700 MN/m^2 in the working range of tension, and showed some hysteresis (Figure 5.5). Both hysteresis and elastic deformation were undesirable characteristics and due in part at least to the nature of the woven fabric hose covering. The tension tests indicated that the magnitude of the hysteresis was not dependent on load. The effects of hysteresis are therefore minimised if the actuators are operated at higher pressures making hysteresis relatively less significant. This result was confirmed experimentally in Figure 5.6.

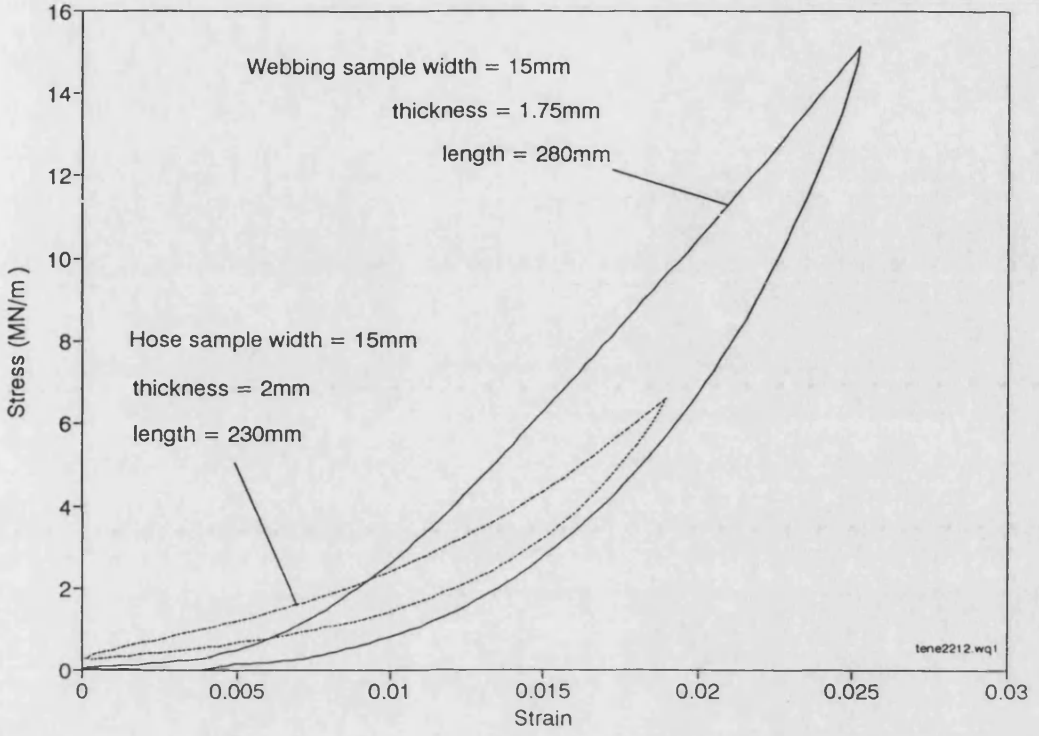

Figure 5.5 Tension vs displacement tests on bladder and webbing material samples

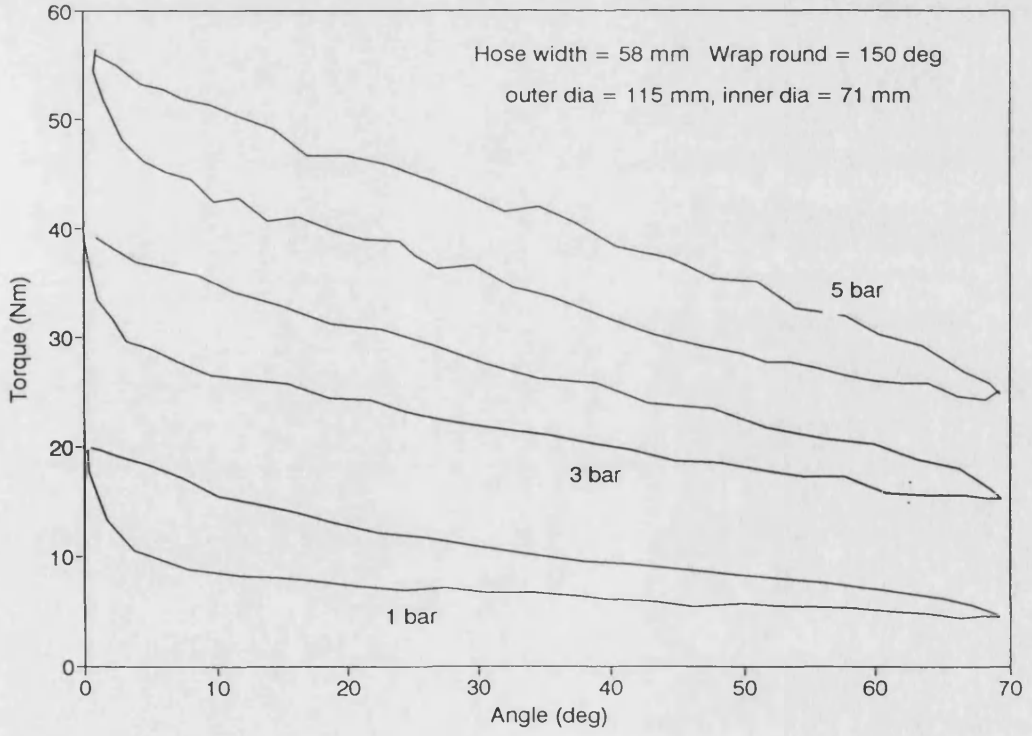

Figure 5.6 Effect of system pressures on torque vs displacement hysteresis characteristic

Alternative materials with improved properties were not readily available, and so techniques for minimising undesirable effects had to be sought. It was suspected that the kinks caused by folding the hose back on itself might contribute to friction during inflation. A single-thickness bladder was therefore constructed by sealing the two open ends with clamps which were pre-formed to the outer radius of the actuator. The bladder was then clamped to the outer cylinder perpendicular to its normal orientation so that the cylinder and the bladder axes were parallel. Webbing was then passed over the bladder and connected to the inner roller in the normal way. Air entered the bladder via a tube fixed by one of the end clamps. The results of the tests, which are illustrated in Figure 5.7, showed no reduction in hysteresis compared to the standard configuration given in Figure 5.6. Some fluctuation in measured torque in these and other figures can be explained by unsteadiness in holding the load cell by hand. These fluctuations are small in comparison to the movements and forces being measured. These results suggested that folding the hose back on itself did not increase hysteresis and since this provides the mechanically most convenient means of clamping and sealing, its use was continued. Should other factors change, such as a requirement for long slender actuators, then this alternative geometry has been shown to be feasible.

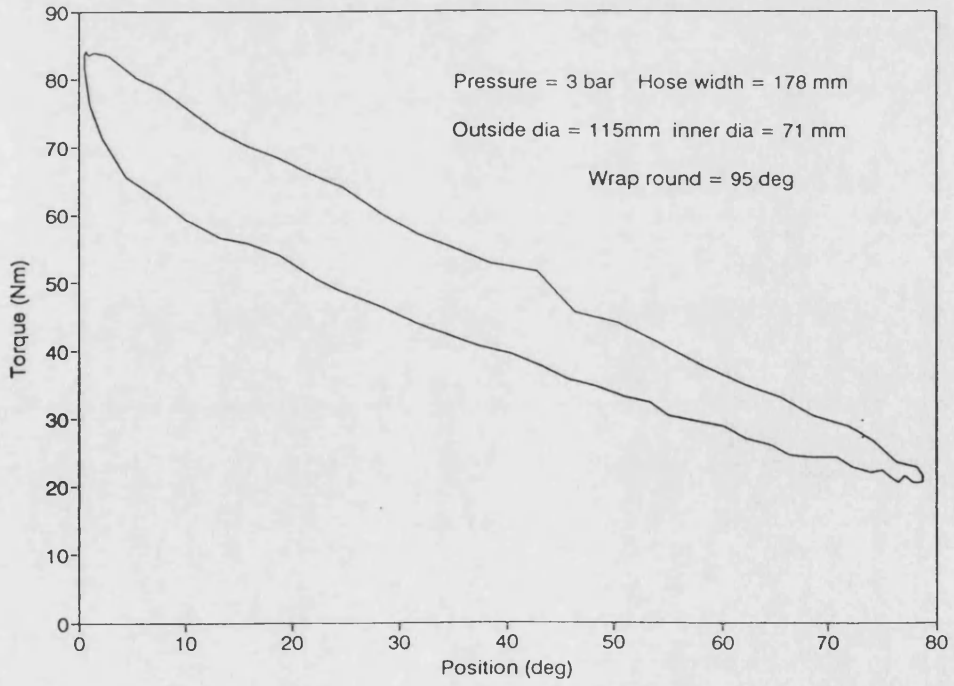

Figure 5.7 Torque vs displacement characteristic of a bladder fabricated from a single thickness of hose and restrained by polyester webbing

Hysteresis in the bladder only occurred when the material was distorted. One way of minimising hysteresis was to limit distortion to that which was required to provide actuator movement. As the bladder inflated, in addition to providing circumferential movement, the outer surface of the bladder swelled up and became rounded. In order to limit this distortion, a 1.5 mm thick aluminium plate was placed between the bladder and webbing. The plate, which was approximately pre-formed to the curvature of the bladder around the tube, was held in place by friction. The function of the plate was therefore to keep the outer cross-section of the bladder flat, but not to transmit tension or to modify circumferential profile. The results of comparative tests with and without the plate are given in Figure 5.8. This shows a small reduction in hysteresis with the plate in place. It had been suggested that this reduction might be due, at least in part, to a reduction in friction between the two surfaces. To test this hypothesis the test was repeated replacing the aluminium sheet with two layers of polythene sheet. The polythene reduced friction and would have indicated if this was a factor. The results did not show a noticeable reduction in hysteresis and so friction at the webbing interface was thought not to be a significant factor. This bore out earlier observations which indicated that for actuators of this geometry, there was no sliding movement between webbing and outer bladder surface.

A development from using a thin plate between the bladder and webbing was to constrain the bladder with a rigid outer shell. It had been noted that the circular profile of the bladder/webbing interface changed only slightly with actuator movement and so loads on the rigid outer shell could be expected to be relatively low. An advantage of the rigid outer shell was that it minimised the collapsed volume of the bladder so that as much as possible of the total volume was used as swept volume. This has a beneficial impact on dynamic performance. For the single-acting experimental rig, a rigid outer shell was constructed in aluminium with a radius equal to that of the fully collapsed bladder. The shell which now transmitted tension had a simple webbing hinge attached to the bladder clamp. The free end could then be attached to the inner roller by any flexible tension transmitting material. This did not need to be the full width of the bladder.

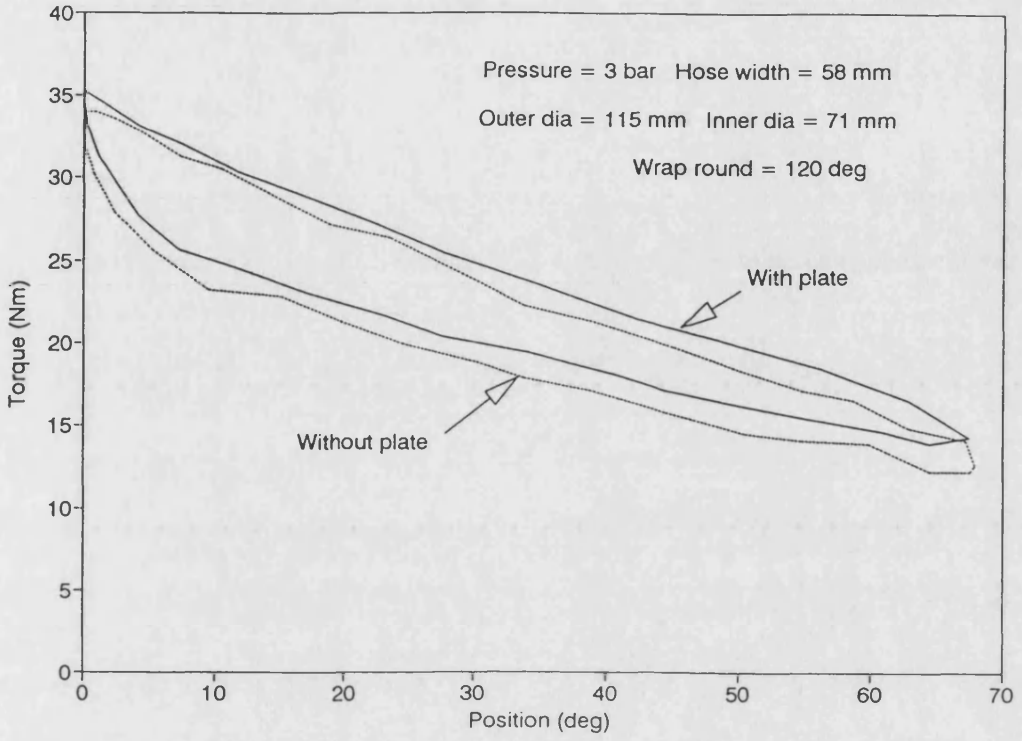

Figure 5.8 Torque vs displacement characteristic with and without a thin aluminium plate between the bladder and polyester webbing

5.2.2 Connecting strap

Another source of hysteresis was from the strap connecting the bladder to the inner roller. Tension tests on the webbing used in the basic actuator revealed some hysteresis and an elastic modulus of approximately 800 MN/m^2 (Figure 5.5). The hysteresis and relatively low modulus were thought to be due to the woven nature of the webbing, in which fibres straighten and slide over one another as they were put under tension. In order to establish what portion of total hysteresis was due to the webbing connecting strap a sample of the material was loaded in an equivalent way to that which it would experience as part of an actuator. The area enclosed in a graphical representation of the force vs displacement cycle represents the work done due to hysteresis which can be compared to that found for the actuator as a whole. This analysis indicated that webbing

hysteresis probably only accounted for a small part (typically <20%) of total actuator hysteresis. However elastic deformation also reduced output stroke. Comparison of webbing stretch with its total linear movement over the normal connecting strap tension and movement range indicated that output stroke was reduced by as much as 10%. This had the further effect of distorting the bladder material where bladder and webbing were in contact.

Looking at alternatives to the webbing, high modulus materials were sought which had their fibres well aligned, so as to minimise internal friction as they came under tension. A plain woven polyaramid (Kevlar) 220 g/m^2 laminating cloth was folded to provide a four-ply web with one weave parallel to the applied tension. The results which were taken with and without the thin aluminium plate, are given in Figure 5.9. This indicates that the Kevlar webbing was marginally superior to the conventional webbing and again showed the value of the aluminium plate.

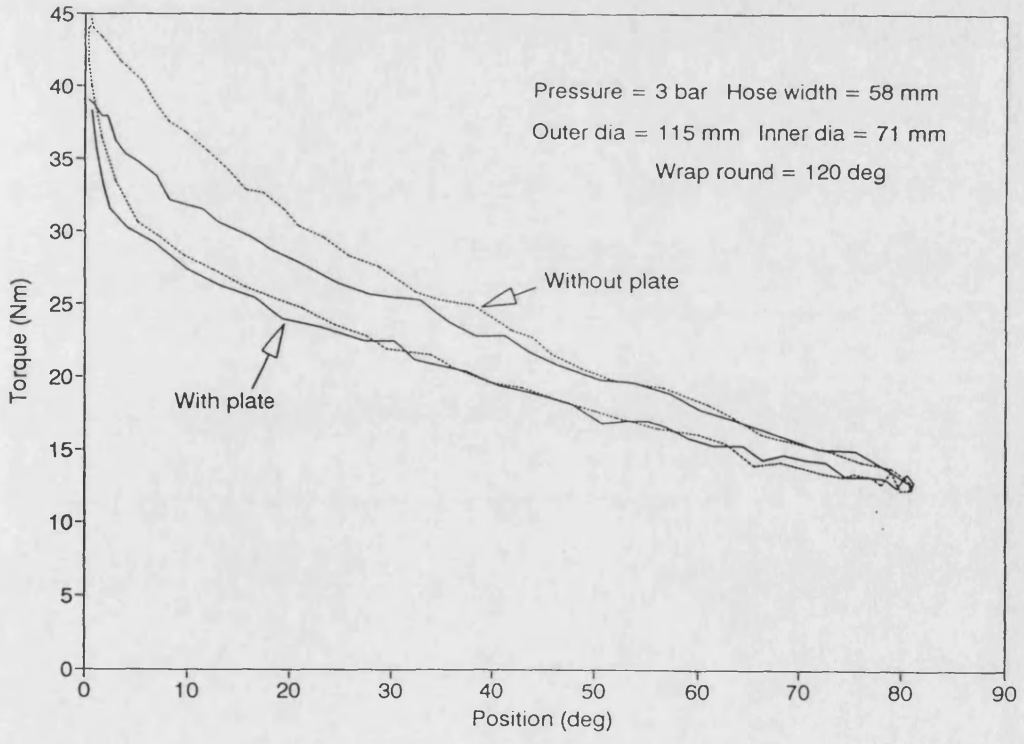

Figure 5.9 Torque vs displacement characteristic with and without a thin aluminium plate between the bladder and Kevlar webbing

Several types of wire and rope were tested in conjunction with the rigid outer shell. It was noted that multiple strands of thinner materials gave less hysteresis. This may be explained by distortion caused as the material was forced to pass under considerable tension over the 15 mm diameter deflecting roller. Thinner materials distort less and so create less hysteresis. With this in mind, thin strips of flexible steel sheet were tried as an alternative to webbing or rope. High yield T301 sheet steel 0.1 mm thick by 46 mm wide was used in conjunction with the solid outer shell. The results illustrated in Figure 5.10 gave less hysteresis (approximately +/- 4% at 300 kPa) than any previous tests. This result contrasted with the hysteresis of approximately +/- 10% revealed in tests with the polyester webbing alone, illustrated in Figure 5.8. The high yield strength of the material, which was established to be 1.8 GN/m^2 in tensile tests provides a high degree of design flexibility. The material did not show any signs of permanent bending where it passed over the deflecting rollers.

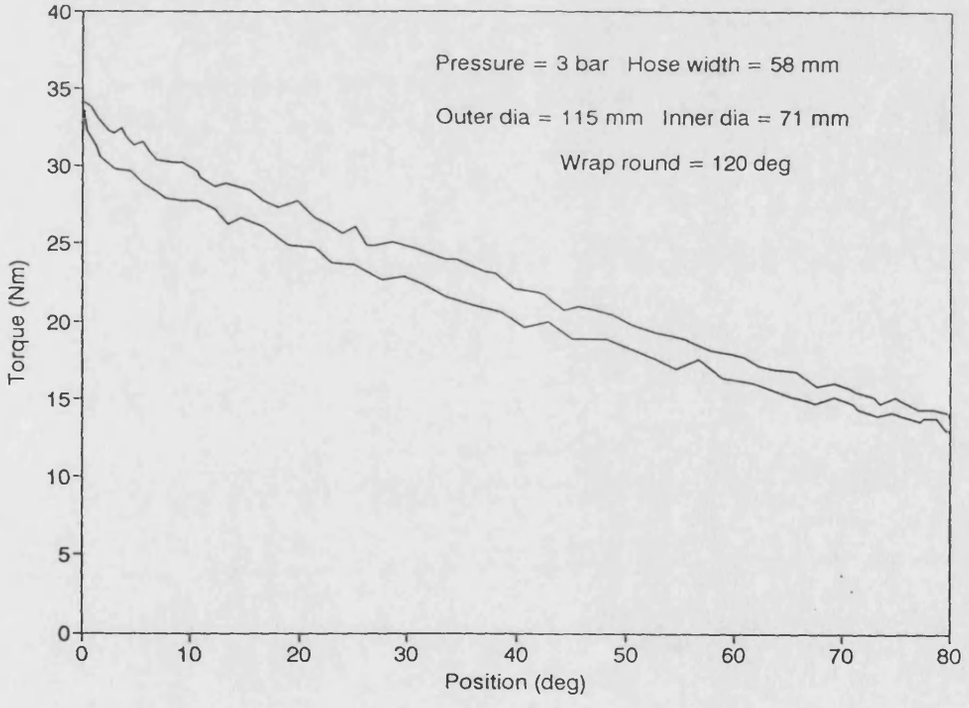

Figure 5.10 Torque vs displacement characteristic with solid outer shell and 0.1 mm thick steel connecting strap

5.3 Robot joint design

5.3.1 Linearity

The relationship between torque and displacement was determined by the ratio of inner roller to outer cylinder diameter. It was proposed that by replacing the circular section inner roller with a cam, it would be possible to further modify the torque-displacement characteristic. Mills (1993) pointed out that since the output torque or force from actuators using flexible inflatable elements[4] varies with position, it is normally necessary to vary pressure to compensate. Changing pressure also affects actuator stiffness and so stiffness in such actuators varies with position. Cam compensation allows the output torque to be modified so that it remains constant over the working stroke. Thus stiffness will not vary with position but could be controlled independently by altering other parameters such as supply pressure. The option to vary stiffness in this way has not been explored in this thesis, and supply pressure remained constant for the experiments reported here. Cam compensation to provide constant output torque also simplifies the position-control algorithm. The desired cam profile was derived using a graphical technique from the torque displacement relationship (Figure 5.11). The basis of the technique was to relate the position of the outer shell to the tension in the material connecting shell to cam. For each shell-position/tensile-force a cam radius could be calculated. The position of the shell and the cam radius define the line along which the connecting material must act. The problem was then to relate this series of lines to cam output angles.

---

[4]He was referring to the McKibben type of flexible inflatable actuator. In this device a rubber tube covered by a diagonally woven fabric sleeve contracts longitudinally as the rubber tube inflates and expands radially.

Where the relationship between force and outer shell displacement was simple, it would have been possible to integrate over the range of movement to derive an expression between cam angle and shell position as required. In this case figures were substituted into Equation 5.6 and the work done for small increments of movement calculated. Cam radii and displacements were then derived by a process of crude numeric integration as illustrated in Table 5.1. A graphical technique was then used to plot the cam from this data as illustrated in Figure 5.11. The same process could be applied to experimentally derived torque vs. displacement data.

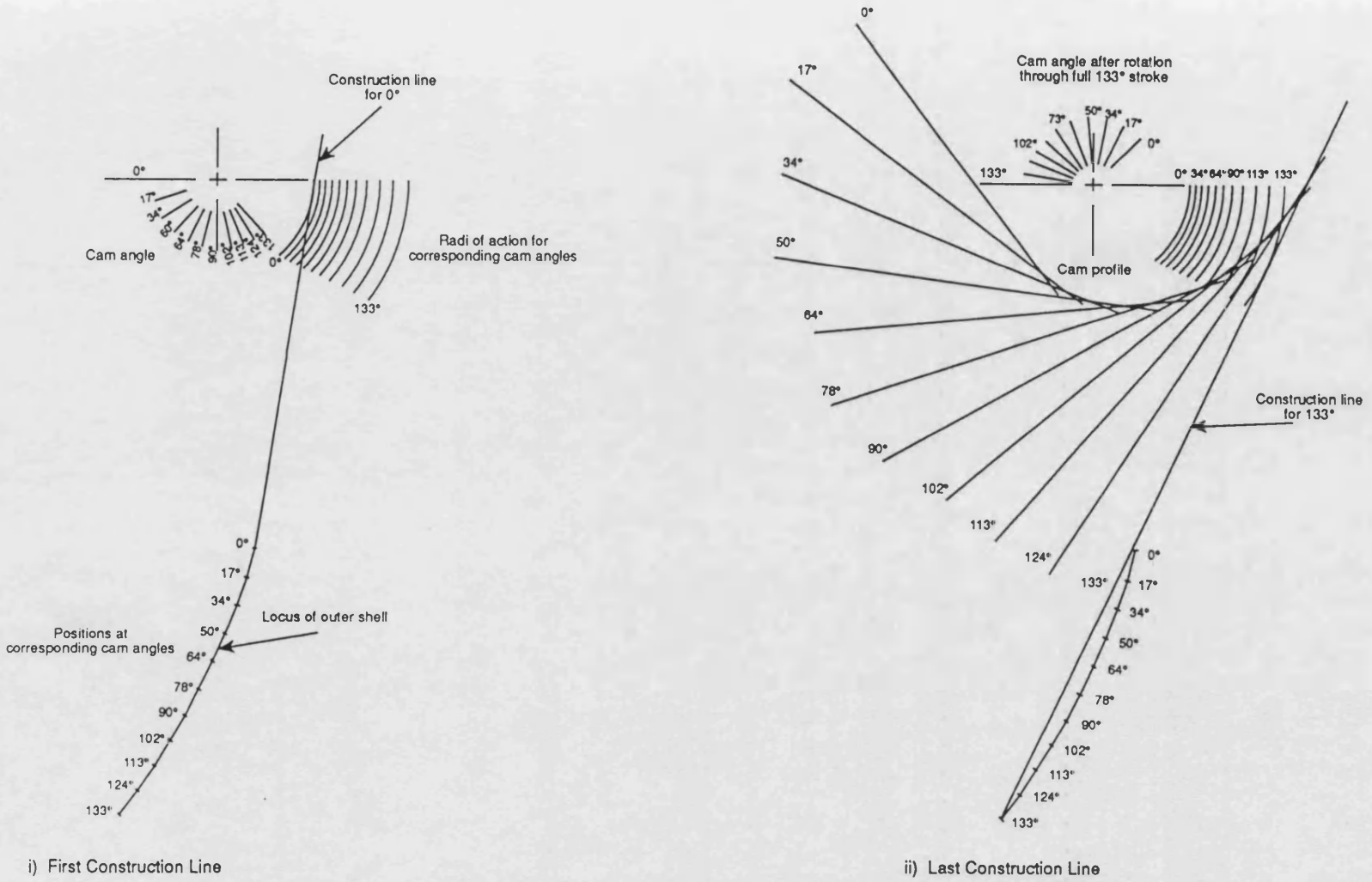

Figure 5.11 Graphical representation of cam plotting procedure.

A = cos((pie-g)/2) B = pie*Rh(1-cosa) C = R(g-a)/(2*pie*a)
D = sina-a*cosa Z = (B-C*D)/A

a = angle of contact from clamp ϕ
g = hose wrap round angle σ

pressure	width	out rad R	in rad r	Rh	angle g	PRr/2
500000	0.16	0.0762	0.026	0.050955	2.094	495.3

Work done = torque (T) * change in angle (b)
Average torque (AT) = sum of work done / total stroke
move (m) = linear movement = b * r * pie / 180
Force (F) = webb tension = T / r
Crad = desired cam radius = AT / F
Cam angle = output angle = sum of: [change in m / average Crad]

angle (g)	angle (a)	A	B	C	D	Z	angle (b)	torque (T)	Work done	move(m)	Force(F)	Crad	Cam angl	Cam deg	Output Torque
2.094	2.094	0.866325	0.239945	0	1.499658	0.276969	0	137.1828	0	0	5276.263	0.019451	0	0	102.6275
2.094	2.0312	0.866325	0.23109	0.002393	1.44431	0.262758	13.32	130.1441	1780.397	0.006041	5005.541	0.020503	0.302419	17.33612	102.6275
2.094	1.9684	0.866325	0.221954	0.004785	1.38721	0.248539	26.64	123.1013	1686.614	0.012083	4734.665	0.021676	0.588885	33.75773	102.6275
2.094	1.9056	0.866325	0.212573	0.007178	1.328584	0.234366	39.96	116.0813	1592.956	0.018124	4464.666	0.022987	0.85942	49.26609	102.6275
2.094	1.8428	0.866325	0.202986	0.009571	1.268662	0.220291	53.28	109.1104	1499.777	0.024165	4196.552	0.024455	1.114105	63.86587	102.6275
2.094	1.78	0.866325	0.193229	0.011963	1.207681	0.206367	66.6	102.2137	1407.418	0.030207	3931.295	0.026105	1.35308	77.56511	102.6275
2.094	1.7172	0.866325	0.183341	0.014356	1.145881	0.192642	79.92	95.41565	1316.211	0.036248	3669.833	0.027965	1.576543	90.37506	102.6275
2.094	1.6544	0.866325	0.173361	0.016749	1.083506	0.179163	93.24	88.73961	1226.474	0.04229	3413.062	0.030069	1.784743	102.3101	102.6275
2.094	1.5916	0.866325	0.163328	0.019141	1.020802	0.165976	106.56	82.2077	1138.509	0.048331	3161.835	0.032458	1.977982	113.3875	102.6275
2.094	1.5288	0.866325	0.153283	0.021534	0.958016	0.153121	119.88	75.84085	1052.603	0.054372	2916.956	0.035183	2.156611	123.6274	102.6275
2.094	1.466	0.866325	0.143263	0.023927	0.895395	0.140639	133.2	69.65866	969.0267	0.060414	2679.179	0.038306	2.321027	133.0525	102.6275
								Average torque (AT)	102.6275						

Table 5.1 Theoretical calculation of flexible actuator characteristics for cam design using Eqn. 5.6.

5.3.2 Joint geometry and construction

An important overall objective of this work was to produce a manipulator with adequate performance for horticultural applications, but at a lower cost than existing precision industrial robots. Simplicity and tolerance to misalignment in assembly were therefore important goals in mechanical design.

Dynamic performance is affected by component weight and becomes increasingly critical with distance from the main axis. Materials have for this reason been selected from aluminium alloys and plastics with steel only used in highly stressed components such as main shafts. Stress analysis has been elementary and restricted to manual calculations. Opportunities should therefore exist to reduce weights further through more sophisticated analysis.

In this and most other applications it was desirable to make the manipulator and therefore its joints as compact as possible. To this end, it was decided to mount the opposing bladders back to back as illustrated in Figure 5.12. Solid outer shells have been used with two connecting steel strips interleaved from each side. Careful selection of steel strip length ensured that the bladder itself started to be compressed before the output arm reached its mechanical limit, thus providing a safety bump stop. The strips themselves were terminated at self tightening roller clamps of the authors design which are light in weight and do not weaken the steel strip.

The simple technique of getting air into the bladders by inserting a pneumatic pipe proved unreliable, as the act of clamping often produced a restriction to the air flow which for reasons outlined in Chapter 6.3.1 is undesirable. In addition local compression of the bladder near to the pipe entry could result in further restrictions to flow. These undesirable effects were eliminated by using a manifold which ensured air entered along the full bladder width. The seal was made with a cyanoacrylate adhesive. The manifolds also provided neat entry points for the air supply and pressure tapping. Restrictions between the two halves of the bladder formed by the crease where the hose

material was folded back on itself were minimized by inserting an open flexible plastic mesh in the hose before it was folded to form the bladder. This provided an air path even if the bladder was fully compressed.

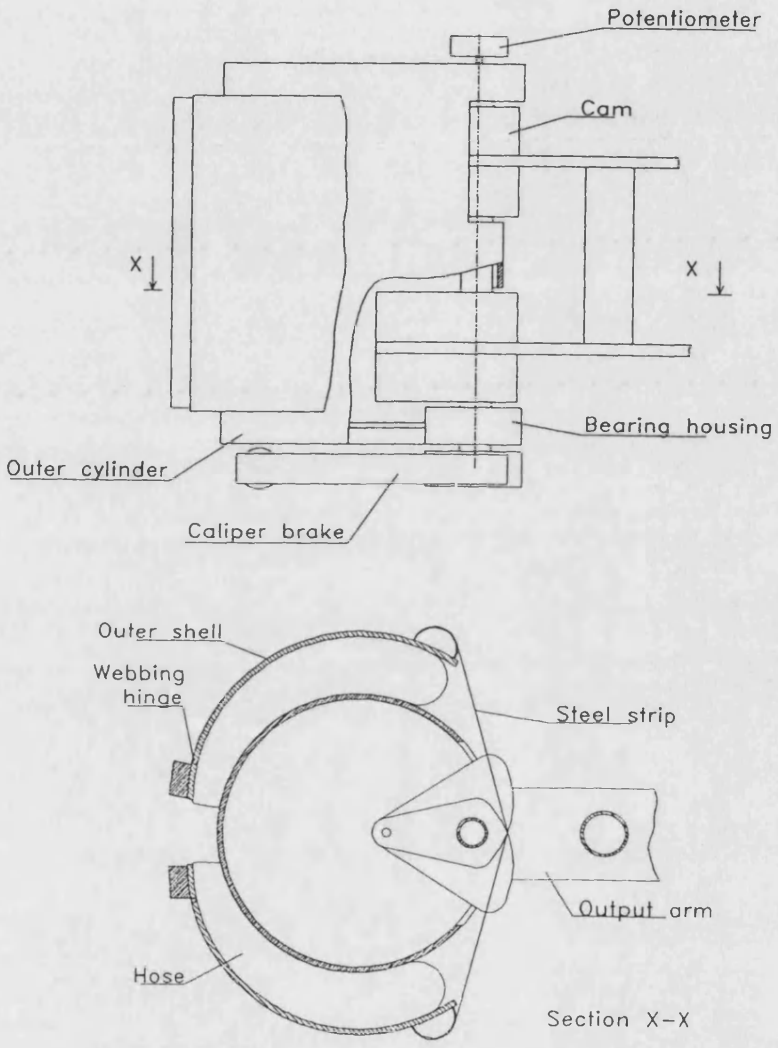

Figure 5.12 Schematic of the improved flexible actuator

The main output shaft axis was offset allowing the connecting steel strip to go directly from the outer shell to the cam. This eliminated the need for deflecting rollers, simplifying design, whilst eliminating one source of hysteresis and component wear. Having made this change, it would be possible to consider mounting the bladder on flat or curved plates on either side of the output shaft instead of round a tube. It has been

calculated that the torque-displacement characteristics would be acceptable. However, the outer cylinder arrangement has been retained as it is structurally superior.

The provision of an offset output shaft allowed the output arm to be connected directly to the cams. This simplified the design and reduced overall length. Torque was no longer transmitted through the shaft allowing significant weight reductions to be made. The assembly, which effectively combined the structure of the actuator with the mechanical requirements of the entire joint, is illustrated in Figure 5.12.

It was known that the addition of Coulomb friction to a system had a stabilising influence, though at the expense of other characteristics, as discussed in Chapter 7. Provision was therefore made for a brake on the output shaft which could be used in experiments, but removed easily if not required. A calliper type brake was designed which fitted on the underside of the joint and acted on an aluminium disk attached to an extension of the main output shaft (Figure 5.12). The callipers were held against the disk by a coil spring, though a small pneumatic actuator could be used and would allow easy adjustment of braking torque, even as part of a dynamic control algorithm. The nylon brake material acting on an aluminium disk was chosen for its ability to provide Coulomb friction with little stiction. A tension testing machine and simple spring loaded brake were used to measure the friction characteristics at a range of speeds which was limited by the experimental equipment. Typical results presented in Figure 5.13 show that there was relatively little stiction and that the coefficient of friction which apparently increases slightly with speed had a value of between 0.2 and 0.25 depending on the cleanliness of the surfaces.

The performance of servo potentiometers is affected by their mounting. In particular it is desirable to minimise loads on their bearings whilst maintaining a backlash free connection to the shaft whose position is being measured. A conventional solution is to use a universal joint, most commonly a helically wound metal or plastic connector, between the two shafts. Unfortunately this would increase overall robot joint height and so the potentiometer was connected directly to the output shaft but connected to the

body by a flexible mounting. The mounting illustrated in Figure 5.14, whilst not providing complete freedom in all five degrees-of-freedom did cope with a reasonable level of misalignment and did have the virtue of compactness.

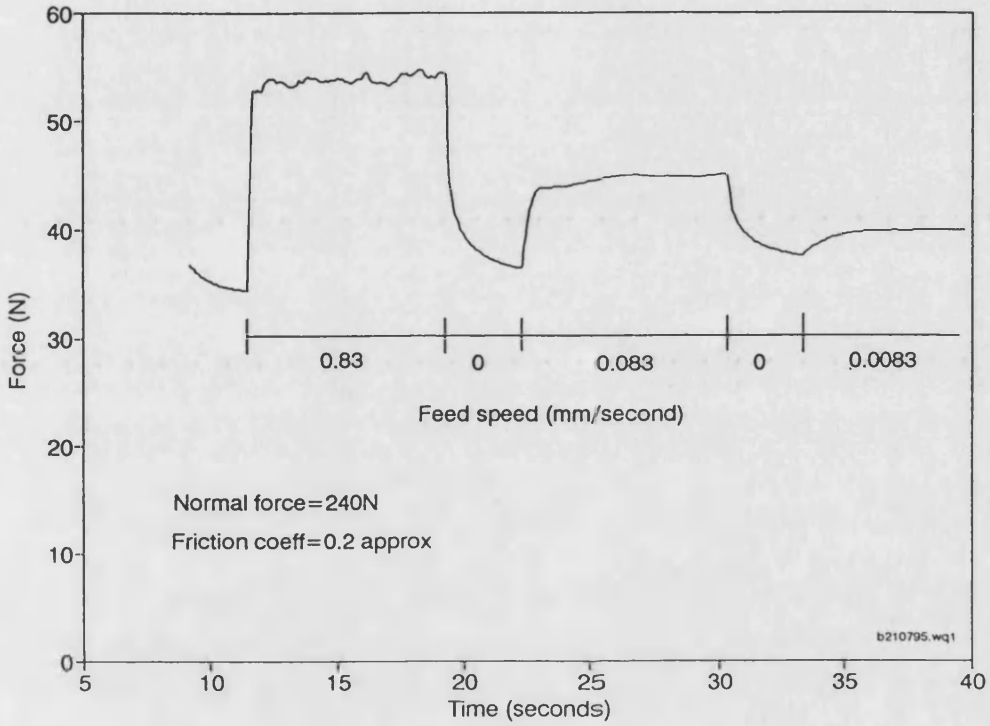

Figure 5.13 Nylon to aluminium friction at varying speed

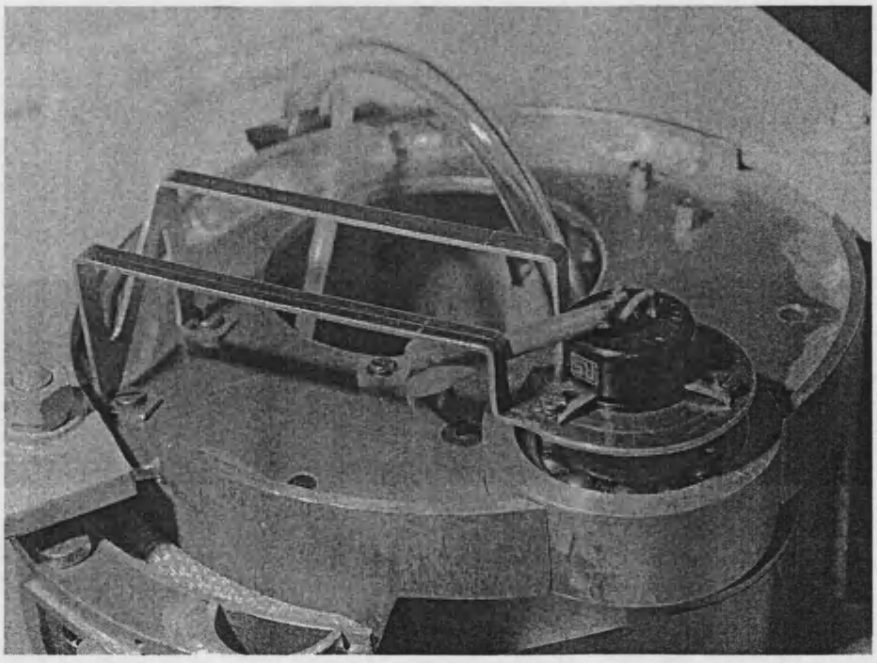

Figure 5.14 Potentiometer mounting

5.4 Robot joint static performance

Comparing the open-loop characteristics of a single bladder for a basic actuator as presented in Figure 5.2 with that of the improved actuator given in Figure 5.15 two notable differences became clear. Firstly cam compensation had resulted in a constant output torque with position. Secondly hysteresis had been reduced from approximately +/-12% to +/-3%. When the caliper brake was applied to the improved actuator, hysteresis was re-introduced as can be seen in Figure 5.16. The form of this Coulomb friction induced hysteresis was however different to that introduced by the distortion of bladder in Figure 5.2. In particular the characteristic was substantially vertical during changes of direction. This provided an improved damping effect as discussed in Chapter 7.

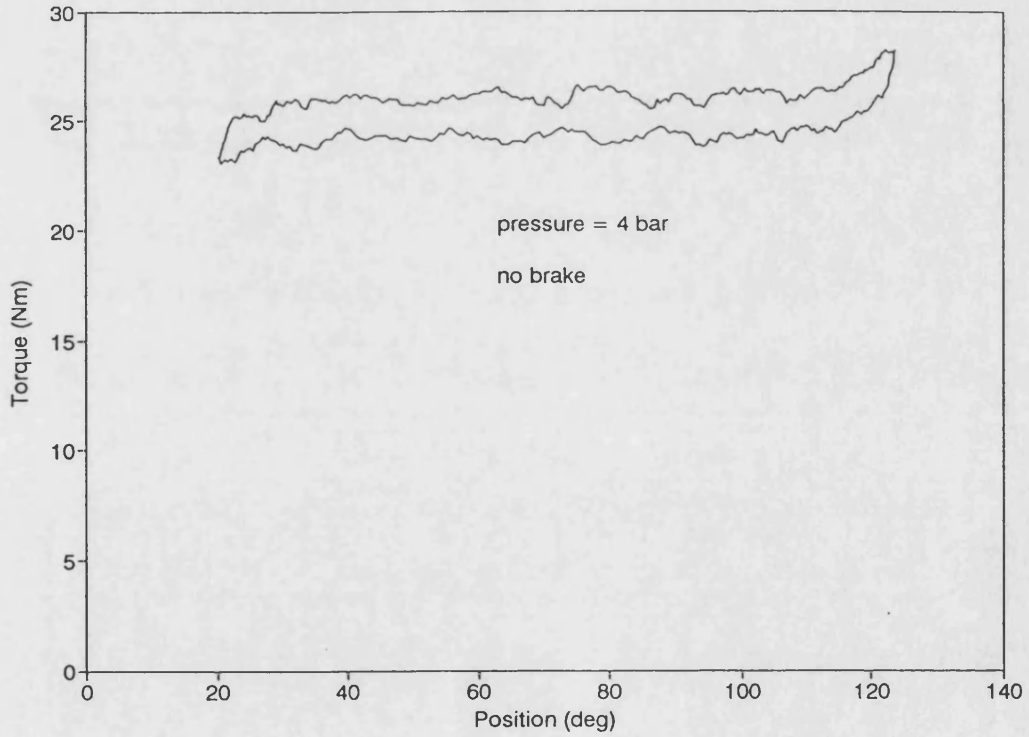

Figure 5.15 Torque vs displacement characteristic for the improved flexible actuator (axis 1) without the brake applied

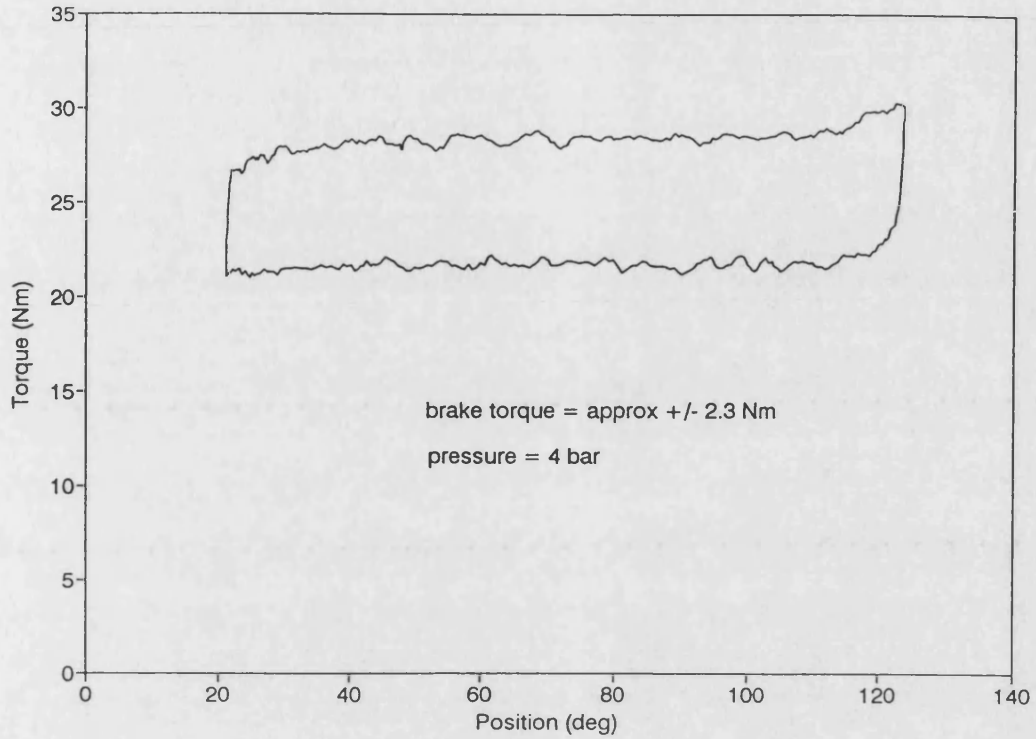

Figure 5.16 Torque vs displacement characteristic for the improved flexible actuator (axis 1) with the brake applied at approximately +/- 2.3 Nm

Two actuators have been constructed. The process of determining their size is covered in Chapter 5.5.2 In the larger joint 160 mm wide hose was wrapped 120° round a 152 mm diameter outer cylinder. It was 25 cm high, weighed 5.5 kg and had a 84 Nm output torque at 400 kPa. The smaller joint used 110 mm hose, wrapped 120° round a 102 mm cylinder. It was 18 cm high, weighed 2 kg and had a 27 Nm output torque at the same pressure. Typical output torque/joint mass can therefore expressed as approximately 35 Nm kg^{-1} per MPa of supply pressure. This compares favourably with other limited stroke rotary pneumatic actuators, for which typical figures are less than 10 Nm kg^{-1}.

5.5 Two degree-of-freedom manipulator

5.5.1 Manipulator geometry

The 0.773 m reach of the experimental manipulator was not critical but was chosen as representative of potential applications. This could have been achieved with a variety of combinations of joint stroke and link lengths. In designing the joints it was convenient to limit working stroke to 120 degrees though the mechanical limit was 140 degrees in order to alow for some overshoot. A range of link length ratios were examined. It can be seen from Figures 5.17a, 5.17b and 5.17c that a 1:1 ratio provides a larger and more compact working area than either 3:2 or 2:3 ratios. A 1:1 ratio using two 0.4 m links was chosen, though the shape of the working area could be modified to suit specific applications by altering this ratio. Repeatability in Cartesian coordinate terms was not uniform across the full working envelope, due to the polar geometry as discussed more fully in Chapter 8. It may therefore be advantageous to arrange for particularly critical operations to be done in higher resolution areas.

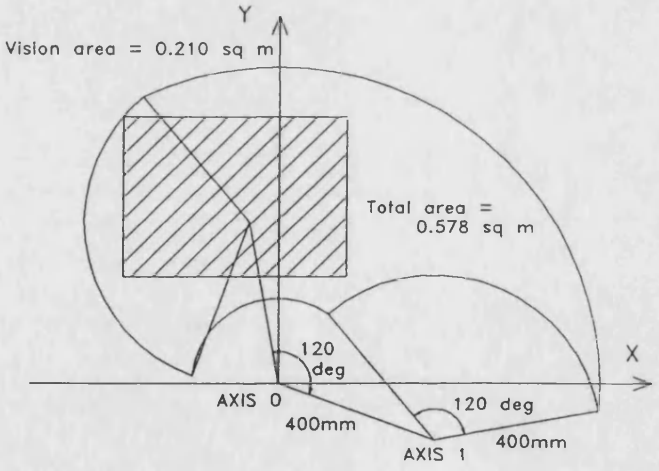

Figure 5.17a Manipulator working envelope for a reach of 0.77 m and a link length ratio of 1:1 with Cartesian co-ordinates and vision guided area (shaded) superimposed.

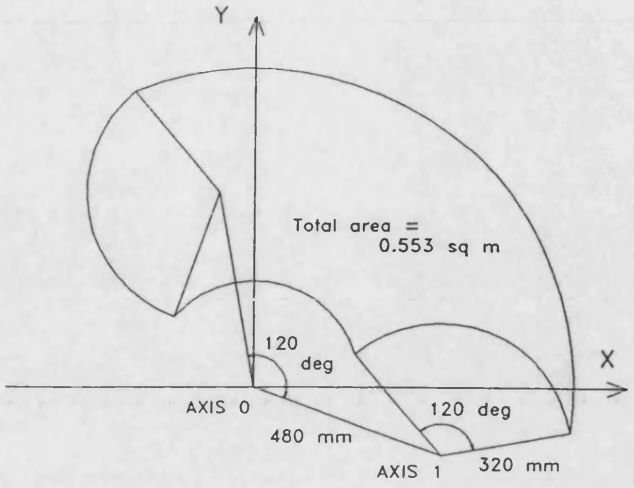

Figure 5.17b Manipulator working envelope for a reach of 0.77 m and a link length ratio of 3:2 with Cartesian coordinates superimposed.

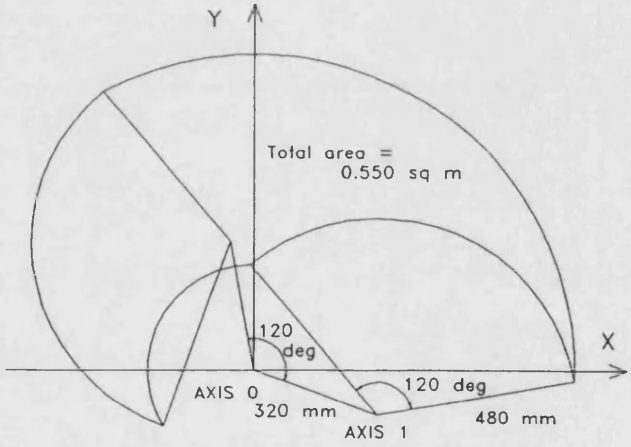

Figure 5.17c Manipulator working envelope for a reach of 0.773 m and a link length ratio of 2:3 with Cartesian coordinates superimposed.

5.5.2 Joint size

In designing a direct drive rotary pneumatic joint of any kind it is necessary to decide on the size expressed as a stroke and torque which in turn determines swept volume.

In this case stroke was determined by design and geometric constraints and the torque by the required dynamic performance based on experience with early experimental devices. At the time these decisions were made the results of the simulation were not available. It was assumed at the initial design stage that for a given level of dynamic performance, torque should be proportional to inertial load. Thus starting with the smaller joint the inertia of the payload, end-effector and second link were estimated as 0.2 kgm^2. An early 40 Nm output torque experimental device [Tillett, 1993b] achieved an adequate response with a 0.3 kgm^2 payload indicating that the required torque would be 27 Nm. Similarly the estimated inertial load on the larger joint was an average of 0.7 kgm^2 indicating a required torque of 93 Nm. In practice design figures of 28 Nm and 82 Nm were chosen after taking practical considerations such as available material sizes into account. It was also anticipated that overall performance would improve between the early and later devices.

Subsequent work in simulation, confirmed by practical experience, showed that the experimental joints perform adequately with payloads well in excess of that specified. This was consistent with the work of Mannetje (1981) who showed that for systems using pressure differential in the feedback loop, position controller gains for a given level of stability can be increased with increasing inertial loads. It follows from this that actuators should be as small as possible, limited by the minimum acceleration acceptable. For future designs sizing would be based on a combination of analysis and experiments in simulation.

Under circumstances in which air flow rate is a limiting factor, either through valve capacity, or the supply itself, it is possible to optimise joint sizes to maximise the rate of response. This can be achieved by developing an expression for cycle time, differentiating it once with respect to swept volume V, equating to zero for the minimum and rearranging to make V the subject. This could be used as a starting point for an assessment in simulation which could take into account dynamic factors such as settling times. However, in this case the valves used had maximum flow rates in excess of those required to provide the maximum desired output velocity.

5.5.3 Link arm design

Accuracy and dynamic stability are both dependant on the rigidity of the structure linking the joints and end-effector. The main objective was simply to produce a stiff and strong structure at minimum weight. A space frame was chosen to link the two joints and a simple tube to link the smaller joint to the end-effector as illustrated in Figure 5.18. Both linking techniques produced an adequate structure, though the tube was neater and would be preferred in a hygiene sensitive application. Stress analysis was limited to simple manual calculations and so it is likely that it would be possible to improve the design.. The weight of the complete manipulator including joints and links was 8.5 kg.

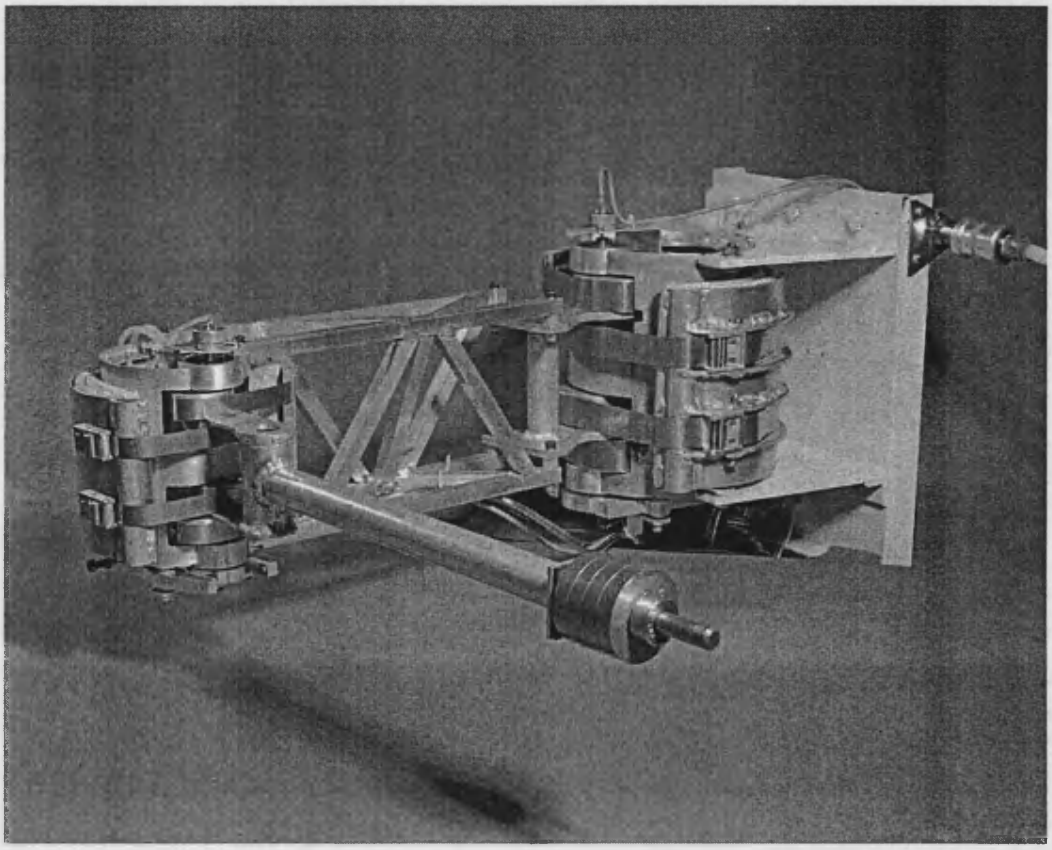

Figure 5.18 Two-axes manipulator with two 0.4 m long links equipped with weights to simulate a payload.

6 Closed-loop Control

For typical horticultural pick-and-place applications such as the demonstration to be described in Chapter 9 a point-to-point position controller is required. In this chapter previous work is reviewed and the implementation of the chosen strategy described. The dynamic performance of the joints is then evaluated experimentally. The objectives of the work described in this Chapter were as follows:

- To review previous relevant research in order to identify control strategies which are appropriate to the flexible actuator and that can be implemented on relatively low cost hardware.

- To develop a practical point-to-point position controller to test the feasibility of using flexible actuators with an outline specification for:
  i. A typical steady-state repeatability of about +/-0.1^0.
  ii. Settling time to be minimized (target time 1s).
  iii. A limited amount of overshoot acceptable.
  iv. Smooth movement, though no specific acceleration limits were set.

- To experimentally evaluate the control system as a whole for both a single joint and a two degree-of-freedom manipulator.

6.1 Review

Although there are important differences between conventional and flexible pneumatic actuators they both operate with the same compressible medium, which is a dominating factor in determining dynamic characteristics. It is likely then that similar control strategies will be appropriate for both types of actuator.

Work on the control of pneumatic actuators has been in progress since at least 1956

[Shearer, 1956; Burrows, 1969]. This review however is limited in scope and concentrates on examples of recent work utilizing digital controllers which could most easily be implemented with commercially available equipment. The aim was not therefore, at this stage, to build up a detailed understanding of the control theory, but more simply to gain a repertoire of control techniques that could be applied to the experimental actuator. A more in depth study leading to an optimised controller would be appropriate if the actuator is developed further. This may use the simulation results of Chapter 7.

One of the earliest microprocessor based controllers was developed by Pu and Weston (1988) at Loughborough University for industrial servo pneumatic drives. Their system used a 5 port flow control spool valve of the same type used in this thesis work. Cylinder output position was measured using encoders from which error, velocity and acceleration feedback terms were derived. Valve control signals were offset by bias values so that the effects of dead band were minimised. The polarity of the bias values depended on the sign of the position error and its magnitude, and were determined by a learning procedure. It was pointed out that the most important factor in determining dead band was the friction in the pneumatic sliding seals. Since friction sometimes varied with position the bias values were also varied. Unfortunately this type of friction is relatively unpredictable and so some error remained. This error was minimised with the addition of an integral term, though at some cost in settling time. The group also used gain-scheduling techniques to increase proportional gain as error reduced to increase system stiffness without adversely affecting stability. Positional accuracy of around 0.04 mm was claimed using these methods. To achieve the fast point-to-point movements required of the industrial situation three phases of control were utilized. The first held the valve fully open, the second fully closed and finally the modified proportional to error algorithm took over to gain precise placement.

A rare example of work on controllers for pneumatic cylinders in agriculture was reported by Street et al. (1990) and Frost et al. (1993) concerning robotic milking. Their control algorithm incorporated feedback of error, velocity, acceleration and error

integral. All these terms were derived using the signal from a potentiometer[5] feeding back actuator position. The algorithm ran within a 5 ms interrupt driven loop producing an output signal which was amplified and used to drive a five-port servo valve. Typical performance of one axis with a 1 m stroke was a maximum velocity of 1.15 m/s, an acceleration of 19 m/s^2, and a steady-state error of ± 2.4 mm.

A number of other researchers have investigated the control problems associated with pneumatic actuators. Amongst the most relevant is the work of Virvalo (1986), who designed a controller broadly similar to that of Street's. Liu and Bobrow (1988) and Mannetje (1981) have proposed controllers utilizing pressure feedback which they claim gave improved performance. Mannetje (1981) showed that system performance could be dramatically improved by the addition of pressure feedback, but that pressure gains were limited by wave propagation time delays. In cylinder based systems he considered that the delay would arise from the distance between valve and piston and between piston and pressure transducer. Using the expression for sonic velocity (λ):

$$\frac{\tau}{l} = \sqrt{\frac{\rho}{\lambda P}} \tag{6.1}$$

The delay results in a phase lag related to frequency:

$$\phi = \omega \tau \tag{6.2}$$

An advantage of the rotary flexible actuator over a cylinder, which has a port at each end, was that its ports were close together and could be connected directly to a single five port valve. However, to reduce the weight of the manipulator the valve for the second actuator was mounted on the supporting frame. The resulting 0.6 m of connecting pipe did therefore contribute a 2 ms lag to the control loop. Fortunately the low relatively low bandwidth requirements of the actuator mean that this does not result in significant loss of performance. The frequency at which a phase lag of 90 degrees occurs based on this lag is 125 Hz, well beyond the bandwidth required.

---

[5]They subsequently changed to Linear Variable Differential Transformers (LVDTs).

Surgenor et al. (1995) investigated continuous sliding mode control (CSLM). This is a form of variable structure control advocated for systems which require a fast response as well as insensitivity to disturbances and variations in system parameters. These requirements match those of pneumatic positioning systems. Surgenor et al (1995), compared CSLM with conventional proportional-velocity-acceleration feedback control and proportional-differential pressure control. They found that similar performance could be achieved with all three control methods, but that CSLM was indeed less sensitive to variations in payload. However the strategy required high sampling rates (2 ms) to achieve stability and a degree of tuning was still required to provide the desired (0.2 mm) steady-state error. The characteristic of the technique used in their implementation, which had the advantage of not requiring a system model, was that of a full scale input of an on/off nature up to the so called 'boundary layer' or tolerance region. Within the tolerance region the controller reverted to a conventional linear state feedback controller. However, for equivalent dynamic performance CSLM control gains were shown to be significantly higher than those of a proportional-velocity-acceleration feedback controller.

Wang (1996) applied fuzzy logic techniques, which provide a formal framework into which non-linear and rule based techniques can integrated. An unusual feature of Wang's system was that he employed an array of six 3/2 way on/off solenoid valves and four restrictors to control a 300 mm stroke double acting cylinder. The fuzzy controller was able to select various combinations of exhaust and supply pressures, with or without restriction. In addition pulse-width modulation techniques were used to provide some flow control at high flow rates. The array of individually cheap components was used to keep costs down, though it was not clear to the author that the number of components and their requisite plumbing would result in a lower cost overall than one employing a single proportional valve. Their results, which were given for the unloaded state only, showed stable responses to step changes in input with typical settling times of about 1.3 s with an rms error of 0.08 mm. Whilst these results demonstrate that fuzzy logic is a viable method of control, they do not prove the approach to be superior to others described in this Chapter.

It could be argued that all of the above control methods utilizing servo valves result in a broadly similar control strategy in the practical implementation. That is one of breaking the control action down into two or more phases, through various formal or ad-hoc strategies. In the first phase the input is designed to get the system moving quickly towards the set point and in the final phase in the vicinity of the set point, there is a predominately linear high gain. The former ensures the fast response and the latter low steady-state errors and high stiffness

6.2 Algorithm

From the discussion above there would appear to be no clear cut optimum control strategy that already exists for the type of system in question. An experimental evaluation algorithm was therefore developed that was very flexible and would allow developments to take place along the lines of those discussed above. It was based on a proportional-to-error, proportional-to-pressure difference and integral-of-error feedback controller with the facility to include gain-scheduling and other rule based techniques to control integral wind up. The generalised controlling equation can be expressed as:

$$U_{out}[a] = K_e[a][](\theta_o - \theta_d) + K_p[a][](P_a - P_b) + N[a] + F[a](\theta_o - \theta_d) + FL[a](\theta_o - \theta_d) \quad (6.3)$$

where:

U_{out}	output voltage to valve
a	array index indicating axes number
K_e	proportional to error gain
K_p	proportional to differential pressure gain
$(P_a - P_b)$	differential pressure between bladders
[ ]	indicates an array whose values vary with error and output velocity
N	bias value

$F(\theta_o - \theta_d)$ short term integration of error function

$FL(\theta_o - \theta_d)$ long term integration of error function

The short-term integral acted in a conventional way whilst position error and velocity are small. At all other times this term was set to zero. The long-term integral corrected for long-term drift in neutral values within the system as a whole. These variations might have been electrical or mechanical in nature, due perhaps to temperature changes or wear for example. The rate of build up of this long-term integral was governed by a number of rules. These included:

1. The presence of an air supply.
2. The attainment of equilibrium indicated by low velocity.
3. The absence of an offset load indicated by a low absolute differential pressure.

6.3 Implementation

A schematic overview of the experimental hardware showing one axis only is given in Figure 6.1.

6.3.1 Solenoid valves and drivers

At the start of the work described in this thesis the range of commercially available low cost servo-pneumatic valves was very limited. Over the period in which this work took place there has been considerable commercial development of valves potentially suitable to drive the experimental manipulator. A detailed investigation of the characteristics of some of the commercial valves that have become available has been conducted in Appendix A. The conclusions of this evaluation work indicate that many of the available valves are suitable for this type of application and that some might improve performance over that reported here.

The flow control valve used in this work was a glandless spool design which was operated directly by a DC solenoid. The effect of friction on the spool was reduced by superimposing a 50 Hz AC signal on the controlling DC current level which caused the spool to oscillate. This valve[6] was rugged and relatively low-cost. The disadvantage of such a simple device was that the control of flow is open-loop and varies considerably with time for a constant input. However, by placing the valve within the position control feedback loop this could be tolerated and the effects minimised.

An unfortunate feature of this particular implementation was that the valve was oversized. As a consequence only 25% of the full 500 mA input range was normally being used in controlling the larger of the two joints. This had two undesirable consequences: firstly the fine controllability of the valve was reduced, and secondly the 200 mA amplitude spool dither signal become a larger proportion of the signal. In order to improve performance the valves were modified to reduce their normal flow range. This was achieved by halving the annular area at each port in the spool sleeve. It was important for reasons explained in Appendix B that the reduction in area was made at the spool sleeve interface rather than by placing a restriction in the output port. Similarly it is important to avoid any restrictions in connections between the valves and the bladders. It was for this reason that the simple pipe entry to the bladders, which tended to get crushed, was replaced with manifolds as described in Chapter 5.3.2.

Experiments were then conducted to measure the effect of the valve modification. When tuned to give a similar response to that achieved with the unmodified valve, pressure ripple due to the spool dither showed a reduction in amplitude (15% on axis 0) and a doubling to 50% utilization of the available signal range. This was expected from a halving of the area, but also implies that further improvements could be made. It should be noted that this was not an ideal method of matching the valve to the system as the mass of the spool remained unnecessarily high. It would be better to utilize a smaller valve if one was available.

---

[6] The M/2999 valve manufactured by Norgren Martonair.

The solenoid valves were driven by power transistors whose output current was regulated by the sum of three signals. The first was a valve bias adjustment, the second was a pseudo-sine wave generated by a two bit counter from the PC and the third was the controlling voltage from a D to A channel.

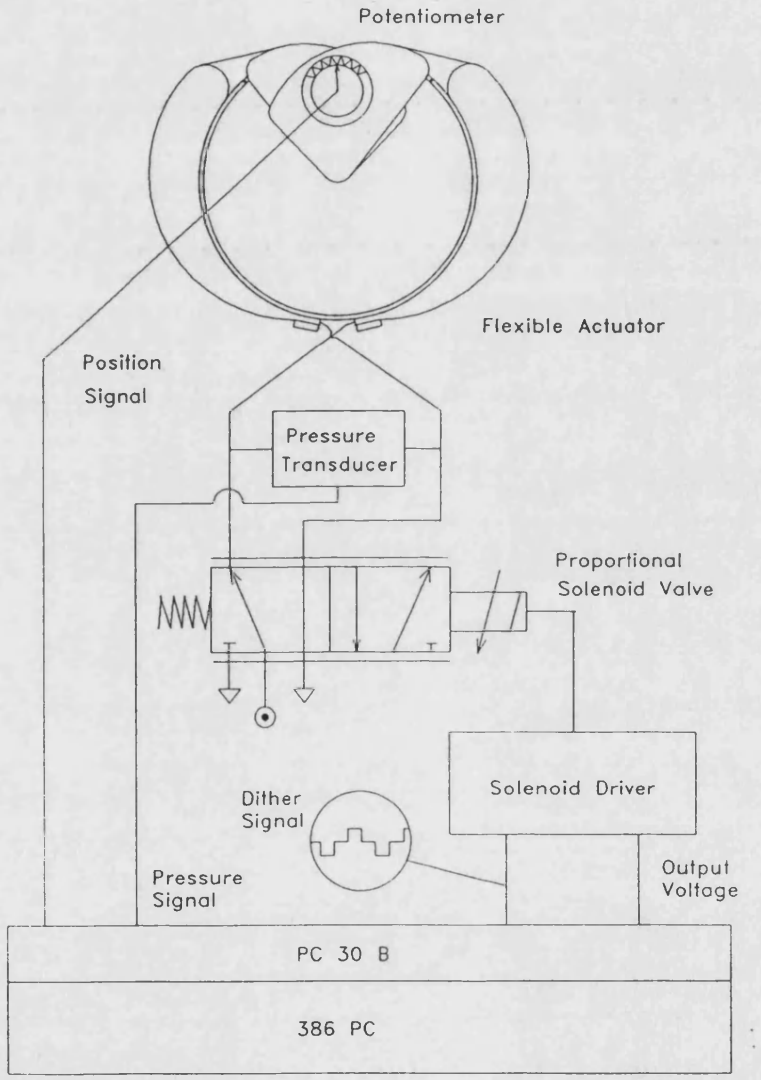

Figure 6.1 Schematic showing a single axis only

6.3.2 Feedback transducers

Two types of feedback transducer were used: Potentiometers to give arm position, and pressure transducers to measure differentially between opposing inflatable elements. The potentiometers were plastic film devices which exhibit high linearity (0.5%) and output smoothness (0.1%) according to the manufacturer's data sheet. The output smoothness proved adequate for dynamic control but the linearity would have resulted in significant errors in absolute accuracy. Accordingly the stroke of the joint was divided into fourteen regions and position determined by linear interpolation between manually derived calibration figures which were stored in a look up table as described in Chapter 8.4. In order to make best use of the 12 bit A to D converter resolution the regulated voltage applied to the potentiometer was sufficient to ensure that its output voltage covered close to the full 0-10 v range over the full mechanical stroke. Electrical protection was provided to prevent accidental overloading of the A to D. The same regulated voltage was fed into a fixed resistor network whose output is placed on a spare A to D channel. Both potentiometer signals were then normalized against this reference which reduced the effect of drift in the reference voltage or A to D converters. Higher quality potentiometers were known to be available (at costs of less than £100) which would potentially improve resolution. However, this improvement could only have been utilized by increasing A to D resolution to 14 bits or more.

The low-cost (£25) piezoresistive pressure transducers provided a 470 mV change in output per MPa. In order to maintain resolution and to minimise the effect of noise the signal was amplified close to the transducer and housed within the joint.

6.3.3 Computing hardware

The 386 33MHz PC on which the controller code ran was equipped with a general purpose input/output board (PC30B). This board provided 12 bit A to D and D to A as well as a number of digital input and output lines. It also contained an on board clock

which was used to trigger the hardware interrupt which prioritized the dynamic control algorithm.

6.3.4 Software

All software was written using Borland Turbo C++, though in general only C attributes were used. A simplified representation of the hardware interrupt driven dynamic control algorithm is given in Figure 6.2.

Input from feedback transducers was smoothed by taking a rolling average over one complete dither cycle (20 ms) of the solenoid valve. This avoided potential aliasing problems caused by the 50 Hz signal which appeared in the pressure and sometimes in the position feedback data. It did however introduce a lag which had an adverse effect on stability. It would thus have been better to use a valve which required no dither or at least utilized a higher dither frequency so that the lag was minimized. A velocity term was calculated using differences between subsequent position values over the 20 ms cycle. This was filtered by limiting accelerations to those which were physically possible. This filtering technique had the advantage of providing no additional lag, though care was required in selecting the maximum slew rate as too low a value would have resulted in phase lags and reductions in amplitude.

Controller parameters were normally read from a data file, though some parameters could be modified interactively at run time. A facility to log a limited amount of data during normal runs was provided. Data were stored in large arrays whilst the controller was running and was placed into a data file as the program was exited. It was also possible to display variables on the screen whilst the code was running.

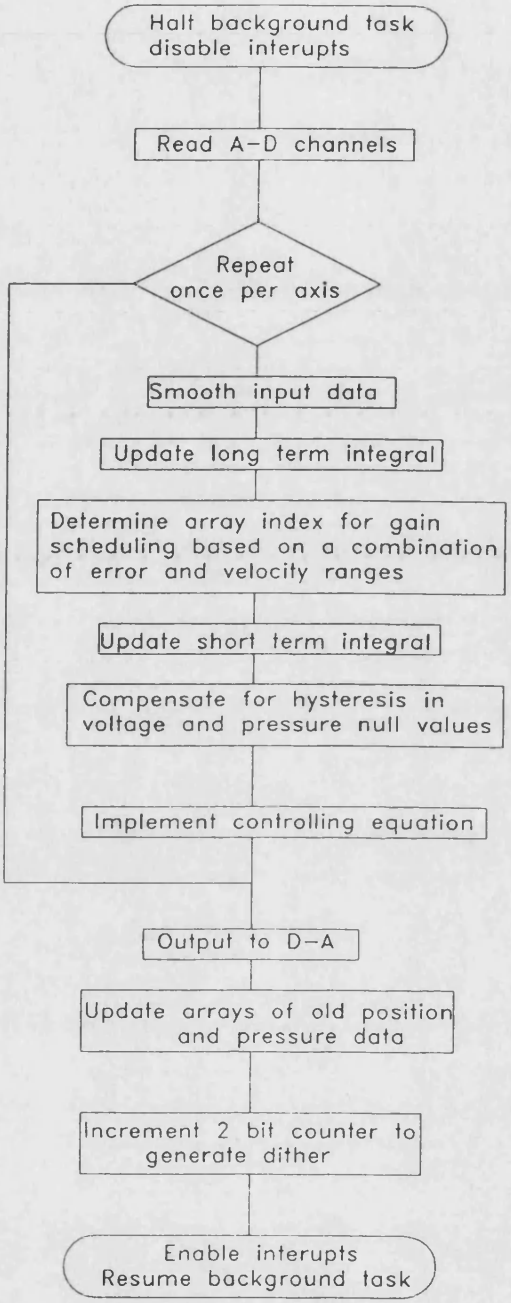

Figure 6.2 Flow chart of hardware interrupt driven control algorithm

6.4 Dynamic performance

6.4.1 One-degree-of-freedom joint

In preliminary tests, the rotary joints suffered from poor stability. Settling times were high and steady-state errors large due to the need to keep proportional gain low. However, with the caliper brake applying Coulomb friction of +/- 8% to bring total hysteresis up to 25 % (Figure 5.16) the behaviour was improved. The reasons for this improvement are investigated in Chapter 7 and confirmed by simulation. Figure 6.3 demonstrates a stable response in the braked configuration with a 0.32 kgm^2 inertial payload (2 kg at 0.4 m). Settling time, which was dependant on payload, was 1.8 s in this example. Repeatability was +/-0.1°. This performance compared well with one of the authors previously reported actuators [Tillett, 1993b] which had similar overall hysteresis most of which arose from the distortion of rubber or woven materials but had no deliberately applied Coulomb friction element (Figure 6.3). In particular for a stable response the maximum payload-to-output-torque ratio was more than doubled. Table 6.1 gives typical controller parameters as applied to the smaller of the two axes.

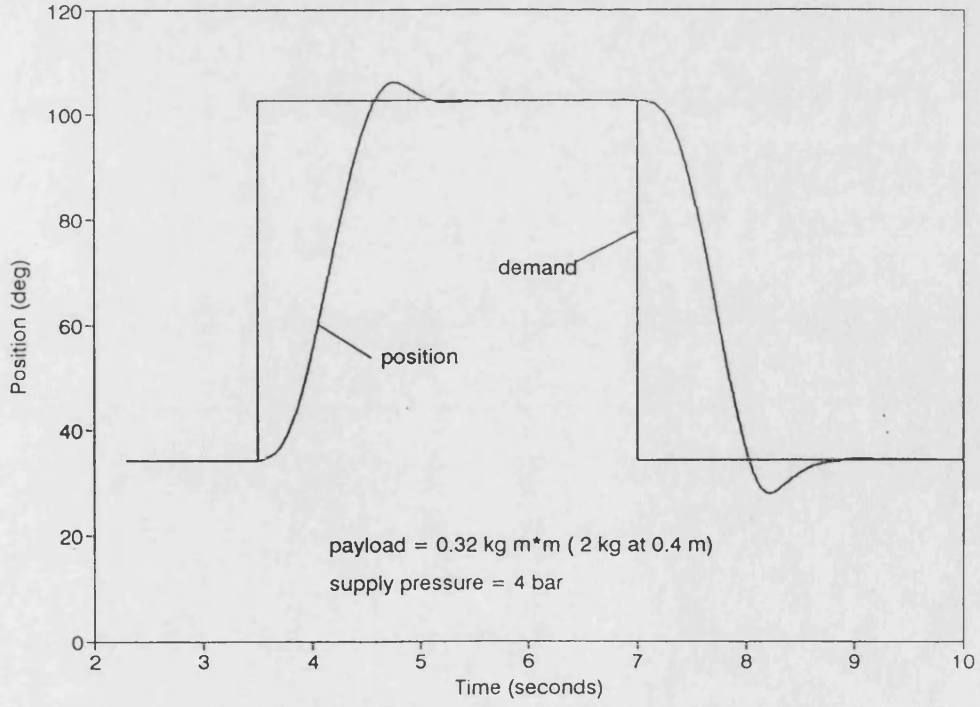

Figure 6.3 Closed-loop response of axis one with 2 kg payload

Parameter	Value			
	Error > 6° or velocity > 80°/sec	6° > error > 3.5° and velocity < 80°/sec	3.5° > error > 1.2° and velocity < 80°/sec	Error < 1.2° and velocity <80°/sec
Error gain, (V/deg^{-1})	1.4	2.9	6.4	15.7
Differential pressure gain, (V/bar^{-1})	46.3	9.3	4.6	0
Velocity gain	0	0	0	0
Integral limit, % of full signal	0	0	0	± 5%
Integral step per 5 ms cycle, % of full signal	-	-	-	0.01
Error dead band on integral, (deg)	-	-	-	0.1
Equilibrium voltage, (V)	Individually set in each of 8 sectors (approx. 5 v)			

Table 6.1 Closed-loop control parameters used to obtain the result illustrated in Figure 6.3

6.4.2 Two degree-of-freedom manipulator

Figure 6.4 gives a typical result for a 1.5 kg payload given step changes in demand position for each axis in turn. This shows that although movement of the smaller joint had little effect on the larger joint, the reverse was not true. The steady-state repeatability was not affected however and was reached within about 1.5 seconds with a 1.5 kg payload. It should be noted that the inertial load on axis 0 was dependent on the geometric configuration. Manipulator repeatability and accuracy are discussed in Chapter 8.2.

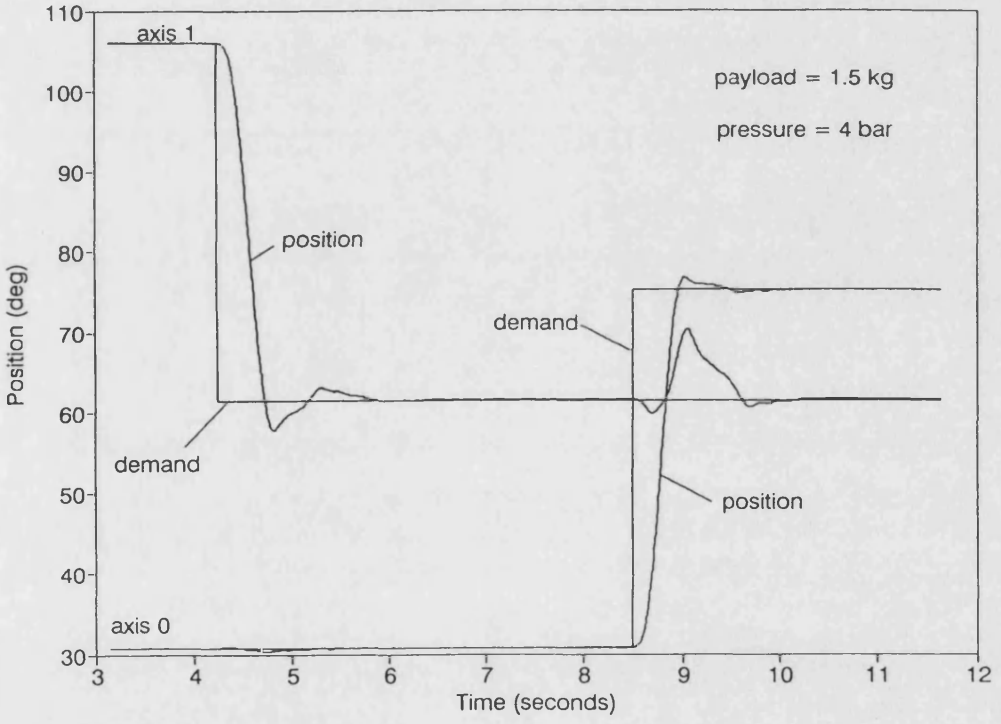

Figure 6.4 Closed-loop response of two-axes manipulator with 1.5 kg payload

6.5 Discussion

Bearing in mind that test payloads were well above the 1 kg design values, the dynamic performance attained above was adequate for simple pick-and-place applications. It is clear however that axes interaction had an adverse effect on dynamic performance and did, under unfavourable conditions, increase overshoots and settling times. In principle this might have been overcome by including an appropriate feedback signal on the motion of one axis into the control loop of the other. Some preliminary decoupling trials were conducted. Joint acceleration was assumed to be proportional to differential pressure. Unfortunately the effects of hysteresis caused significant errors and may have accounted for the poor results obtained. Deducing acceleration from the second differential of position was not thought practical due to the relatively high noise on this signal. A better source of data might have been accelerometers, though this was not pursued. Future progress would probably be best made by developing the simulation model to include two axes and conducting an investigation in simulation before progressing to practical trials.

Pneumatic actuators in general are known to provide poor trajectory control. This aspect of performance was not investigated here but might be worthy of further investigation as even very poor trajectory following may be useful in some applications. In particular the problem of axis interaction described above will need to be addressed.

Subsequent experience with conventional cylinder based pneumatic robots (e.g. Appendix A) has shown that it is often useful to place upper and lower limits on the output signal (U_{out}). This provides a controlled ramp response to a step input which often allows higher proportional gains to be used. It is likely that the performance of the flexible rotary joint could be improved in this way.

7 Dynamic Analysis and Simulation of Pneumatic Servo System

In order to provide a tool for future investigation of the effect of various design parameters (notably hysteresis) on system performance a simulation model has been constructed. Model parameters matched those of the experimental system allowing validation to take place. The bulk of the work described in this Chapter is also covered in Tillett et al, (1997). The objectives of the work described in this Chapter were:

- To develop a simulation model of the dynamic behaviour of a single flexible actuator.

- To validate the model against experimental results.

- To use the model to investigate the influence of design factors including:
  i. Transient pressure feedback in closed-loop control
  ii Different forms of hysteresis

A feature of the bladder driven joint, whose development was described in Chapter 5, was an absence of sliding motion between the components that make up the joint. This results in a joint with no inherent friction. A change in shape of the inflatable bladders, on the other hand, did introduce hysteresis through internal distortion of the rubber-backed woven material of which the bladder was constructed. It is likely that this hysteresis is partially caused by internal friction. However, the characteristics of the hysteresis caused by the distortion of this material and that caused by sliding friction were different.

7.1 Review

The dynamic characteristics of the rotary pneumatic joint were very similar to those of conventional pneumatic cylinders and so it was possible to base this work on earlier studies. The literature contains two approaches to pneumatic system modelling. In one followed by Backé and Eschmann (1993) the system was broken down into a series of components which were modelled as a sequence of alternate resistances and capacities. The mass flow rate between components was calculated from pressures and temperatures and from parameters describing resistance, eg conductance and critical pressure ratio which were measured experimentally. The advantage of this approach, which yielded good results, was its ability to model non-linear characteristics such as those associated with choked flow. Frictional non-linearities were also incorporated into this model. The other approach followed by Liu and Bobrow (1988) utilized a linearized analysis of the pneumatic components and was based on earlier studies by Shearer (1956). Their results, which did not take frictional effects into account, showed reasonable agreement between experiment and simulation, but the match was not as good as that achieved by Backé and Eschmann (1993). In this study, the latter approach using a linearized analysis of the pneumatic components has been chosen for its relative simplicity. However, non-linearities due to the distortion of the inflatable bladders have been incorporated into the model in an attempt to improve its accuracy and to provide a means of investigating the bladders effect on performance.

7.2 Analysis

7.2.1 Experimental system

The axis 0 joint of the experimental manipulator was used as the basis for the experimental system, the mechanical and control aspects of which are fully described in Chapters 5 and 6 respectively. A diagrammatic representation of the apparatus is given in Figure 7.1.

The control equation used for these experiments was a simplified version of the one described in Chapter 6 (equation 6.3). In particular there were no integral terms and no use was made of non-linear techniques such as gain scheduling, though a proportional to velocity term was added. The controller could be represented as follows:

$$U_{out} = K_e(\theta_o - \theta_d) - K_p(P_a - P_b) - K_v\dot{\theta}_o \qquad (7.1)$$

where

U_{out} output voltage to valve

K_e proportional to error gain

K_p proportional to differential pressure gain

K_v proportional to velocity gain

θ_o output angle

θ_d demand angle

P_a-P_b differential pressure between bladders

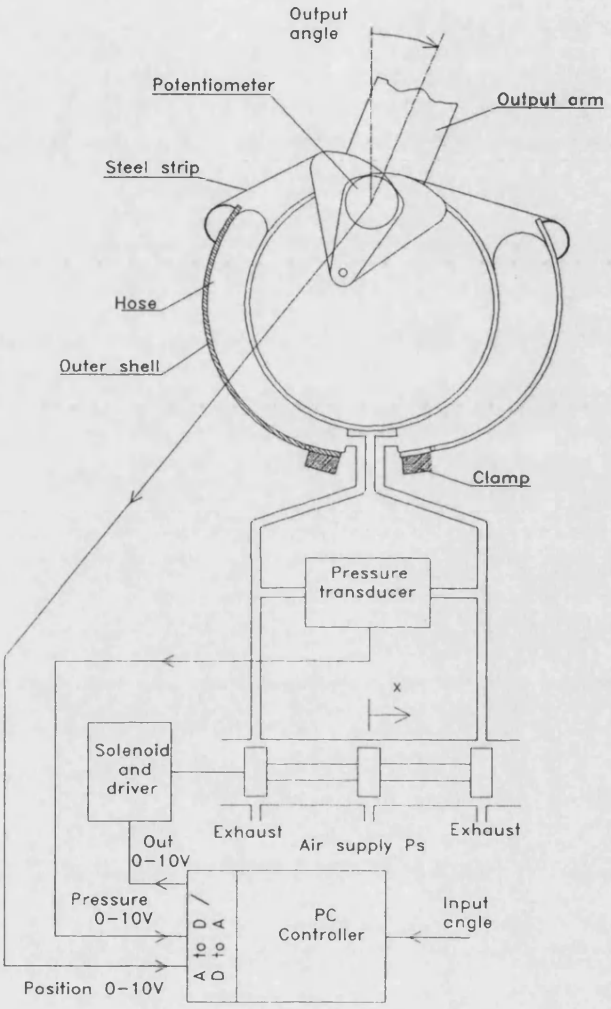

Figure 7.1 Schematic of the one degree-of-freedom experimental system.

7.2.2 Linearized servo system

The objective of this analysis was to derive linearized differential equations for the components of the system depicted in Figure 7.2 so that they could be presented in a transfer function form suitable for inclusion in a SIMULINK model.

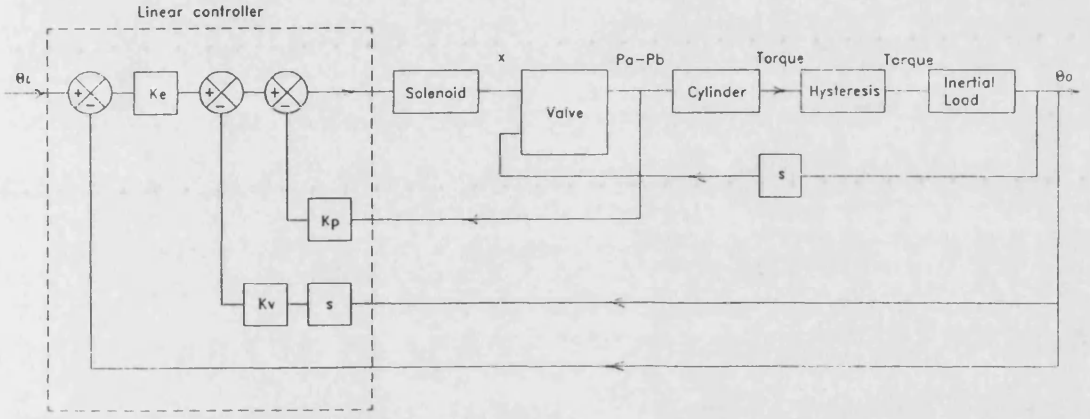

Figure 7.2 Block diagram of the one degree-of-freedom experimental system with the controller depicted as linear for simplicity.

It has been shown by Shearer (1956) using continuity and energy equations that for one chamber (subscript a) of a pneumatic cylinder (or one bladder of the flexible rotary actuator) mass flow $\dot{m}$ can be expressed as:

$$\dot{m}_a = \frac{P_{ai}\dot{v}_a}{RT_s} + \frac{V_{ai}\dot{p}_a}{\gamma RT_s} \tag{7.2}$$

where P is the pressure and V is the volume of the chamber. R is the gas constant and T_s is the supply temperature, γ is the ratio of specific heats, lower case denotes a change from initial conditions and subscript i indicates an initial value. Dot notation has been used to indicate the rate of change with time. Assumptions made by Shearer in this derivation include perfect gas, adiabatic change and compressible flow. Similarly the equation for the other side (subscript b) can be represented as:

$$\dot{m}_b = \frac{P_{bi}\dot{v}_b}{RT_s} + \frac{V_{bi}\dot{p}_b}{\gamma RT_s} \tag{7.3}$$

Shearer (1956) also proposed the following linearized pressure-flow characteristic representation for a pneumatic spool value:

$$\dot{m}_a = C_1 x - C_2 p_a \tag{7.4}$$

$$\dot{m}_b = -C_1 x - C_2 p_b \tag{7.5}$$

where X is spool displacement and:

$$C_1 = \frac{\delta \dot{M}_a}{\delta X}\Big|_{P_{ai}} = \frac{\delta \dot{M}_b}{\delta X}\Big|_{P_{bi}} \tag{7.6}$$

$$C_2 = \frac{\delta \dot{M}_a}{\delta P_a}\Big|_{X_i} = \frac{\delta \dot{M}_b}{\delta P_b}\Big|_{X_i} \tag{7.7}$$

These relationships were also used by Burrows (1969) to obtain the characteristic equation of a pneumatic servo system and to show the effect of cylinder position on stability. A similar manipulation of these equations was performed for this thesis in order to obtain a relationship between spool position and actuator pressures P_a and P_b.

Considering the volume of each bladder:

$$V_{ai} = V + \theta_i \alpha \tag{7.8}$$

$$V_{bi} = V - \theta_i \alpha \tag{7.9}$$

where V = volume in either bladder at mid-stroke, θ_i is actuator initial output angle and α is first moment of area.

Following a displacement θ from the initial conditions:

$$v_a = \theta \alpha \tag{7.10}$$

$$v_b = -\theta \alpha \tag{7.11}$$

Combining (7.2) with (7.4) and (7.3) with (7.5) and substituting (7.8), (7.9), (7.10) and (7.11):

$$C_1 x - C_2 p_a = \frac{P_{ai} \alpha \dot{\theta}}{RT_s} + \frac{(V + \alpha \theta_i) \dot{p}_a}{\gamma RT_s} \tag{7.12}$$

$$-C_1 x - C_2 p_b = \frac{-P_{bi} \alpha \dot{\theta}}{RT_s} + \frac{(V - \alpha \theta_i) \dot{p}_b}{\gamma RT_s} \tag{7.13}$$

Combining (7.12) and (7.13), rearranging and converting from dot to Laplace notation where s represents $\frac{d}{dt}$:

$$\frac{\alpha s \theta}{RT_s} \left((P_{ai} + P_{bi}) - \frac{\alpha s \theta_i / \gamma RT_s (P_{ai} - P_{bi})}{(C_2 + Vs/\gamma RT_s)} \right)$$

$$= 2C_1 x - \left(C_2 + \frac{Vs}{\gamma RT_s} - \frac{(\alpha \theta_i / \gamma RT_s)^2 s^2}{(C_2 + Vs/\gamma RT_s)} \right) (P_a - P_b) \tag{7.14}$$

Initial pressure conditions are assumed to the same in each bladder :

$$P_{ai} = P_{bi} = P_q$$

where P_q is the quiescent pressure.

Equation (7.14) can then be rearranged to give:

$$\frac{2\,\alpha\, s\,\theta\, P_q}{RT_s} = 2\,C_1 x - G(s)(P_a - P_b) \qquad (7.15)$$

where G(s) =

$$C_2 \left\{ \frac{(1 - (\alpha\,\theta_i / V)^2)\,\tau^2 s^2 + 2\,\tau s + 1}{1 + \tau_s} \right\} \qquad (7.16)$$

and the time constant

$$\tau = \frac{V}{\gamma\, RT_s\, C_2} \qquad (7.17)$$

Thus an expression has been derived for P_a - P_b in terms of x and s θ, which was the result needed for the valve transfer function block in the block diagram model of Figure 7.2.

7.2.3 Measurement of system parameters and representation of hysteresis

Linearized valve coefficients, C1 and C2 were evaluated experimentally by measuring flow at a range of differential pressures and spool positions. The large amplitude pressure ripple caused by spool dither prevented the use of conventional flow meters particularly for low flows. Accordingly flows were deduced from the rate of charge of pressure vessels. The spool displacements and differential pressures used were in the lower range of flow rates as this best represents the system when settling about a set point. Details of the analysis and experimental procedure are given in Appendix C. The results produced a value of 1.5 $kgs^{-1}\,m^{-1}$ for C_1 and 0.4 10^{-8} ms for C_2.

In Chapter 5 it was shown that the most important source of hysteresis was due to relative motion between reinforcing fibres and the rubber matrix within the bladders.

The bladders change shape for two reasons, firstly due to changes in actuator output position and secondly due to changes in inflation pressure. The characteristics and parameters of both have been investigated experimentally. In one experiment an actuator output arm was connected to a strain-gauge load cell which was in turn mounted on a lead screw actuated carriage to facilitate actuator movement over a limited stroke. Pressure in both bladders was held constant but unequal so that a nominally constant output torque could be maintained. The actuator was then cycled through part of its stroke whilst torque and position were logged. The results illustrated in Figure 7.3a show +/- 1.5 Nm hysteresis which is +/-2% of maximum output torque. This has been modelled as having a modified trapezoidal characteristic as depicted in Figure 7.3b. For constant input pressures, output torque changes due to actuator movement vary first stepwise and then linearly with angular position up to the hysteresis boundary. Once beyond the hysteresis boundary output torque becomes saturated and the output force remains constant. Work by Chou and Hannaford (1996) with an inflatable reinforced rubber actuator of the McKibben type indicated that hysteresis characteristics were independent of velocity over a wide speed range. Within the limited speed capacity of the apparatus (0.01 rad s^{-1}) these results were confirmed and so hysteresis has been modelled as independent of speed.

In a second experiment output position was fixed and the pressure in one bladder was varied, whilst that in the other remained constant. The resulting plot of torque vs pressure given in Figure 7.3c, indicates a hysteresis of +/-0.15 Nm (+/- 0.2%), a figure which remains fairly constant when the experiment was repeated at other operating pressures. It is likely that a proportion of this hysteresis was due to very small (0.25 degrees in the results illustrated) movements within the apparatus. Hysteresis due to variations in inflation pressure have therefore been shown to be small in comparison to those due to changes in output position and have not been included in the model.

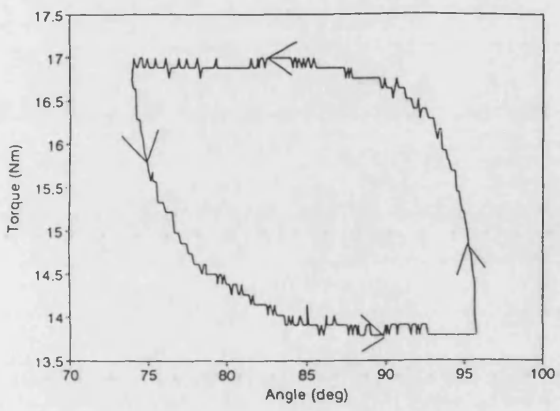

(a) Measured hysteresis due to movement of output arm with no brake P_a = 2.1 bar, P_b = 2.7 bar

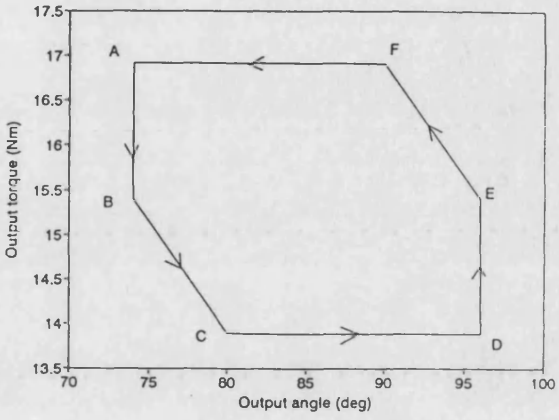

(b) Model of bladder distortion induced hysteresis due to movement of output arm, P_a = 2.1 bar, P_b = 2.7 bar

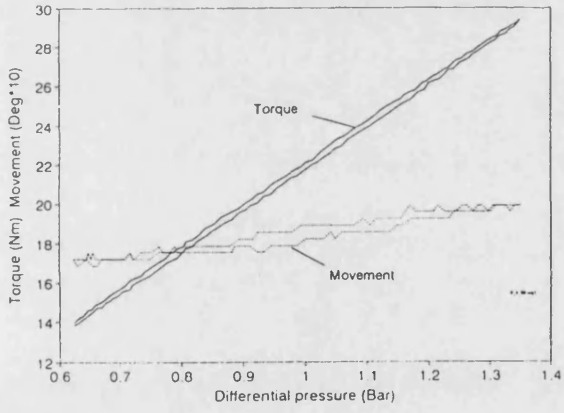

(c) Measured hysteresis due to changes in pressure (P_a - P_b) with no brake and output arm clamped

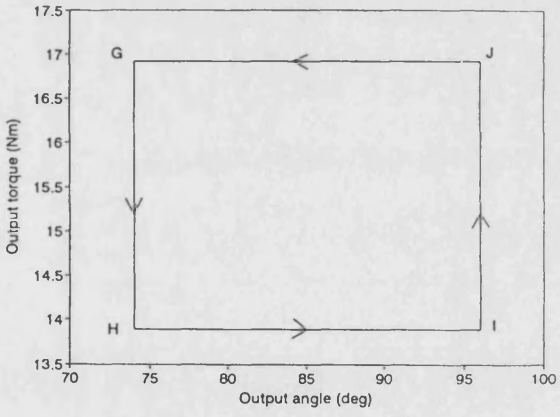

(d) Model of Coulomb friction induced hysteresis due to movement of output arm

Figure 7.3 Measured and idealized hysteresis in the output torque characteristic

Two types of caliper brake applied friction were considered to be of possible significance: Coulomb and stiction. Coulomb friction was considered as a constant torque which opposed motion; when there is no motion it opposed (but does not exceed) the applied force as depicted in Figure 7.3d. Stiction was regarded as a force which generally exceeded Coulomb friction at speeds below a threshold. It too opposed motion and when there is no motion opposed (but does not exceed) the applied force. Tests using a tension testing machine described in Chapter 5.3.2 indicated that a pure Coulomb friction model adequately represented the caliper brake.

7.3 Simulation

7.3.1 Model construction

The dynamic model was constructed within the SIMULINK/MATLAB program [SIMULINK Users Guide, 1993]. This environment was well-suited to a block diagram representation of the system. The SIMULINK equivalent representation of the block diagram illustrated in Figure 7.2 is given in Figure 7.4.

The digital controller block was made up of a sub-system which included analogue-to-digital and digital-to-analogue conversions, as well as the control algorithm itself. The control algorithm was written in the MATLAB language and called as an S-function m-file. MATLAB code is very similar to the C-code used in the experimental controller so that in most cases the code and its structure could be copied directly, thus minimising the risk of differences between the experimental and model controllers.

The solenoid sub-system was a simple combination of offset, gain and saturation blocks to convert the controller output voltage linearly to a spool displacement. No account was been taken of solenoid and spool dynamics as these were considered very fast in comparison with the actuator itself. Spool friction and valve bias value drift were also neglected. A sine-wave was superimposed on the solenoid input to model valve dither.

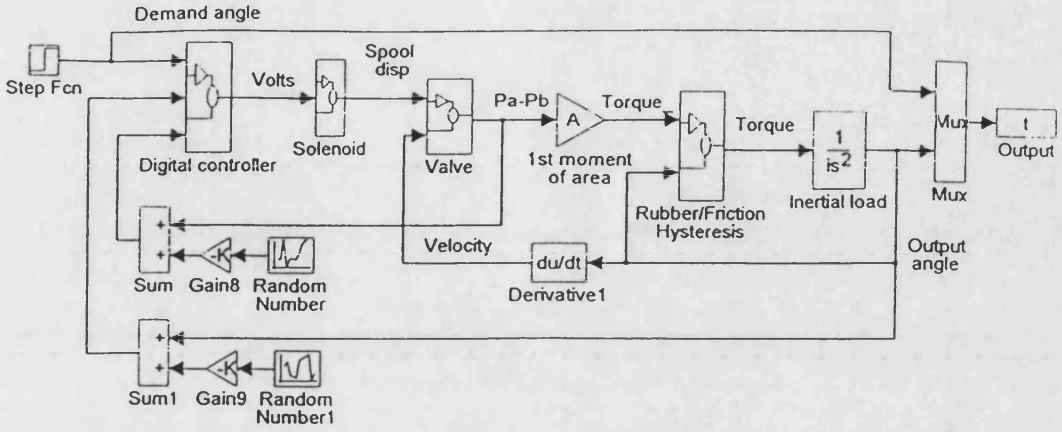

(a) Overall system

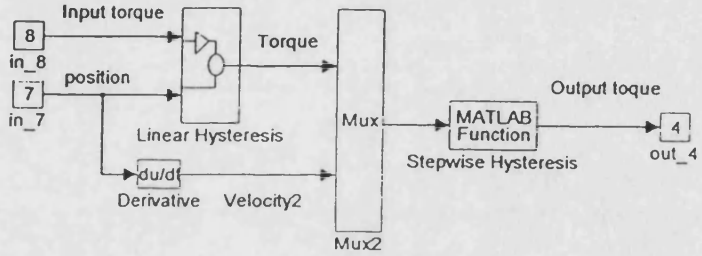

(b) Hysteresis sub-block

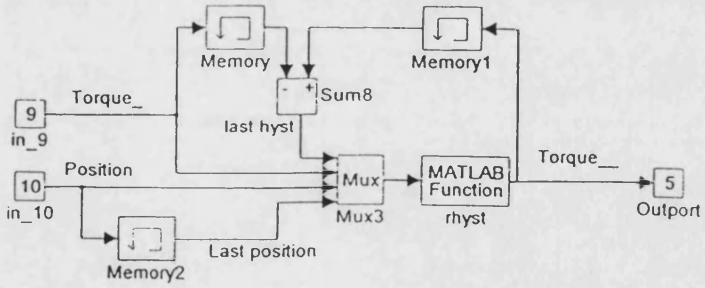

(c) Linearly varying hysteresis with history dependance

Figure 7.4 SIMULINK block diagram representation

The valve sub-system consisted of a block diagram representation of the transfer function derived as equation 7.15 in Section 7.2.2.

The actuator hysteresis block consisted of two sub-systems acting in series. The first modelled that element of hysteresis which varies linearly with output position (ie B-C and E-F in Figure 7.3b). The second modelled hysteresis which results in a stepwise change with the polarity of output motion (A-B and D-E in Figure 7.3b and G-H and I-J in Figure 7.3d). Both utilised MATLAB function m-files taking angle and torque as inputs. In the former, memory blocks were used to record the recent history of movement and in the latter a derivative block calculated angular velocity. The output of the hysteresis block for parameters relating only to the distortion of the bladders is given in Figure 7.3b and for parameters relating to pure Coulomb friction in Figure 7.3d.

The inertial load was a pure double integrator with output arm inertia as a denominator constant.

Normally distributed noise with variance equivalent to 2 on the 12 bit analogue-to-digital input was injected into the feedback paths to simulate the noise measured by the experimental system transducers.

7.3.2 Model validation

A series of experiments were conducted to make direct comparisons between model and experimental system performance. Except where stated, all simulation results include the experimentally measured +/-2% hysteresis due to bladder distortion as illustrated in Figures 7.3a and 7.3b. In Figure 7.5, a series of three comparisons was made for proportional-to-error controllers with gains (K_e) only and with no applied friction. The three gains were chosen to represent to a first approximation overdamped, underdamped and critically damped responses respectively. Figure 7.5a shows the

simulation and Figure 7.5b the experimental results obtained with a 1.7 kgm^2 payload (I) and K_e set to 1.2 V rad^{-1}. Figures 7.5c and 7.5d give the result for the same payload but with an increased proportional to error gain, K_e = 3.7 V rad^{-1}. In Figures 7.5e and 7.5f payload has been decreased to 0.4 kgm^2, K_e = 3.7 V rad^{-1}. In all three cases there was good correlation between simulation and experiment.

The performance of a proportional-to-error controller, K_e = 3.7 V rad^{-1}, with +/-8% Coulomb friction applied with the brake and a payload of 1.7 kgm^2 is illustrated in Figures 7.6a and 7.6b. In Figures 7.6c and 7.6d the payload was reduced to 0.4 kgm^2 and the gain increased to 7.4 V rad^{-1}. In both cases correlation between simulation and experiment was good, though not as good as the previous three runs, indicating that the Coulomb friction model provided a reasonable but not perfect representation of the physical system. As expected the Coulomb friction provided a degree of damping, reducing oscillations around the set point. However, this damping has been provided at the expense of significantly increased steady-state errors. In the experimental system steady-state error was variable between runs but values lie in a restricted band. The experimental results given in Figures 7.6b and 7.6d are typical, but in general steady-state errors were lower than those predicted in simulation. Some of the discrepancy, up to 0.007 rad, may be due to unmodelled elastic flexing of the brake assembly which will tend to distort in such a way as to reduce error. It should be noted that although Coulomb friction increases steady state error for a given proportional gain the resulting increased dynamic stability allows that gain to be increased with a consequent reduction in steady state error.

The use of velocity feedback is illustrated in Figure 7.7. System parameters were as follows: I = 1.7 kgm^2, K_e = 3.7 V rad^{-1}, no applied friction and a velocity feedback gain of 0.3 V rad^{-1} s. This value was arbitrarily chosen to illustrate a clear effect, but is representative of values normally used in the controller The results which display reasonable agreement between simulation and experiment, showed that velocity damping had only a limited value in damping the system.

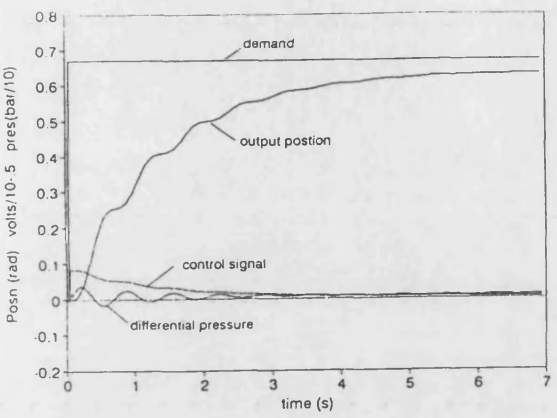

a) Simulation results, K_ϵ = 1.2 V rad^{-1}, I = 1.7 kgm^2

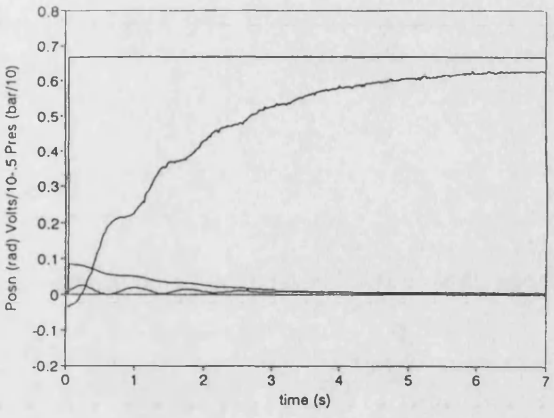

b) Measured results, K_ϵ = 1.2 V rad^{-1}, I = 1.7 kgm^2

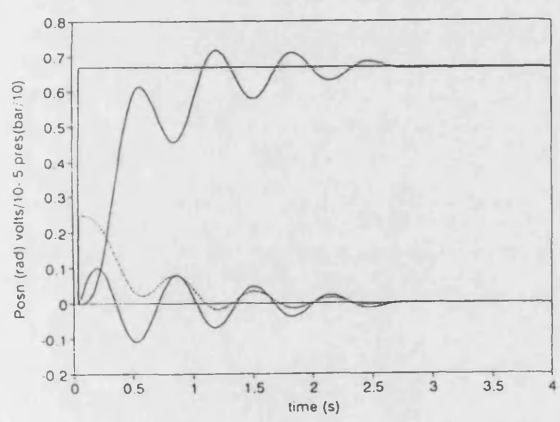

c) Simulation results, K_ϵ = 3.7 V rad^{-1}, I = 1.7 kgm^2

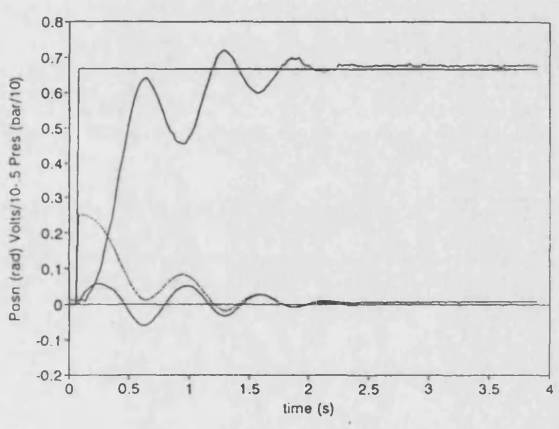

d) Measured results, K_ϵ = 3.7 V rad^{-1}, I = 1.7 kgm^2

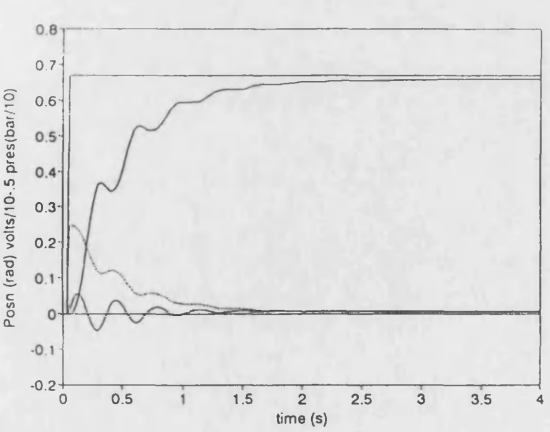

e) Simulation results, K_ϵ = 3.7 V rad^{-1}, I = 0.4 kgm^2

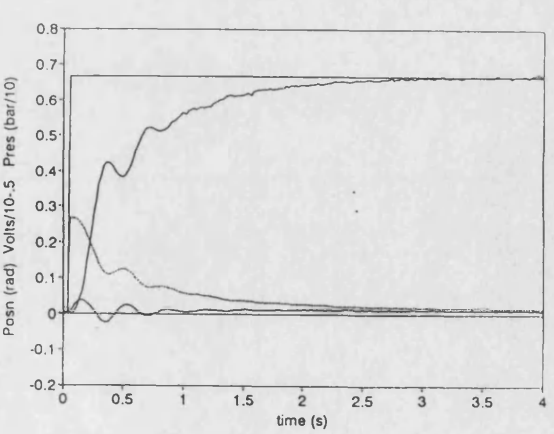

f) Measured results, K_ϵ = 3.7 V rad^{-1}, I = 0.4 kgm^2

Figure 7.5 Comparison between simulation and experimental results with no brake applied and a proportional to error controller

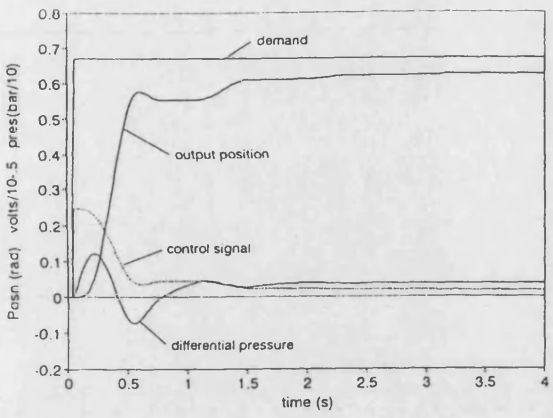

a) Simulation results, K_e = 3.7 V rad^{-1}, I = 1.7 kgm^2

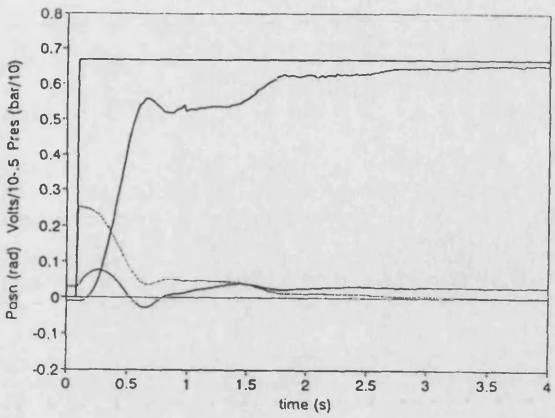

b) Measured results, K_e = 3.7 V rad^{-1}, I = 1.7 kgm^2

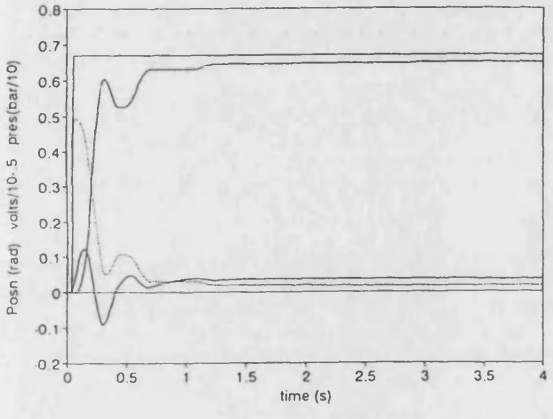

c) Simulation results, K_e = 7.4 V rad^{-1}, I = 1.7 kgm^2

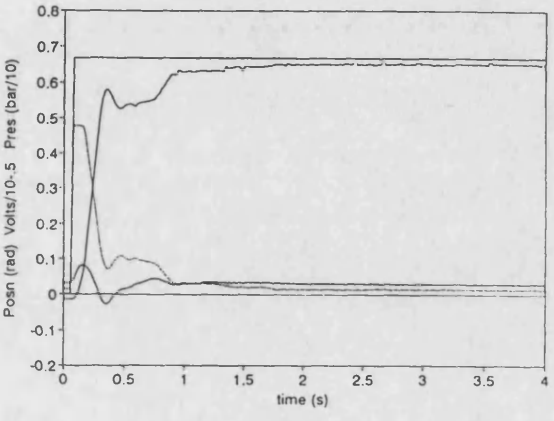

d) Measured results, K_e = 7.4 V rad^{-1}, I = 1.7 kgm^2

Figure 7.6 Comparison between simulation and experimental results with +/- 8% Coulomb friction applied through the brake and a proportional to error controller

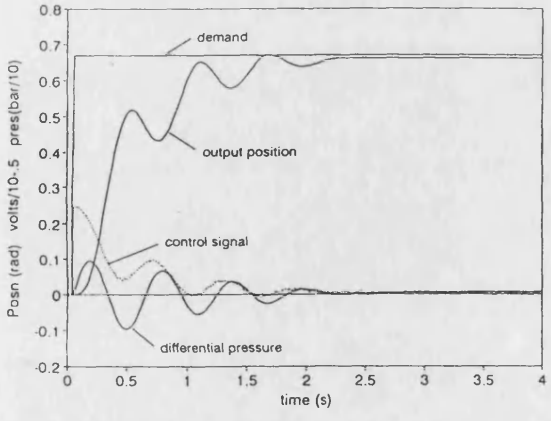

a) Simulation results, K_e = 3.7 V rad^{-1}, K_v = 0.3 V rad^{-1}s, I = 1.7 kgm^2

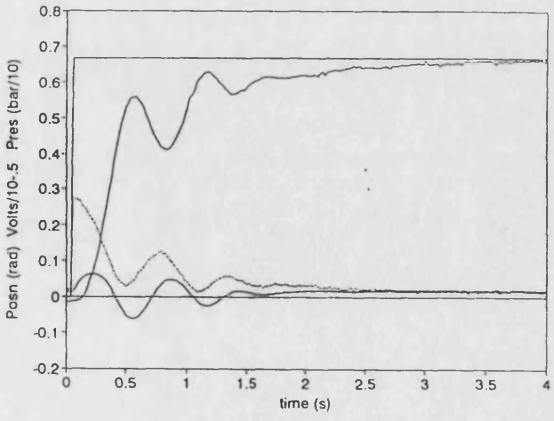

b) Measured results, K_e = 3.7 V rad^{-1}, K_v = 0.3 V rad^{-1}s, I = 1.7 kgm^2

Figure 7.7 Comparison between simulation and experimental results with a velocity damping term included in a proportional to error controller, no brake applied

Differential pressure feedback was used in the last response illustrated in Figure 7.8, where $I = 1.7\ kgm^2$, $K_e = 4.9\ V\ rad^{-1}$, $K_p = 17\ V\ MPa^{-1}$ and no friction has been applied. Both simulation and experiment gave similar initial rates of response and steady-state errors. However, the experimental result was less damped, probably due to the over estimation of differential pressure within the simulation. This trait could be seen in all results (Figures 7.5-7.8). Differential pressure was related to the second differential term of the simulation position output and is therefore likely to highlight any differences between real and simulated behaviour. Prediction of pressures would also seem to have been the least accurate aspect (approximately +/-20%) of Backé and Eschmann's (1993) simulation, though they gave few results and did not comment directly on it. The effectiveness of differential pressure as a damping term was clear from Figure 7.8. However, a steady-state position error was caused as the controller drives to bring differential pressure to zero in the presence of hysteresis. The situation could be worse in the case of the rotary actuator, if due to manufacturing defects for example, the cam profile did not produce a perfectly constant output torque throughout its stroke. In such a case the steady-state differential pressure will vary slightly with position. A solution developed by Shearer (1956) and others was to use transient pressure feedback which will go to zero at the steady-state. In 1956 Shearer proposed to achieve this pneumatically, though it would now be most conveniently implemented electrically or as a digital filter. A preliminary investigation of this technique applied to the rotary actuator has been conducted in simulation.

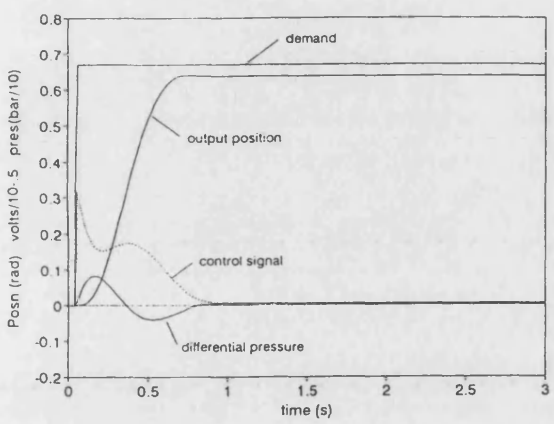

a) Simulation results, K_e = 3.7 V rad^{-1}, K_p = 1.7 V bar^{-1}, I = 1.7 kgm^2

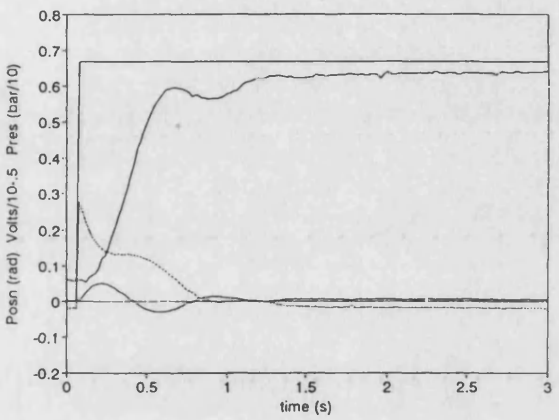

b) Measured results, K_e = 3.7 V rad^{-1}, K_p = 1.7 V bar^{-1}, I = 1.7 kgm^2

Figure 7.8 Comparison between simulation and experimental results with a pressure differential between bladders damping term included in a proportional to error controller, no brake applied

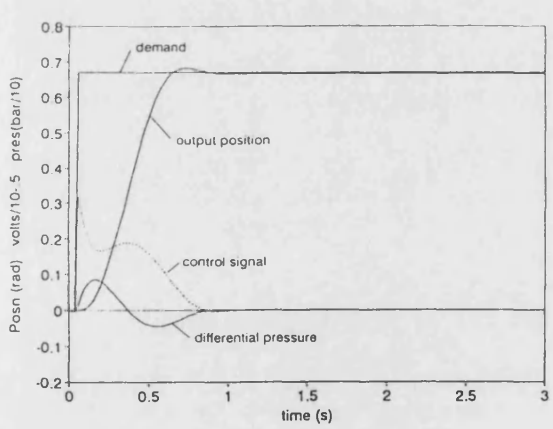

Figure 7.9

Simulation result showing the effect of transient pressure feedback in a proportional to error controller, no brake applied, K_e = 4.9 V rad^{-1}, K_{tp} = 1.7 V bar^{-1}, I = 1.7 kgm^2

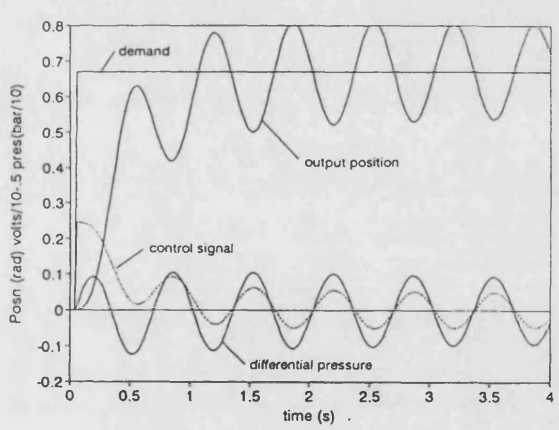

Figure 7.10

Simulation result showing the effect of removing hysteresis from model, when all other parameters are the same as those used to obtain Fig 7.5c K_e = 3.7 V rad^{-1}, I = 1.7 kgm^2

7.4 Investigations in simulation

7.4.1 Use of transient pressure feedback

Transient pressure feedback was implemented in simulation as a continuous transfer function of the form:

$$\frac{\tau_f s}{(1+\tau_f s)} \tag{7.18}$$

acting as a high pass filter and placed between the analogue-to-digital converter and point at which noise is injected. Best results were obtained with a time constant τ_f=1s, which can be expressed as a 1 rad/s cut off frequency at the -3dB breakpoint. The results given in Figure 7.9 relate to the same parameters used to obtain Figure 7.8 except that the pressure gain K_{tp} was altered to act on the transient pressure and retained the value 17 V MPa^{-1}. The Figure shows a very marginally less damped response, but with a significant reduction in steady-state error. The apparent effectiveness of this technique in simulation suggested that it might be worth implementing on the experimental system for further evaluation. This is reinforced by the promising results achieved when a first order RC band pass filter was used to provide transient pressure feedback to a pneumatic servo system based on a conventional cylinder and a proportional flow control spool valve. These experimental results including filter design details are given in Appendix D. An alternative, or complementary solution to the problem of providing adequate damping, whilst maintaining a fast response rate and low steady-state errors, may lie in using one of the many non-linear control strategies that have been proposed for pneumatic systems [Pu and Weston, 1988; Wang, 1996; Surgenor et al., 1995]. The use of such strategies has not been investigated here, but could form the basis of future work with the simulation model.

7.4.2 Effects of hysteresis

The significance of the magnitude and type of hysteresis was investigated in simulation as illustrated in Figures 7.10 to 7.12. For reference in Figure 7.10 all parameters were identical to those used to obtain Figure 7.5c except that hysteresis has been eliminated. The marked change in response indicates the importance of including hysteresis within the model and shows that hysteresis contributes to system damping. It should be noted that the apparent stabilizing effect of hysteresis is related to its presence within position control systems. In such systems oscillations around the set point result in a change in direction of movement, which hysteresis opposes, thus removing energy from the system. In trajectory following applications oscillations will result in varying speeds about the desired level, but the direction of motion may remain unchanged and so there will be no damping effect. In both cases hysteresis will result in increased steady-state errors. This effect has been demonstrated in Figure 7.11 in which the addition of +/- 10% of Coulomb friction failed to affect the oscillations about the ramped input, though it did increase steady-state error. Viersma (1980) discussed a similar result for hydraulic servo systems and concluded that Coulomb friction does not improve stability, though he only considered a constant speed input. In general, hysteresis has adverse effects on the performance of trajectory or velocity control systems, but the picture is less clear for position control. This is particularly true for pneumatic systems, which can be easier to stabilize about a stationary set point with some hysteresis present.

If hysteresis has some desirable features, it would be valuable to know which forms should be minimised and which, under some circumstances, might be deliberately introduced. In Figure 7.12 hysteresis of the type introduced by distortion of the bladders (ie as represented by Figure 7.3b) is compared with that due to pure Coulomb friction (ie as represented by Figure 7.3d). In order to exaggerate the differences, hysteresis levels were set artificially high at +/-6% in both cases. Other parameters were the same as those used to obtain Figure 7.5c. The results indicated that Coulomb friction induced hysteresis provided more damping than that caused by distortion of the

bladders. Steady-state errors were the same in both cases indicating that it would be preferable to design out hysteresis due to the distortion of bladders and replace it, if required, with pure Coulomb friction.

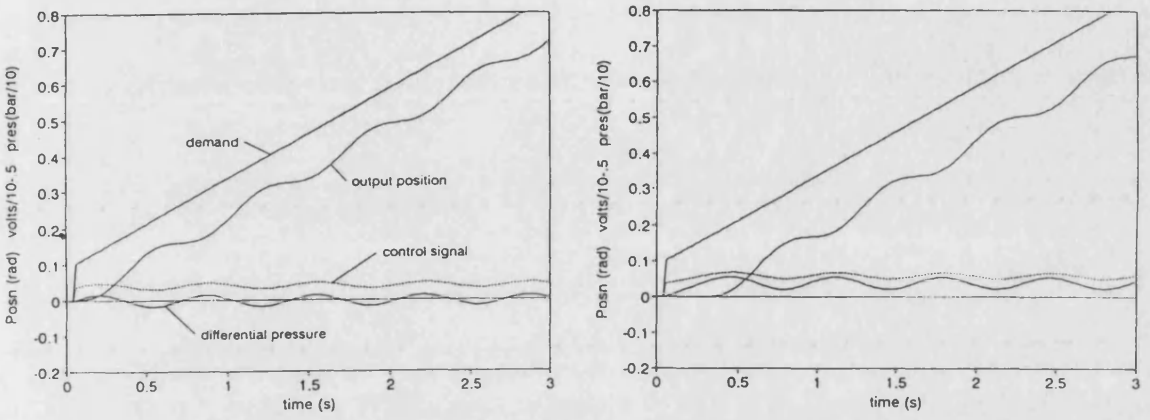

a) Simulation result with no hysteresis, $K_\epsilon = 3.7$ V rad^{-1}, $I = 1.7$ kgm^2

b) Simulation result with +/- 10% Coulomb friction induced hysteresis, $K_\epsilon = 3.7$ V rad^{-1}, $I = 1.7$ kgm^2

Figure 7.11 Investigation in simulation of the effect of Coulomb friction on a proportional to error control system with a ramp input

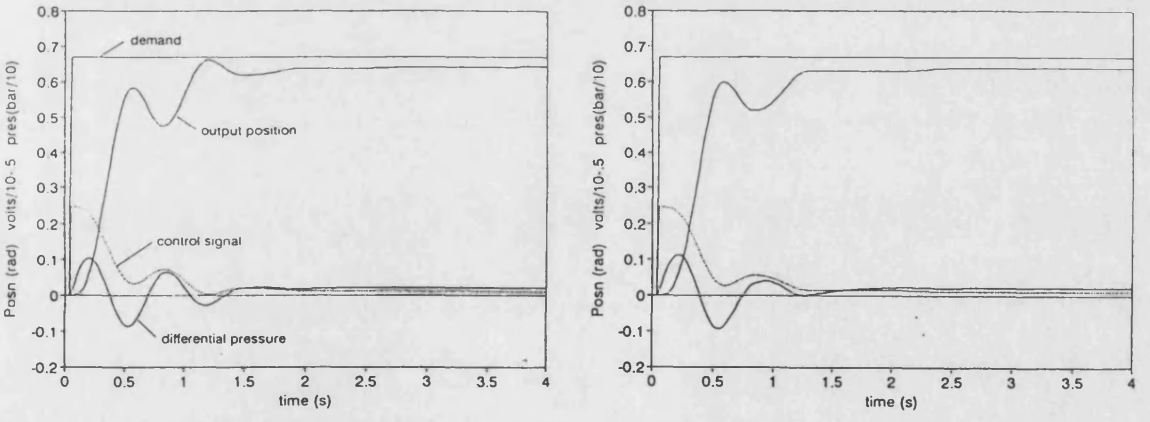

a) Simulation run with +/-6% hysteresis due to bladder distortion, $K_\epsilon = 3.7$ V rad^{-1}, $I = 1.7$ kgm^2

b) Simulation run with +/- 6% hysteresis due to Coulomb friction, $K_\epsilon = 3.7$ V rad^{-1}, $I = 1.7$ kgm^2

Figure 7.12 Investigation in simulation of the differences between Coulomb friction and rubber distortion induced hysteresis in a proportional to error control system with a step input

7.5 Conclusions

The simulation model successfully predicted all major modes of behaviour. It provided an accurate representation of the position response of the experimental system under proportional to error or proportional to error and velocity feedback control. The simplified models of rubber and Coulomb friction induced hysteresis modified simulation performance in line with experimental results.

In general differential pressures predicted in simulation were up to 60% greater than those measured in the experimental system. This discrepancy caused the damping effect of pressure feedback terms to be over estimated in simulation.

The model provides a useful mechanical and control design tool for pneumatic positioning systems in general and those utilizing flexible rotary actuators in particular.

An investigation in simulation of different forms of hysteresis, showed that Coulomb friction induced hysteresis had a greater damping effect than the same level of hysteresis caused by the distortion of the rubber bladders. This result applies only to position control, as hysteresis has been shown not to provide damping in trajectory control applications.

8 High Level Control and System Evaluation

The purpose of the high level control system was to provide a user friendly interface and to provide a means of linking the various sub-systems required to perform demonstration tasks. A schematic of the system, given in Figure 8.1, shows that two PC's were used. The host PC contained the image grabbing card and conducted the image analysis. The resulting data was passed via an RS 232 serial link to the slave PC which contained the input/output card and conducted high level robot control as a background task to the dynamic control algorithm. The complete system has been evaluated with respect to repeatability over the whole working area and accuracy within the image guided region. The objectives of the work described in this Chapter were as follows:

- To provide a high level control structure which provides an interface with the user and sub-systems such as the vision system and end-effector.

- To develop and implement a coordinate transformation between robot polar coordinates and work space Cartesian coordinates.

- To develop and implement calibration procedures to take account both of non-linearities in joint position transducers and in the computer vision system.

- To determine experimentally the repeatability of the manipulator over its full working area and its accuracy in the region of vision guidance.

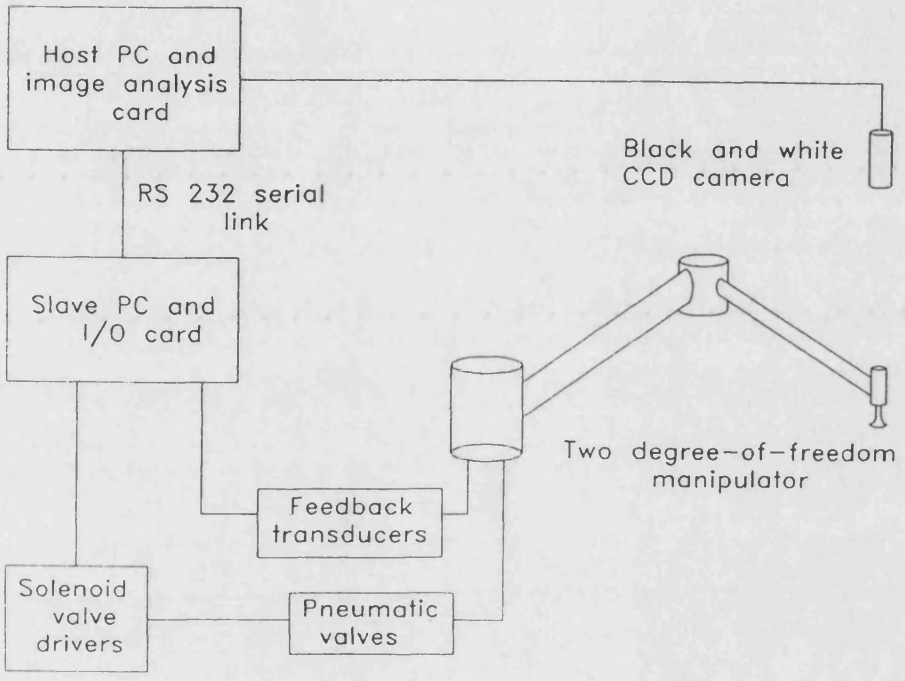

Figure 8.1 Schematic diagram of demonstration system

8.1 High level control

8.1.1 High level language

The high level control software, which was initially developed by another worker for an automatic plant micro-propagation system behaved as a program interpreter to interpret all user messages. It was written in 'C' and contained a number of features which are standard to general robot systems. These include user interfaces, a text editor and some command functions such as MOVETO and WHERE which caused the robot to move or display its position respectively. In addition, it was necessary for the author to write new functions specific to the horticultural manipulator. These included functions to perform operations such as coordinate transformations, end-effector control, calibration procedures and at the highest level, functions to perform the packing demonstration.

8.1.2 Coordinate transformations

One of the key additional functions required of the high level control was to transform between vision co-ordinates, which were Cartesian, to robot co-ordinates which were polar. The geometry was simplified by arranging the two link lengths to be the same and by the fact that strokes were less than 180° making the structure determinate. The principle behind the transformation outlined in Appendix E was to convert Cartesian co-ordinates to polar co-ordinates around axis 0. The polar radius R_a defined joint 1 angle and the polar angle defined joint 0 angle.

8.1.3 Joint angle calibration

Transformations from polar manipulator joint co-ordinates to Cartesian vision co-ordinates and vice versa were performed using the simple geometric relationships

outlined in Appendix E. However non-linearities, notably in the joint position potentiometers, caused errors in absolute accuracy. The +/- 0.5% linearity specification of the potentiometers led to 0.7° error, equivalent to roughly 6 mm error in absolute position. One could argue that even this relatively poor figure would have been acceptable for the chosen demonstration, as it did not affect repeatability, which was all that matters when placing into pre-taught positions. Also within the vision guided area where accuracy was important the vision to robot calibration would to a large extent have calibrated these non-linearities out. However, a simple calibration procedure was devised in order to widen the manipulator's capability. Accordingly the rotary stroke of each joint was sub-divided into 14 roughly equal sectors. For each of the 15 joint angles defining these sectors, actual angles were matched to 12 bit joint transducer readings and stored in a look up table. In making a co-ordinate transformation, the two nearest calibration angles were taken from the look up table and linear interpolation performed between them.

For example:

$$Pos_0(x,y) = Pos_0(n-1) + \frac{[Pos_0(n) - Pos_0(n-1)]\,[\alpha_0(x,y) - \alpha_0(n-1)]}{[\alpha_0(n) - \alpha_0(n-1)]} \qquad (8.1)$$

where: $\alpha_0(x,y)$ = Joint 0 angle for Cartesian position x,y

$Pos_0(x,y)$ = 12 bit transducer output for Cartesian position x,y

n = look up calibration table index where the values for (x,y) fall between n and n-1

8.1.4 Computer vision

A version of the same high level robot control software was run on the host PC's which contained the image grabbing card and included functions relating to image analysis. Image resolution was 512 x 512 pixels with 0 to 255 grey levels. The monochrome camera was mounted 1.1 m vertically above the working surface giving a 0.4 x 0.5 m

field of view and so providing a resolution of slightly better than 1 mm. The general strategy used to locate tomatoes was based on one originally developed for mushroom identification [Tillett R. D. and Batchelor, 1991]. First, a tomato centre was estimated by locating a bright area in an image processed with a relatively high threshold value. This technique worked well, because tomatoes have a generally convex shape which when lit from above acts as a Lambertian reflector. Viewed from above, the centre of the tomato appeared brighter than its sides. The image was then processed using a lower threshold value to obtain another binary image. A chain code method [Rosenfeld and Kak, 1982] was then used on this image starting from a tomato centre, proceeding outward until an edge was detected and then using knowledge that tomatoes appear approximately circular to track round its outline.

Once the chain code information of the tomato's outline had been gathered, the shape, location and size of the tomato were calculated. The results of applying the algorithm to a tomato image Figure 8.2 (a) are shown in Figures 8.2 (b), (c) and (d). Figure 8.2 (b) shows tomatoes were well separated using a high threshold value; Figure 8.2 (c) shows how the identified tomatoes matched the original image; Figure 8.2 (d) shows the final located tomatoes which are numbered in order top to bottom, left to right.

8.1.5 Vision to robot calibration

The calibration procedure used was previously applied to some vision guided micro-propagation robotics [Tillett R. D., 1989]. It compensated for rotational, offset and scalar differences between robot Cartesian and vision coordinates. This procedure resulted in the derivation of six linear interpolation constants which require six equations for solution. These can be obtained by selecting three points within the field of view. However, in this application the non-linearities in the video camera system due to lens distortion were known to be significant. To reduce the effect of these, the camera field of view was divided into eight sectors using nine points and calibration

performed independently within each. The position of the calibration points is illustrated in Figure 8.3.

(a) (b)

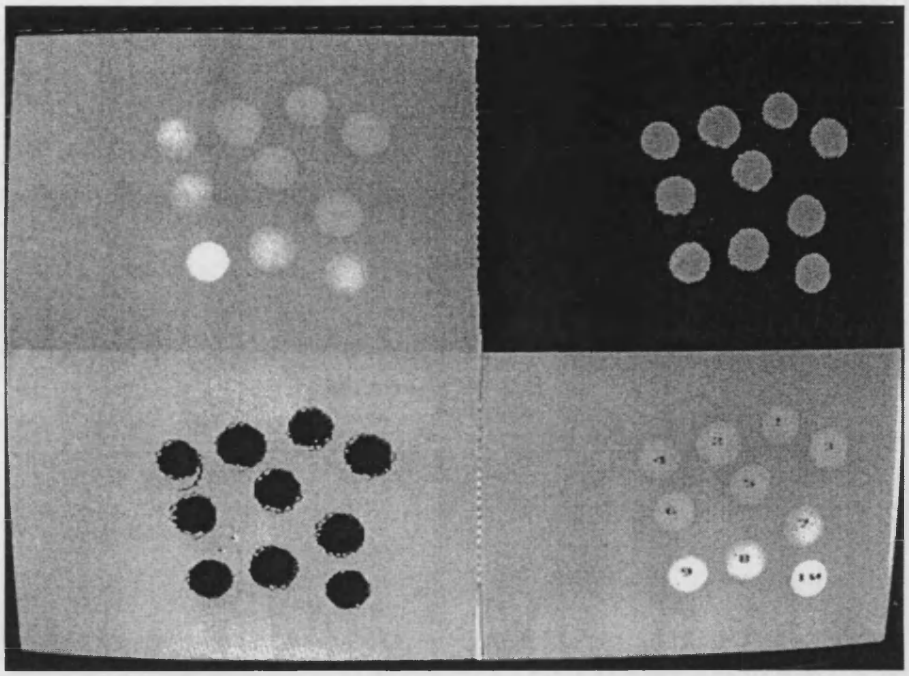

(c) (d)

Figure 8.2 Tomato location algorithm

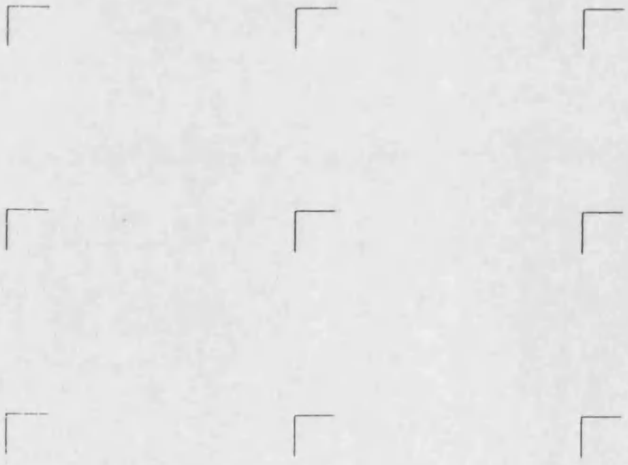

Figure 8.3 Vision to robot coordinate calibration pattern

8.2 Experimental evaluation of overall system

8.2.1 Repeatability

The repeatability of the manipulator as a whole was assessed by sending the arm under dynamic control to the same co-ordinates and measuring actual position relative to a nominal point marked on the bench. A sequence of nine points was chosen to cover the full working envelope. Return to each point was demanded five times and position was measured to the nearest millimetre in x and y co-ordinates according to a Cartesian co-ordinate frame for which the axis of joint O formed the origin as illustrated in Figure 5.17 (a). The standard deviation in position at each point individually and overall was then calculated.

As one would expect from geometrical considerations, the relative errors in x and y were dependent on position. In one extreme, with joint 1 almost fully extended and the arm end point near the x axis, the standard deviation in x was recorded as 1.8 mm and 0 mm in y. Similarly, with the arm remaining fully extended but rotated by approximately 70° towards the y axis, the standard deviations were calculated as 0.7 mm in x and 1.3 mm in y. Taken as an average over the entire working envelope, the repeatability expressed as a standard deviation was 1.1 mm in x and 0.7 mm in y. If error was normally distributed, one would have expected approximately 99% of moves to be within 2.5 standard deviations of the mean position, ie within 3.3 mm in x and 1.8 mm in y. Of the 45 measurements used to obtain this result the peak error was 3 mm in x and 2 mm in y.

As discussed in Chapter 6.4.2 repeatability could have been improved by a combination of higher resolution A to D conversion and better quality potentiometers. For the configuration described here the linear resolution of axis 0 at the end-effector with a fully extended manipulator (0.7 m radius) was 0.5 mm. Neglecting noise on the potentiometer signal this could have been reduced to 0.1 mm by increasing A to D

resolution from 12 to 14 bits. Clearly linear resolution was also directly related to arm link lengths.

8.2.2 Accuracy under vision guidance

Having established the repeatability of the manipulator over the whole range of movement in Chapter 8.2.1, accuracy and repeatability in the vision field of view is considered here. Accuracy in this context is considered relative to points identified on the imaging system. In order to measure accuracy experimentally, the field of view was marked out by an array of five by five points (25 in all, of which 24 were used) each defined by the intersection of two lines which could be seen on an image generated by the camera. For convenience, nine of these points were also used to calibrate the camera to robot co-ordinates as described in Chapter 8.1.5. Once the system had been calibrated, an image of the test points was taken and a cursor was guided manually to each point in turn recording the robot co-ordinates calculated by the image calibration algorithm at each point. In order to reduce experimental error introduced by uncertainty over the precise point position due to the poor clarity and pixel resolution of the image, each point was recorded twice and a mean co-ordinate used. These co-ordinates were then entered into the manipulator controller which sequenced from one point to the next. At each point, end-effector position was measured to the nearest millimetre relative to the original grid, in both x and y co-ordinates. This procedure was repeated four times.

Analysis of these results gave an overall rms error in x of 2.1 mm and 2.0 mm in y with a standard deviation in x of 0.7 mm and 0.6 mm in y. The standard deviations which reflect the repeatability of the manipulator are better than those calculated in Chapter 8.2.1. This is to be expected, as the vision-to-robot accuracy trials were conducted over a limited area in which the geometrical configuration was favourable. Using these figures and assuming that the distribution of error due to repeatability was normal, we could expect 99% of moves to be repeatable to within 2.5 standard deviations. Over the

camera field of view this corresponds to 1.8 mm in x and 1.5 mm in y.

In addition to dynamic and joint measurement repeatability, there was some variability in vision-to-robot location error, for which only overall mean values have been stated. This variability has not been quantified due to the difficulty of dissociating it from dynamic and joint measurement repeatability. However, since only one of the 96 data points exceeded an error of 5 mm in x or 4 mm in y, it would have been reasonable to expected all but a limited number of vision guided moves to have reached their target within these limits. These figures included experimental measurement error in both vision and manipulator positions, which were thought to contribute approximately 1 mm to maximum errors. Actual accuracy may therefore be understated slightly.

9 Demonstration Application

The scope of potential applications for horticultural robotics in general is, as was indicated in Chapter 2, very wide. It ranges from fruit harvesting to micro-propagation. The experimental manipulator at the stage of development described here had two degrees-of-freedom, which limited applications to those which require fully proportional movement on one plane only. Vertical movement, which need not be fully proportional, could be provided within the end-effector. Examples of such applications include transplanting, mushroom harvesting or fresh produce packaging. The latter was chosen as it is a very generic task which can be conducted in at least partially controlled lighting conditions, so reducing some of the problems associated with image analysis. Tomatoes were chosen as a specific crop as they are of commercial importance to the UK industry and are available year round for experiments. Alternative techniques using conventional machinery for packaging tomatoes do exist, but they do not offer the flexibility of a robotic system in terms of an ability to pack a very wide range of produce sizes into a variety of different packs. Flexibility is a generic feature of robotic systems and the experimental device could equally well have been used to pack a wide variety of products. The work described in this Chapter is also covered in Tillett et al, 1995. The objectives of the work described in this Chapter were as follows:

- To demonstrate that the low-cost experimental manipulator was capable of performing real horticultural tasks.

- To design an end-effector which was simple yet capable of carrying out the tomato packing task.

- To develop a strategy for conducting the task and to evaluate its performance experimentally.

9.1 End-effector design

The specification for the end-effector was that it should be a lightweight device capable of handling without damage a range of common fresh tomato size grades, that is diameters ranging from about 35 mm to 70 mm. It also had to be capable of working despite some misalignment and of selecting an individual from within a group, some of which may have been touching.

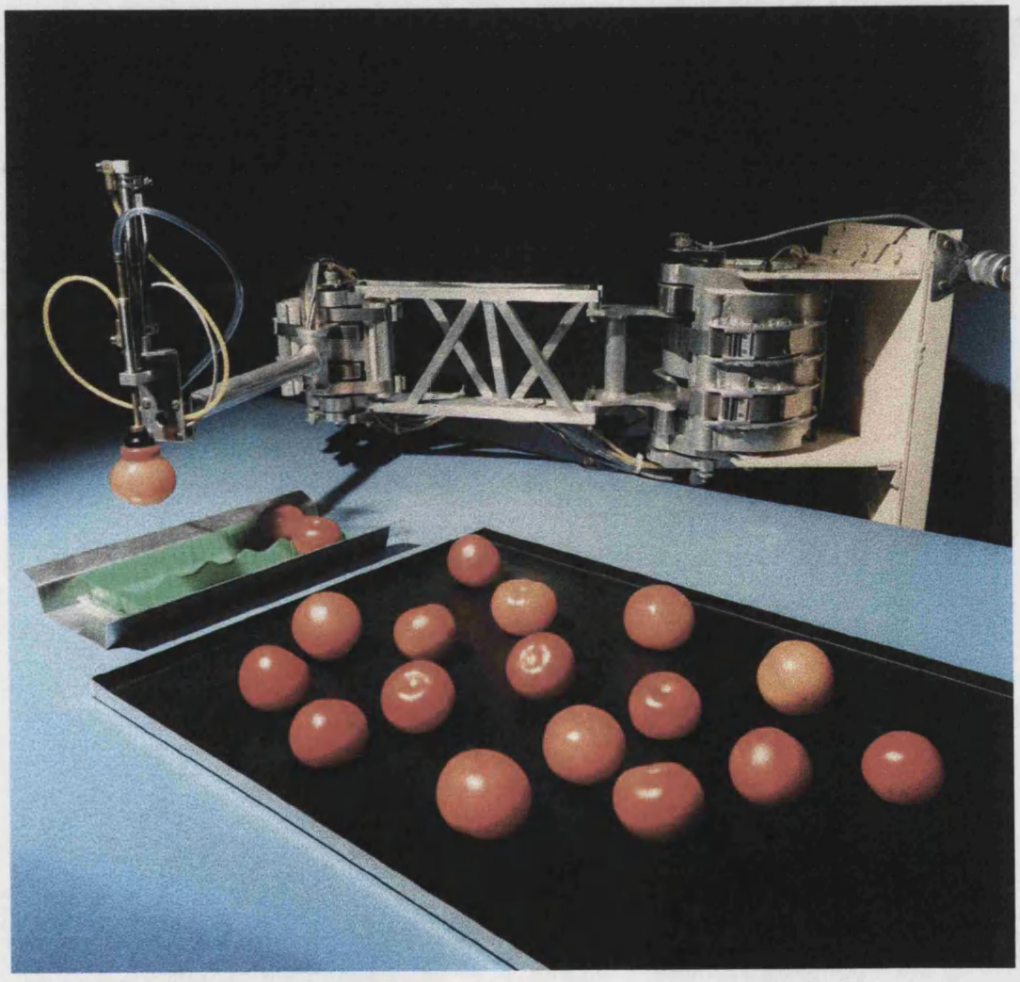

Figure 9.1 Experimental two degree-of-freedom manipulator packing tomatoes

The end-effector assembly, which was mounted 0.4 m from the smaller manipulator joint consisted of a 10 mm diameter non-rotating pneumatic cylinder and a sprung vacuum tube to which a suction-cup was attached. The arrangement is illustrated in Figure 9.1. The 100 mm stroke of the cylinder was chosen to provide adequate clearance when raised and carrying a large tomato, and to extend far enough down to be sure of coming into contact with a small tomato. Over-travel of the fixed stroke assembly was taken up first by the bellows in the suction-cup and then by the spring which pushed the suction-cup and vacuum tube down relative to the cylinder rod. Digital feedback was provided by reed switches on the cylinder which were activated by piston movement. A vacuum detection switch was used to indicate when the suction-cup had sealed onto something. The rate of piston movement in each direction was set by pneumatic restrictions. Piston movement and suction on/off were achieved with conventional pneumatic solenoid valves which were controlled via suitable drivers from the PC digital I/O.

Suction-cups have been used with some success both in industry and research to handle a variety of horticultural produce including apples [Bourely et al., 1990], citrus [Harrell et al., 1990; Juste and Fornes, 1990], mushrooms [Reed and Tillett R.D., 1994] and tomatoes [Balerin et al., 1991], the latter as part of a harvesting research project. Suction-cups are simple devices which can be made to satisfy all the criteria listed above and were therefore chosen for this application. Suction-cups to handle flat objects such as paper or sheets of glass are normally fairly stiff. These devices have insufficient compliance to conform to the shape of curved materials and fail to lock on. To overcome this, suction-cups with flexible skirts and one or more bellows are produced. Trials showed that a 30 mm diameter double bellows cup made from food grade silicon rubber performed best. This suction-cup was tolerant to misalignment of up to approximately 70% of the difference between tomato and suction-cup radii. An interesting feature of handling near spherical objects in this way is that initial misalignment is compensated as the bellows pulls the object into alignment with the end-effector. This effect is illustrated in Figure 9.2.

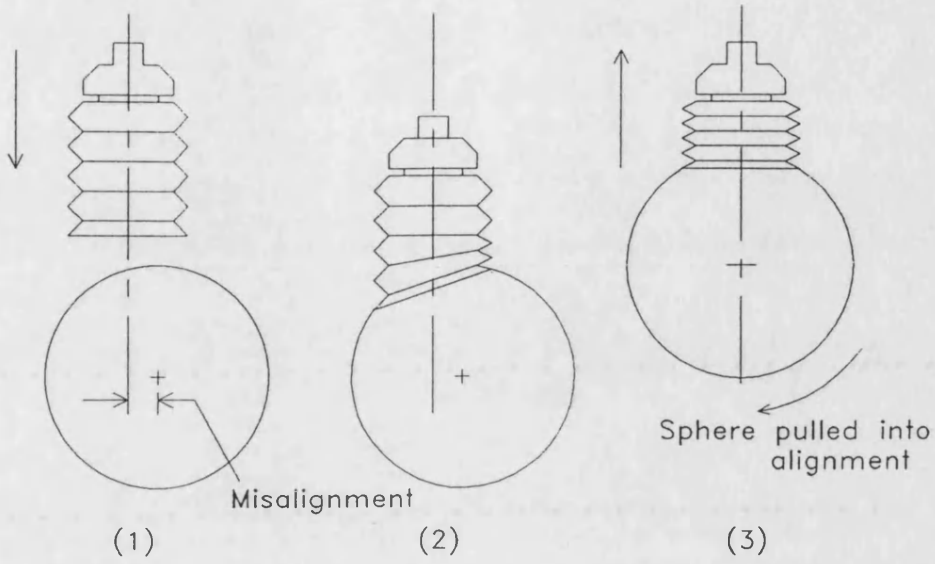

Figure 9.2 Suction-cup alignment correction

The skirt and bellows of the suction-cup were found to have sufficient compliance to seal over the indentation left after the stem is removed. Unfortunately, if the stem leaves are left on the tomato the seal may be broken, resulting in a failure to pick up. Although it is not necessary to leave the stem leaves in place for culinary or storage purposes it is regarded as an important marketing point. From a commercial point of view an inability to function on tomatoes with stems intact is a serious drawback. To overcome this problem an end-effector with three 20 mm diameter cups arranged in an equilateral triangle was devised. If centred over a tomato with stem uppermost it is likely that at least one of the suction-cups would lock on. This did provide a limited degree of success. However, the tomato was then centred on whichever cup sealed first, or part way between two if a pair locked on together. The resulting indeterminacy in position gave unsatisfactory results. It might have been possible to overcome this problem if independent pressure switches for each suction cup were used to deduce where the tomato was located. This technique might have been extended to picking up multiple fruit from a random selection in a bin or in a tray, possibly without vision guidance, though this option was not pursued.

Initial trials of a technique for handling tomatoes with stem leaves intact showed that it would be possible to pick-up successfully if the approximate position of the leaves were known. The method involved deliberately offsetting the end-effector away from the stem, lowering the suction-cup so that it partially made contact, then moving the end-effector laterally towards the stem so that the tomato rolled onto the suction-cup. Compliance in the suction-cup bellows ensured that accurate positioning was not critical to this operation. Automatic picking using this technique was not possible as the image analysis algorithms to locate stem leaves had not been developed though this was known to be feasible. All trials described here have been conducted on tomatoes from which the stems leaves were removed. Further work would be required if this specific task was to be done commercially.

9.2 Task strategy

The process followed in this application started with the presentation of a random distribution of tomatoes in a picking area. Commercially the picking area might have been a conveyor belt, but for experimental purposes a simple tray, painted black for colour contrast, was used. A monochrome CCD camera was placed vertically above the picking area to take images of the tomatoes and transmit them as a video signal to the host PC which contained the image grabber card. The image analysis algorithm running on this PC calculated the size and location of tomatoes within the field of view. This information was sent down a serial line to the slave PC which ran the dynamic and high level control code. The high level control algorithm decided which tomatoes were to be packed on the basis of size grade. It worked from top right to bottom left and used the dynamic control algorithm to set the manipulator in motion to pick the tomatoes. The co-ordinates of the packing area, which was adjacent to the picking area, were pre-recorded and coincided with a jig containing a plastic tray of a type commonly found in supermarkets. The feeding of empty trays was not automated and so the robot stopped when the tray was full or it had run out of appropriately sized tomatoes.

9.3 Performance

Trials were also conducted to establish the performance and reliability of the system as a whole. The task chosen for this trial was the packing of loose, randomly organised tomatoes into a plastic tray of eight. A total of twenty trays were packed with a mean cycle time of 20.7 s. Of the 160 tomatoes packed, there were only four failures to pick up individual tomatoes. However, since the vision system had identified alternative tomatoes and the robot had detected the failures, these were recovered automatically and all twenty trays were filled. The failures that did occur were all as a result of the suction-cups failing to make a seal with the fruit. This was most likely to occur where manipulator position error and tomato stem indentation position combined to require the suction-cup to distort more than usual to make a seal. It is thought that the end-effectors vertical speed, vacuum pressure and flow rate were also be influences, though no tests were conducted to quantify the effect of these factors. No assessment was made of the damage to the tomatoes, although none was evident except in very ripe fruit where skins occasionally split after repeated handling by the suction-cup.

10 Conclusions

This research has covered a broad range of topics as indicated by the points below. However the most significant novel aspects are concerned with the analysis and design of the flexible rotary actuator. There are two aspects of particular importance. The first is concerned with the identification of sources of hysteresis and the development of design techniques which minimise them. The second covers modelling of geometric changes which cause the output torque to vary with stroke. This led to a novel cam compensation technique allowing torque to remain constant over the full stroke. Together these innovations considerably improve the performance of the actuator as demonstrated experimentally.

- A need to maintain the competitiveness of the UK horticultural industry combined with demand for consistent product quality and improved worker welfare are likely to provide a requirement for horticultural robots in the longer term.

- In the current economic environment the cost of industrial robotic equipment is difficult to justify for the majority of potential applications. Furthermore, industrial robot technology only goes part way towards meeting horticultural needs, particularly with respect to robustness and hygiene, though in general accuracy is over specified.

- Financial justification is easier for applications which are not seasonal or have long seasons. Tasks which can be achieved with relatively simple low-cost technology are similarly favoured. Packing of horticultural products into supermarket packs is one such application.

- Pneumatic robotic devices potentially offer low-cost, hygiene and robustness. Simulation and experimental work has shown that adequate dynamic performance can be achieved for many of the simpler applications.

- Rotary pneumatic drives provide the most flexibility in work space layout. They are also easier than linear drives to encapsulate for reasons of hygiene. Existing rotary pneumatic actuators are unsuited to horticultural robot applications and so an alternative direct drive robot joint has been developed.

- The kinematic characteristics the basic actuator from which the flexible robot joint was developed have been analysed and are now well understood. This knowledge has been used in the design process to improve performance. In particular rubber-induced hysteresis has been reduced from +/-12% to +/-3% and the output torque characteristic modified to remain constant over the 140 degree stroke.

- The problem of controlling the flexible rotary actuator is essentially similar to that of controlling other direct drive pneumatic actuators. The modified PI controller with differential pressure feedback combined with +/- 8% Coulomb friction provided joint repeatability of +/- 0.1° with a typical settling time of 0.8 s which is regarded as adequate for many applications, though capable of improvement.

- A non-linear dynamic model of the rotary flexible joint has been derived and implemented in the SIMULINK/MATLAB simulation environment:

  The simulation model is a sufficiently accurate representation of the experimental system to provide useful insights into design factors affecting performance.

  System stability can be improved by the addition of Coulomb friction at the cost of increased steady-state error for given levels of proportional-to-error gain. Used in conjunction with higher proportional gains particularly with non-linear control techniques such as gain-scheduling, Coulomb friction can improve overall point-to-point position control performance.

During continuous unidirectional motion friction acts as a constant offset load which does not damp out oscillations. This combined with large system time constants makes pneumatic servo systems less well suited to applications such as profile following or pick-and-place of moving objects.

In designing flexible actuators it is desirable to minimise hysteresis due to the distortion of rubber. Hysteresis deliberately applied to improve dynamic stability should be adjustable and as near as possible to pure Coulomb friction.

- An experimental manipulator has been constructed using two of the flexible joints with 0.4 m links. High level control and vision guidance have been added to facilitate evaluation. Overall the manipulator meets criteria for low-cost and robust construction, combined with adequate performance. Table 10.1 contrasts the performance achieved with the specification for general horticultural and industrial manipulators set out at the start of this thesis in Table 3.1

  In trials to establish manipulator accuracy under vision guidance, rms error was calculated to be 2.1 mm in x and 2.0 mm in y with standard deviations of 0.7 mm and 0.6 mm respectively.

  The manipulator has been successfully demonstrated packing loose tomatoes into plastic trays of eight under vision guidance. This task is performed in about 21 s with high reliability.

- The experimental manipulator described would form a suitable basis for a commercial two degree-of-freedom device, conducting vision guided horticultural pick-and-place operations.

Feature	Horticultural use	Industrial manufacturing use (Puma 562)	Horticultural manipulator performance
Speed	1.5 ms^{-1}	1.2 ms^{-1}	0.8-2.0 m/s
Acceleration	20 ms^{-2}	20 ms^{-2} (estimated)	24 ms^{-2}
Reach	0.7 m	0.864 m	0.77 m
Payload	1 kg	4 kg	> 2 kg
Dynamic (trajectory) accuracy	± 20 mm	± 1 mm (estimated)	not measured
Static accuracy / repeatability	± 2 mm	± 0.1 mm	2.3 mm
Typical (half stroke) point-to-point settling time	1 s	2 s (estimated)	1 s
Guidance / sensors	Vision and others	Proximity detectors	Vision / potentiometer
Actuator type	Pneumatic	Geared DC servo motors	Flexible rotary pneumatic actuator
Degrees of freedom	3	6	2
Geometrical configuration	Spherical with common vision and mechanical coordinates	Revolute	Revolute
Robustness	Capable of withstanding collisions in a semi-structured environment	Not capable of withstanding collisions	Compliant direct drive
Washability	Hose down	Not washable	Potentially, though sensors need protecting
Tolerant to dust and dirt	Yes	Not tolerant	Yes
Hygiene	Required for some applications	Not easily converted	No, though could be covered

Table 10.1 Typical manipulator specifications and achieved performance

11 Future Work

The simulation work has shown that the experimental actuators are oversized for the payloads used in the demonstration application. There is a need for work, some of which could be done in simulation, to investigate the optimum sizing for actuators and valves in order to minimise response times whilst retaining some tolerance to minor external loads and variations in inertial payloads.

Experience with other pneumatic systems and in simulation suggests that it would be possible to improve the dynamic performance of the experimental manipulator. This might be achieved through alternative control algorithms, sliding mode control or fuzzy logic for example, and might employ alternative feedback signals such as the use of transient pressure feedback. Some improvements might also be achieved using alternative correctly sized flow control valves.

Compensation for interaction between axes would improve overall performance. This might be achieved through model based predictions to provide compensating inputs or alternatively accelerometers might be used to provide appropriate feedback signals. Use of such compensation techniques would become increasingly important as the number of degrees-of-freedom increase. In applications requiring proportional movement in a vertical plane allowance would have to be made for the effect of gravity on valve bias values as geometrical configuration changes. The use of asymmetric actuators or special cam compensation profiles may have a role in reducing the effects of gravity.

Whilst the design of the joint is inherently tolerant to dirty and moist environments, no special effort has been made to eliminate dirt traps that would be required in food processing applications. Hygienic operation could probably be achieved by enclosing the joint in a flexible cover, though further work would be required to establish the feasibility of this approach.

References

[Backé and Eschmann, 1993] Backé W. and Eschmann R. SSP - A simulation program for pneumatics. 6th Bath Int Fluid Power Workshop, pp 64 - 77, September 1993.

[Baldur and Blach, 1985] Baldur R. and Blach W. Inflatable manipulator RI/SME Robots 9th Conference, Detroit, 2-6 June 1985.

[Balerin et al., 1991] Balerin S., Bourely A. and Sevila F. Mobile robotics applied to fruit harvesting: The case of greenhouse tomatoes. Proceedings of the 1991 Symposium on Automated Agriculture for the 21st Century, ASAE, Chicago, Illinois, 503-517, 16-17 December 1991.

[Baylou, 1987] Baylou P. Agricultural Robots. 10th Triennial world congress of the Int Fed of automatic control, Pergamon, Oxford, 114-122, 1987.

[Billington and Grundon, 1990] Billington W. P. and Grundon P. M. Cutting and/or manoeuvring apparatus and methods. UK Patent Application 90163239, Date of filing 25 July 1990.

[Boddy and Taylor, 1992] Boddy C. L. and Taylor J. D. Advanced techniques for robot arm control. IMechE Mechatronics Forum, University of Salford, 27th May 1992.

[Bourely et al., 1990] Bourely A., Rabatel G., Grand D'Esnon A. and Sevila F. Ten years of CEMAGREF experience on apple, grape and orange. Ag Eng 90, Agricultural Engineering International Conference, Berlin, Germany, October 1990

[Burrows, 1969] Burrows C. R. Effect of position on the stability of pneumatic servo mechanisms. Journal of Mechanical Engineering Science, 11 (6), 615-616, 1969.

[Chou and Hannaford, 1996] Chou C. and Hannaford B. Measurement and modelling of McKibben pneumatic artificial muscles. IEEE Transactions on robotics and automation, Vol.12, No. 1, February 1996.

[Cleary, 1995] Cleary M. Rise of the gourmet robots. Professional Engineering, 20th Sept 1995.

[Deleplanque et al., 1985] Deleplanque H., Bonnet J. G. and Postaire J. G. An intelligent robotic system for in vitro plant production. Proceedings of 5th International Conference on Robotic Vision and Sensory, Amsterdam, Netherlands, 29-31 October 1985.

[Dils, 1992] Dils M. Air springs vs air cylinders. Machine Design, May 7, 96-98, 1992.

[Foroughi et al., 1987] Foroughi F., Rahnejat H. and Bera H. Tactile sensors for robot handling . Proceedings of the Institute of Mechanical Engineers, Vol 201, No. B1, pp 51-58, 1987.

[Frost et al., 1993] Frost A.R, Street M.J. and Hall R.C. The development of a pneumatic robot for attaching a milking machine to a cow. Mechatronics Vol.3. No. 4. pp 409-418. 1993.

[Fujita, 1989] Fujita N. The application of robotics to mass propagation systems. 40th Meeting of the American Tissue Culture Association, Orlando, USA, 11-14 June 1989.

[Grand D'Esnon et al., 1987] Grand D'Esnon A., Rabatel G., Pellenc R., Journeau A. and Aldon M. J. MAGALI: A self-propelled robot to pick apples. ASAE Paper 87-1037, 1987.

[Gunkel and Throop, 1992] Gunkel W.W. and Throop J.A. Robotic pruning of grapevines. Paper presented at the 1992 Vineyards and Technical Seminar, Wineries Unlimited, Philadelphia, February 1992.

[Hague and Tillett, 1996] Hague T. and Tillett N. D. Navigation and control of an autonomous horticultural robot. Mechatronics Vol. 6, No. 2, pp.165-180, 1996.

[Hall et al., 1994] Hall R. C, Street, M. J and Spencer D. S. Robotic milking. International workshop on advanced robotics and intelligent machines research. University of Salford, Manchester, 28-29 March, 1994.

[Harrell, 1987] Harrell R. Economic analysis of robotic citrus harvesting in Florida Transactions of the ASAE, Vol 30 (2), 298-304, 1987.

[Harrell et al., 1990] Harrell R. C., Adsit P. D., Munilla R. D. and Slaughter D. C. Robotic picking of citrus. Robotica, Vol 8, pp 269-278, 1990.

[Harrell et al., 1989] Harrell R. C., Slaughter D. C. and Adsit P. D. A fruit tracking system for robotic harvesting. Machine Vision and Applications, 2: 69-80, 1989.

[Harris and Laurenson, 1992] Harris M. and Laurenson I. A hydraulically-actuated parallel-linking robot. Advance Vol 4, 1992.

[Hennequin and Fluck, 1987] Hennequin J. R. and Fluck P. Motorised joint. International Patent classification, PCT/GB87/00473 Filing date, 21 October 1987.

[Hennequin, 1990] Hennequin, J. R. Wheelchair mounted pneumatic manipulator. IMechE Symposium on Robotics in Medicine, 14 June 1990, IMechE HQ, London.

[Herman et al., 1992] Herman T., Bonicelli B. and Sevila F. On line predictive algorithm for high speed and power hydraulic arms. AG ENG 92, Agricultural Engineering International Conference, Uppsala, Sweden, June 1992.

[Humberg and Reid, 1989] Humberg D. S. and Reid J. F. Background Separation and Filtering for Images of Emerging Asparagus. ASAE paper no. 89-7503, Dec 1989.

[Iida et al., 1993] Iida M., Umeda M. and Namikawa K. Development of agricultural hydraulic robot. Proceedings of Int. Conf. Of Agric. Machinery and Process Eng. Souel, Korea.Vol 3, 820-829, 1993.

[Immega, 1986] Immega G. B. ROMAC muscle powered robots. Society of Manufacturing Engineers Conference on Robotics Research, Scottsdale, Arizona, 18-21 August 1986.

[Jacobsen et al., 1984] Jacobsen S. C., Wood J. E., Knutti D. F. and Biggers K. B. The UTAH/M.I.T. Dextrous Hand: Work in Progress. The International Journal of Robotics Research. Vol 3, No 4, Winter 1984.

[Juste et al., 1990] Juste F., Castillo S., Motto E., Fornes I. and Paniagua J. Contributions to Robotic Harvesting of Citrus in Spain. Ag Eng 90, Agricultural Engineering International Conference, Berlin, Germany, 24-26 October 1990.

[Juste and Fornes, 1990] Juste F. and Fornes I. Contributions to robotic harvesting of citrus in Spain. Proceedings of the AG-ENG 90 Conference. Berlin (G), October 1990.

[Kawamura et al., 1986] Kawamura N., Namikawa K., Fujivra T. and Ura M. Study on agricultural robot, Memoirs of the College of Agriculture, Kyoto University, No. 129, pp 29-46, 1986.

[Kawamura et al., 1987] Kawamura N., Namikawa K. and Fujiura T. Study on agricultural robot (vii) hand of fruit harvesting robot. Kansai Branch Report of the Japanese Society of Agricultural Machinery (In English), No. 62, pp 66-67, 81, 1987.

[Khodabandehloo, 1993] Khodabandehloo K. (editor) Robotics in meat, fish and poultry processing. Blackie Academic and Professional, Chapman and Hall, ISBN 0-7514-0087-4, 1993.

[Kondo et al., 1995] Kondo N., Fujiura T., Monta M., Shibano Y., Mohri K. and Yamada H. End-effectors for petty tomato harvesting robot. Greenhouse Environment Control and Automation, Acta Horticulturae 399, pp 239-245, 1995.

[Kozai et al., 1991] Kozai T., Ting K. C. and Aitken-Christie J. Considerations for automation of micro-propagation systems. Proceedings of the Symposium on Automated Agriculture for the 21st century, ASAE, 16-17 December, Chicago, Illinois, pp 503-517, 1991.

[Kurata, 1994] Kurata K. Cultivation of grafted vegetables 2. Development of grafting robots in Japan. HortScience, Vol. 29(4), April 1994.

[Kutz et al., 1987] Kutz L. J., Miles G. E., Hammer P. A. and Krutx G. W. Robotic transplanting of bedding plants. Transactions of the ASAE, 30(3), pp 586-590, 1987.

[Levi et al., 1988] Levi P., Falla A. and Pappalaro R. Image controlled robotics applied to citrus fruit harvesting. Proceedings of the 7th International Conference on Robot Vision and Sensory Controls, Zurich, IFS Publications, pp 327-338, 2-4 February 1988.

[Levpolz and Lofmark, 1991] Levpolz V. and Lofmark. A flexator based robotic rehabilitation exerciser M Eng Final Report, University College, London, 12 May 1991.

[Liu and Bobrow, 1988] Liu S. and Bobrow J. E. An analysis of a pneumatic servo system and its application to a computer-controlled robot. Transactions of the ASME 110, 228-235, 1988.

[Mannetje, 1981] Mannetje J. J. Pneumatic servo design method improves system band width twenty fold. Control Engineering, June, 79-83, 1981.

[Marchant et al., 1997] Marchant J. A., Hague T. and Tillett N. D. Row following accuracy of an autonomous vision guided agricultural vehicle. Computers and Electronics in Agriculture, 16(2), 165-175, 1997.

[Marchant and Moncaster, 1990] Marchant J. A. and Moncaster M. E. Robotics and automation in agriculture. Outlook on Agriculture, Vol 19, No. 4, pp 221-228, 1990.

[McKay, 1996] McKay S. Linear motors on the verge of universal acceptance. Drives and Controls, June 1996.

[Mills, 1993] Mills J. K. Hybrid actuator for robust manipulators: design, control and performance, Mechatronics, Vol. 3, No. 1, pp 19-38, 1993.

[Monta et al., 1995] Monta M., Kondo N., Shibano Y. and Mohri K. End-effectors for agricultural robot to work in vineyard. Greenhouse Environment Control and Automation, Acta Horticulturae 399, pp 247-254, 1995.

[Morgen, 1983] Morgen R. J. Steppers vs DC servomotors. Machine design, 22 September 1983.

[Namikawa et al., 1992] Namikawa K., Umeda M., Iida M. and Suguri M. Watermelon harvesting hydraulic robot. Proc of JICA-IPB 5th Int. Conf. On Eng. Application for the Development of Agric in the Asia and Pacific Region. B233-B240, Indonesia, Oct 15th, 1992.

[Naugle et al., 1989] Naugle J. A., Rehkugler G. E. and Throop A. J. Grapevine cordon following using digital image processing. Transactions of the ASAE, 31(1) pp 309-315, 1989.

[Nix, 1997] Nix J. Farm management pocketbook - 27th Edition. Department of Agricultural Economics, Wye College, University of London, 1997.

[Norman et al., 1991] Norman D. W., Throop J. A. and Gunkel W. W. Electro hydraulic robot design for mechanised grapevine pruning. ASAE paper no. 91-1598, 1991.

[Okamoto et al., 1993] Okamoto T., Kitani O. and Torii T. Robotic transplanting of Orchid protocorm in mericlone culture. ASAE Paper No 93-3090, Summer meeting, Washington, 20-23 June, 1993.

[Parrish and Goksel, 1977] Parrish E. A. and Goksel A. K. Pictorial pattern recognition applied to fruit harvesting. Transactions of the ASAE, 20 (5), pp 822-827, 1977.

[Prior et al., 1993] Prior S. D., Warner P. R., White A. S., Parsons J. T. and Gill R. Actuators for rehabilitation robots. Mechatronics Vol. 3, No. 3, pp 285-294, 1993.

[Pu and Weston, 1988] Pu J. and Weston R.H. Motion control of pneumatic drives. Microprocessors and Microsystems 12, (7), pp 373-382, 1988.

[Rabatel et al., 1991] Rabatel G., Bourely A. and Sevila F. Object detection with machine vision in outdoor complex scenes: the case of robotic harvest of apples. European Robotics and Intelligent Systems Conference, Corfu, Greece, June 1991.

[Ranky and Ho, 1985] Ranky P. G. and Ho C. Y. Robot modelling: Control and applications with software IFS (Publications) Ltd, UK, 1985.

[Reed et al., 1995] Reed J. N., He W. and Crook S. Harvesting mushrooms by robot. XIVth International congress on the science and cultivation of edible fungi. Oxford, 17-22nd Sept, 1995.

[Reed and Tillett R. D., 1994] Reed J. N. and Tillett R. D. Initial experiments in robotic mushroom harvesting. Mechatronics, Vol 4, No 3, pp 265-279, 1994.

[Rosenfeld and Kak, 1982] Rosenfeld A. and Kak A. C. Digital picture processing. Vol 2. Academic Press, London, 1982.

[Schertz and Brown, 1968] Schertz C. E. and Brown G. K. Basic considerations in mechanising citrus harvest. Transactions of the ASAE, **11**(2), pp 343-348, 1968.

[Sevila et al., 1992] Sevila F., Balerin S. and Thompson P. Control of an agricultural robotic arm based on a mobile platform. AG ENG 92, Agricultural Engineering International Conference, Uppsala, Sweden, June, 1992.

[Sevila et al., 1990] Sevila F., Baylov P. and Piquel J. C. Computer vision systems and growth modelization softwares applied to grapevine woods, as pruning robots design and control tools. AG Eng 90, Agricultural Engineering International Conference, Berlin, Germany, October 1990.

[Shearer, 1956] Shearer J. L. Study of pneumatic processes in the continuous control of motion with compressed air. Transactions of ASME, pp 233-249, February 1956.

[Simonton, 1990] Simonton W. Automatic geranium stock processing in a robotic work cell. Transactions of the ASAE, 33 (6), pp 2074-2080, 1990.

[Simonton, 1991] Simonton W. Robotic end-effector for handling green house plant material. Transactions of the ASAE, 34(6), pp 2615-2621, 1991.

[SIMULINK Users Guide, 1993] SIMULINK Users Guide. The MathWorks, Inc. April 1993.

[Sittichareonchai et al., 1989] Sittichareonchai A., Sevila F., Fatour J-M., Costans A., Brons A. and Davenel A. A robot to harvest grape: A feasibility study. ASAE paper no. 89-7084, 1989.

[Stone, 1992] Stone R. Virtual reality interfaces for telerobotics. IMechE Mechatronics Forum, University of Salford, 27th May 1992.

[Street et al., 1990] Street M. J., Hall R. C. and Wilkin A. L. A pneumatic milking robot, structure, performance and first results. Robotereinsatz in der Landwirtschaft am Beispiel des Melkens Tagung Braunschweig-Volkenrode, 5-6 December 1990.

[Surgenor, 1995] Surgenor B. W., Vaughan N. D. and Uebing M. Continuous sliding mode control of a pneumatic positioning system. 8th Bath International Fluid Power Workshop, September 1995.

[Taylor and Brooking, 1994] Taylor M. G. and Brooking G. N. Y-cut dressing of sheep carcases using a robot. MIRINZ 28th Meat Industry Research Conference, Auckland, New Zealand, pp 181-186, 1994.

[Thollot and Bonicelli, 1992] Thollot J. and Bonicelli B. Distributed control architecture on hydraulic robotized arms. AG ENG 92. Agricultural Engineering International Conference, Uppsala, Sweden, June 1992.

[Thompson et al., 1995] Thompson P., Rombaut M., Rabatel., Pierrot F., Liegeois A. and Sevila F. Design and control of mobile manipulator for weed control. Int. Conf. Advanced Robotics, Barcelona, 20-22 September 1995.

[Tillett, 1993a] Tillett N. D. Robotic Manipulators in Horticulture: A review. Journal of Agricultural Engineering Research, 55, pp 89-105, 1993.

[Tillett, 1993b] Tillett N. D. Flexible pneumatic actuators for horticultural robots - A feasibility study. Mechatronics, 3 (3), pp 315-328, 1993.

[Tillett, 1995] Tillett, N. D. Robotics and food - low margins need different solutions. Industrial Robot, Vol. 22 No. 5, 1995.

[Tillett et al., 1995] Tillett N. D., He W. and Tillett R. D. Development of a vision guided robot manipulator for packing horticultural products. Journal of Agricultural Engineering Research 61, pp 145-154, 1995.

[Tillett and Lane, 1992] Tillett N. D. and Lane A. G. A gantry crane system for handling outdoor container grown nursery stock. Journal of Agricultural Engineering Research. 51, pp 285-296, 1992.

[Tillett et al., 1992] Tillett N. D., Miles S. J., Holt J. B., Wilkin A. L. and Scott M. A. An experimental automatic repotting machine for hardy ornamental stock. Journal of Agricultural Engineering Research 53, pp 289-303, 1992.

[Tillett et al., 1994] Tillett N. D., Vaughan N. and Bowyer A. An improved flexible pneumatic joint for horticultural robots. Mechatronics, 4 (7), pp 653-671, 1994.

[Tillett et al., 1997] Tillett N. D., Vaughan N. and Bowyer A. A non-linear model of a rotary pneumatic servo system. Proc. Instn Mech. Engrs, Part I, Vol. 211 No. 12, 1997.

[Tillett, R. D., 1989] Tillett, R. D. A calibration system for Vision-guided Agricultural Robots. Journal of Agricultural Engineering Research, 42, pp 267-273, 1989.

[Tillett, R. D., 1991] Tillett R. D. Image analysis for agricultural processes: A review of potential opportunities. Journal of Agricultural Engineering Research, 50, pp 247-258, 1991.

[Tillett, R. D. and Batchelor, 1991] Tillett R. D. and Batchelor B. G. An algorithm for locating mushrooms in a growing bed, Computers and Electronics in Agriculture, Vol 6, pp 191-200, 1991.

[Tillett, R. D. and Reed, 1990] Tillett R. D. and Reed J. N. Initial development of a mechatronic mushroom harvester. I Mech E International Conference on Mechatronics: Designing Intelligent Machines, Cambridge, UK, pp 109-114, 12-13 September 1990.

[Viersma, 1980] Viersma T. J. Analysis, synthesis and design of hydraulic servosystems and pipelines. Elsevier Scientific Publishing Company, ISBN 0444418695, 1980.

[Virvalo, 1986] Virvalo T. Designing a pneumatic position servo system. Power International, pp 141-147, June 1986.

[Wallin, 1993] Wallin P. Advanced robotics in the food industry. Industrial Robot, Vol.20, No.4, pp 12-13, 1993.

[Wang, 1996] Wang H. Hybrid fuzzy logic algorithm for position control of pneumatic actuator with 3/2-way solenoid valves. Proc of the Inst of Mech Eng, Part C, Journal of Mech Eng Sc. Vol. 210 Part. 2, pp 167-176, 1996.

[Wheeler, 1990] Wheeler C. G. Harvesting of delicate produce. UK Patent Application GB 2237 491 A. Date of filing, 20 October 1990.

[Wilson, 1995] Wilson M. Developments in industrial robotics. Computing and Control Engineering Journal, pp 156-160, August 1995.

[Winters, 1990] Winters J. M. Braided artificial muscles: mechanical properties and future uses in prosthetics/orthotics. Proceedings of the 13th annual conference RENSNA, pp 173-174, 1990.

[Wolf et al., 1990] Wolf I., Bar-or J., Edan Y. and Peiper U. Developing grippers for a melon harvesting robot. ASAE paper 90-7594, 1990.

[Woodcock, 1990] Woodcock B. Picking 24 hours a day, seven days a week, 52 weeks a year .... Journal of the Mushroom Growers Association, 210, pp 204-205, 1990.

APPENDIX A - Servo-Pneumatic Valve Evaluation

A1 Introduction

Three alternative commercially available control valves each from different manufacturers are evaluated here for their suitability for a low cost agricultural pneumatic robot application. Additionally for reference a prototype Martonair flow control valve used in earlier non-horticultural work has also been included. This prototype valve was the forerunner of the M/2999 production valve which was used in the horticultural manipulator work described in this thesis. The two valves have similar characteristics, though the M/2999 had a higher flow range in its unmodified form.

The first two valves, the prototype and Isoflex valves from Martonair, both control flow by altering the position of a spool. The spool is balanced between a spring and a solenoid so that its position is proportional to solenoid current. Control of spool position is open-loop so frictional forces or other factors may result in spool position errors. The effects of friction are reduced by applying a 50 Hz signal to the solenoid causing the spool to oscillate. The principle differences between the prototype and Isoflex valves lie in their construction. The newer Isoflex valve is manufactured to higher tolerances and utilizes low friction coatings.

The third valve, manufactured by Festo, is also a solenoid operated spool valve. However, it differs from the Martonair valves in that a position transducer connected to the spool provides an internal feedback signal for closed-loop control of spool position. This makes the valve less sensitive to internal friction and other disturbances, though internal complexity and cost are increased.

The remaining device is a pressure regulating valve manufactured by SMC. The valve consists internally of two poppet valves which control the flow of air from exhaust and supply pressure ports to the outlet according to internal mechanical feedback

mechanisms whose set point is determined by the input signal. Cylinder position can be controlled by using two proportional valves one each side of the piston to control the differential pressure, or using one proportional valve and a fixed pressure regulator. The latter has been chosen for this evaluation.

The approach taken was to measure key parameters such as hysteresis and flow range, and to assess performance in a simple control system. The experimental approach is described in Section A2 and the results given in Section A3. In Section A4 there is further discussion of the results and related issues such as cylinder selection and control algorithm design. Overall conclusions are summarised in Section A5.

A2 Valve evaluation

A2.1 Apparatus

A simple mechanism consisting of a direct link between a cylinder and output arm as illustrated in Figure A.1a was chosen for these experiments. The output arm was linked to a fixed frame by a universal joint. A link which joined the output arm part way along its length supported it vertically. The 1.5 kg payload was chosen to be representative of potential payloads. The cylinder of a standard type manufactured by Martonair had a 4 cm diameter and a 10 cm stroke. Position was measured using a Penny and Giles LVDT of similar stroke providing a 0-10 V output.

The controller was PC based using a proprietary PC30B interface board featuring 12 bit analogue input and output. The algorithm ran at 5 ms intervals triggered from a hardware interrupt and was written in 'C'. The controller was a linear one that can be expressed as follows:-

$$U_{out} = k_c (\theta_o - \theta_d) - k_v \dot{\theta}_o - k_a \ddot{\theta}_o + N \qquad (A.1)$$

Where U_{out} = controlling voltage to valve

k_e = proportional to error gain

k_v = velocity gain

k_a = acceleration gain

N = neutral valve

θ_o = output position

θ_d = demand position

The output U_{out} was constrained between limits U_{upper} and U_{lower}.

Whilst the performance could have been improved by a more sophisticated control algorithm, the simplicity of this was preferable for the purpose of comparing valves.

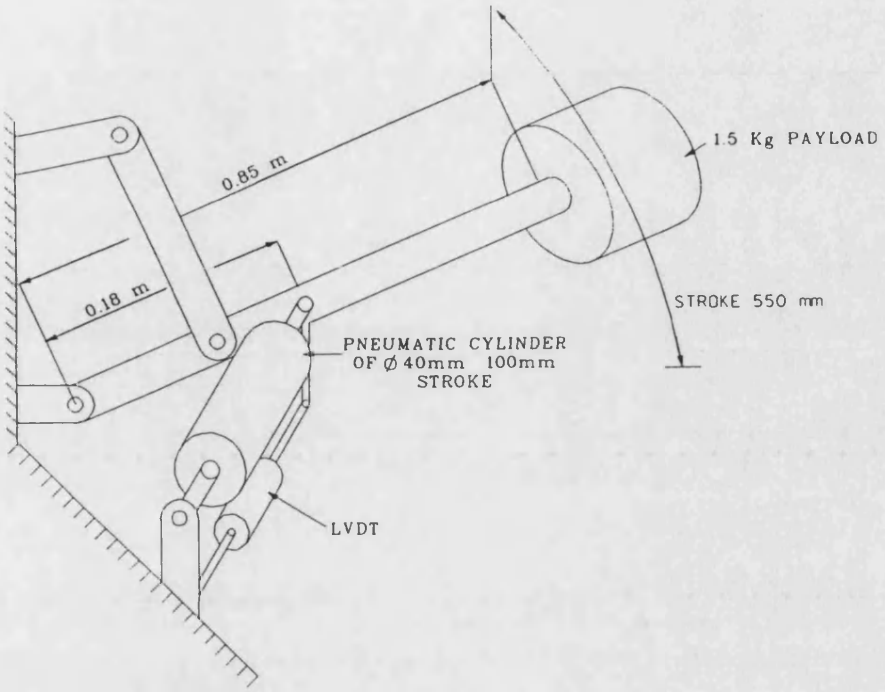

Figure A.1a Mechanical apparatus.

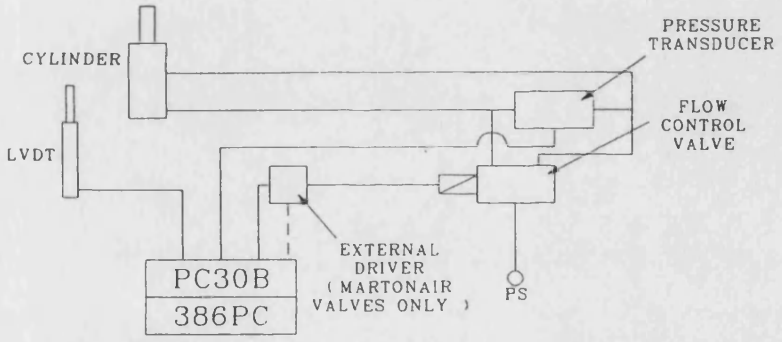

Figure A.1b Schematic for flow control valves.

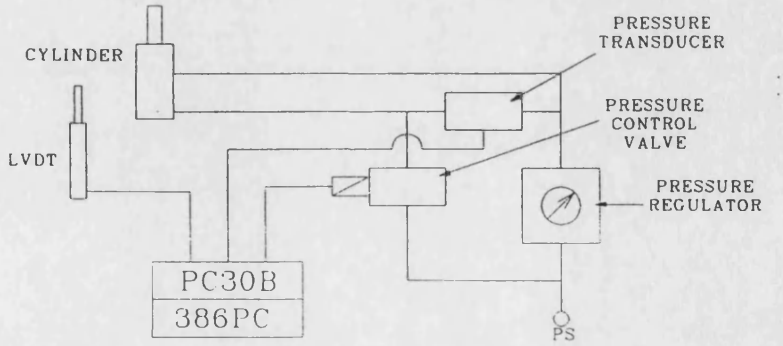

Figure A.1c Schematic for SMC pressure control valves.

The control algorithm included the facility to alter gains externally from potentiometers during experimental runs. It also had the facility to log data for up to 40 seconds (at 20 ms intervals). This data could include all control variables as well as differential pressure across the cylinder piston.

For the SMC and Festo valves the controlling voltage could be taken directly from the analogue output and power supplied from a separate 24 V supply. The Martonair valve did not come with an appropriate driver[7] and so one was constructed based on that used in the horticultural manipulator work (Figures A.1b and c).

A2.2 Procedure

A2.2.1 Hysteresis measurement

Hysteresis is an undesirable non-linearity which is likely to degrade performance. Whilst manufacturers do provide information on hysteresis, it was decided to measure it in the application situation so that a fair comparison could be made between valves. To achieve this the system was configured so that valve input voltage was controlled in open-loop mode from a potentiometer via the PC. The voltage was slowly adjusted until the cylinder just started to progressively retract and the corresponding 12 bit A to D value noted. This was repeated for the cylinder extending. The difference between these two valves represented the hysteresis of the system as a whole. That is hysteresis in the valve plus effects due to cylinder friction, which was as one would expect higher than that quoted by the manufacturers for the valve alone. Friction in the cylinders gave a jerky motion at low speed and so an assessment of when movement became progressive was a little subjective, however the results did show differences between valves.

---

[7]The standard driver introduces a 50 Hz dither signal that cannot be synchronised with the controller thus risking aliasing effects.

A2.2.2 Position control

The position control task was a sequence of five steps of varying magnitude designed to cover the range of movements encountered during teat attachment. Tuning of the controller was an iterative procedure involving adjustment of the three gains in Equation 1 and the upper and lower limits on the output. In general, output limits were adjusted to provide the rate of response required, approximately 0.7 ms^{-1}, proportional gain to give satisfactory steady state error, ± 2 mm, and the velocity acceleration terms to damp out first and higher order oscillations respectively. The desired response had little or no overshoot. In practice steady state error sometimes had to be compromised to achieve a better trade off with stability.

A2.2.3 Stiffness measurement

The stiffness of the system was evaluated by applying offset loads at the end of the arm, at a radius of 0.8 m, and recording output error. The load was applied through a hand held spring balance up to 50 N in 10 N increments. As each load level was reached there was a pause of approximately five seconds whilst the position stabilised, after which the error reading was taken. The procedure was repeated for both +ve and -ve loads. The result is expressed as a modulus of stiffness (M) defined as load applied in N (at 0.8 m radius) divided by the linear movement at the end of the arm in mm.

A3 Results

A summary of the results presented in detail below is given in Table A1.

A3.1 Martonair prototype flow control valve (for reference)

Hysteresis was found to be ± 24 counts of the 12 bit (4096) output. The upper and lower limits on output used in position control to achieve a maximum linear speed of 0.7 ms^{-1} were ± 300 counts from the null value. Thus hysteresis as a percentage of working range was 8%. The closed-loop time response illustrated in Figure A.2 revealed a well behaved dynamic response settling within one second to a steady state error of less than 2.1 mm. The modulus of stiffness (M) measured from Figure A.3 was 1.7 N mm^{-1} near the zero error point.

One of the less desirable features of this value compared to the others tested was its very high leakage flow rate at the steady state. A flow meter was placed in the air supply pipe and a reading of 14 l min^{-1} at 4 kPa recorded.

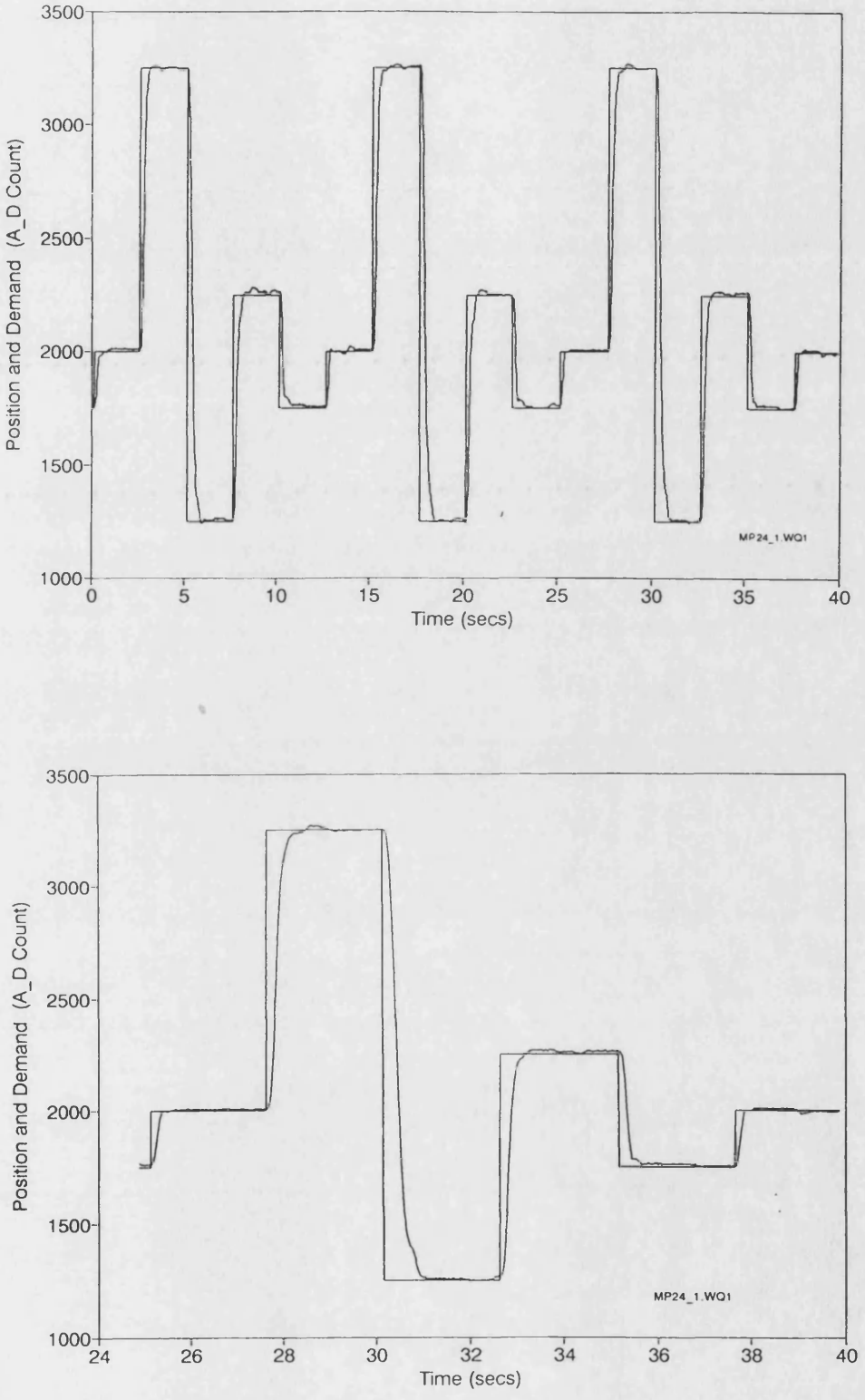

Figure A.2 Martonair prototype flow control valve time response. $k_e = 35$, $k_v = 144$, $k_a = 461$, $U_{upper} = N + 300$, $U_{lower} = N - 300$.

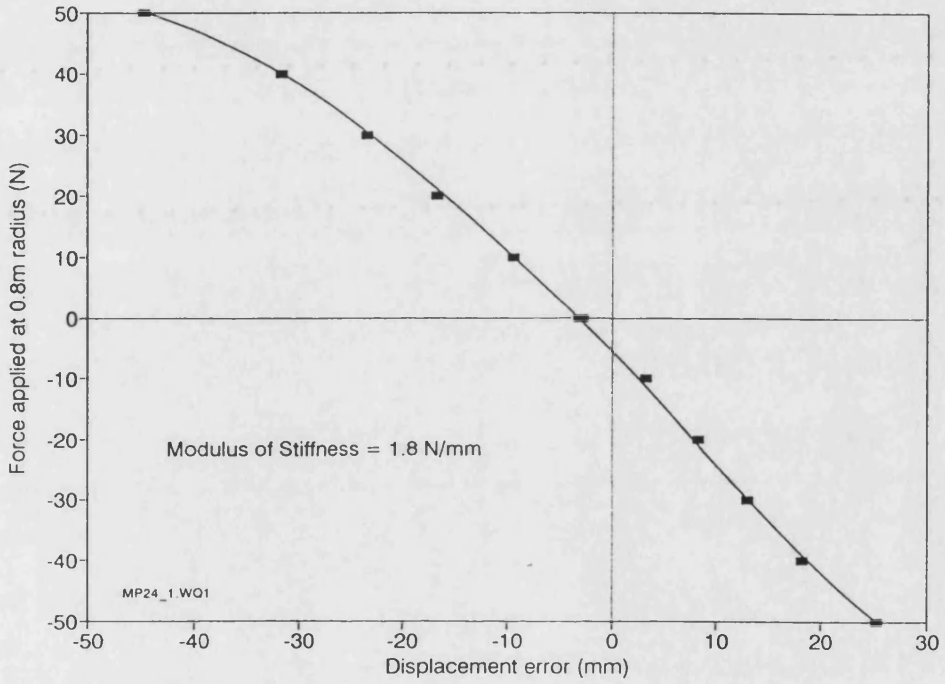

Figure A.3 Martonair prototype flow control valve static stiffness. $k_e = 35$, $k_v = 144$, $k_a = 461$, $U_{upper} = N + 300$, $U_{lower} = N - 300$.

A3.2 Martonair Isoflex flow control valve

Hysteresis was found to be ± 18 counts. The upper and lower limits used to achieve a maximum linear speed of 1.0 ms^{-1} were ± 350 counts from the null value. Thus hysteresis as a percentage of working range was 5%. The closed-loop time response illustrated in Figure A.4 showed a relatively well behaved system, though there was a tendency to go into a slow hunting cycle with a period of about a second and a stroke of typically 12 mm. At other times positioning to a steady state error of less than 2.2 mm was achieved within one second. The major cause of the hunting is thought to be a combination of the integrating nature of the flow control valve within a position control system combined with cylinder friction. This phenomenon is best explained by reference to Figure A.5 in which the system has been configured deliberately to encourage hunting. It is clear that whilst the control input may remain constant if an error exists which takes the valve out of its dead band differential pressure across the piston will build up until it exceeds the frictional force. If this movement overshoots the set point the procedure is repeated. There are several ways in which the tendency for the system to hunt in this way can be reduced, though the most obvious, reducing cylinder friction may have implications for stability as discussed later. The modulus of stiffness measured from Figure A.6 was 7.4 N mm^{-1}, though the tendency to hunt did produce some scatter near to the zero point.

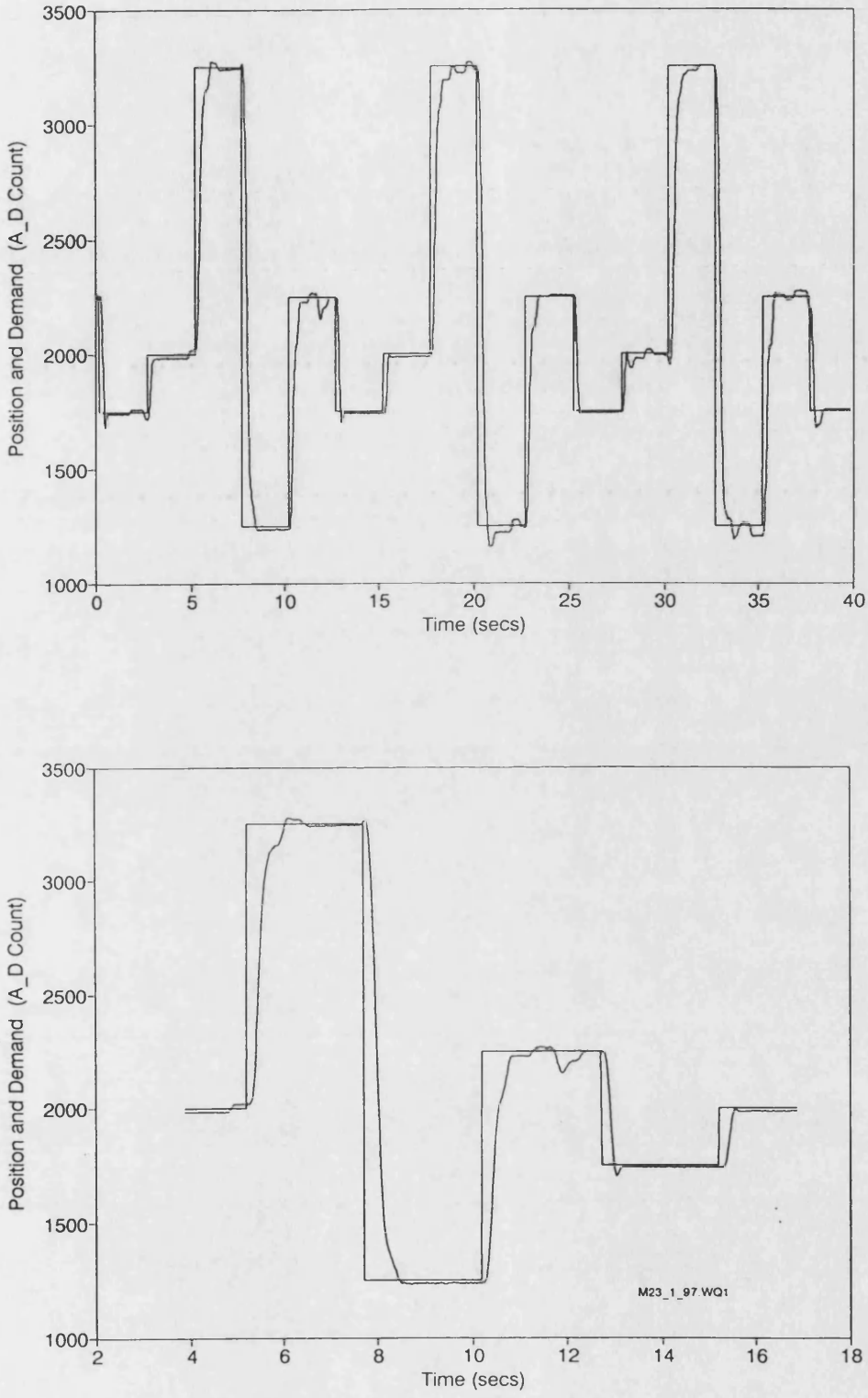

Figure A.4 Martonair Isoflex flow control valve time response. $k_e = 32$, $k_v = 128$, $k_a = 531$, $U_{upper} = N + 350$, $U_{lower} = N - 350$.

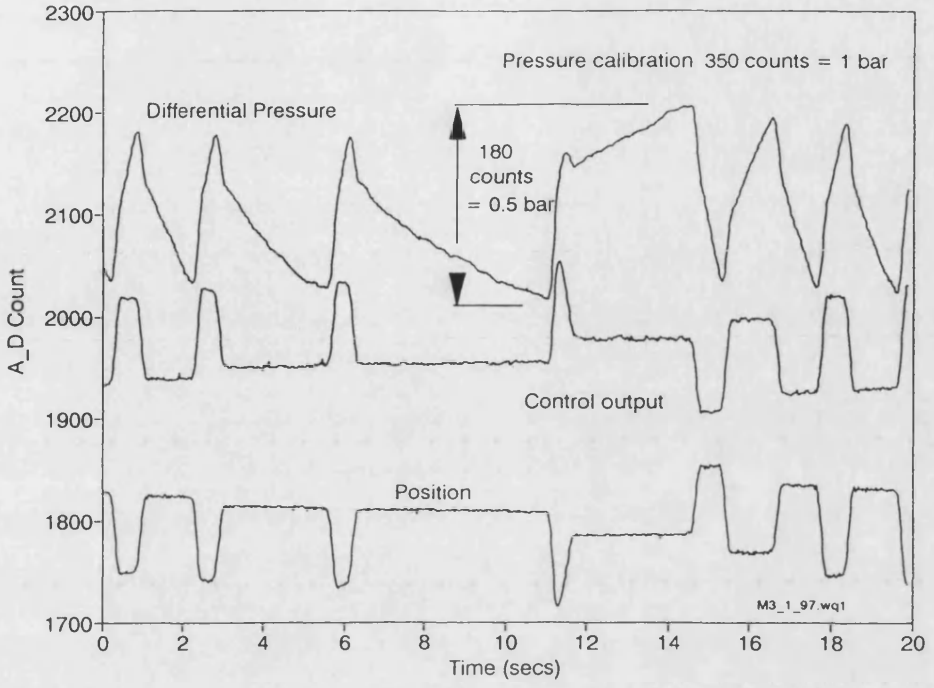

Figure A.5 Martonair Isoflex flow control valve deliberately configured to demonstrate hunting. $k_e = 18$, $k_v = k_a = 0$.

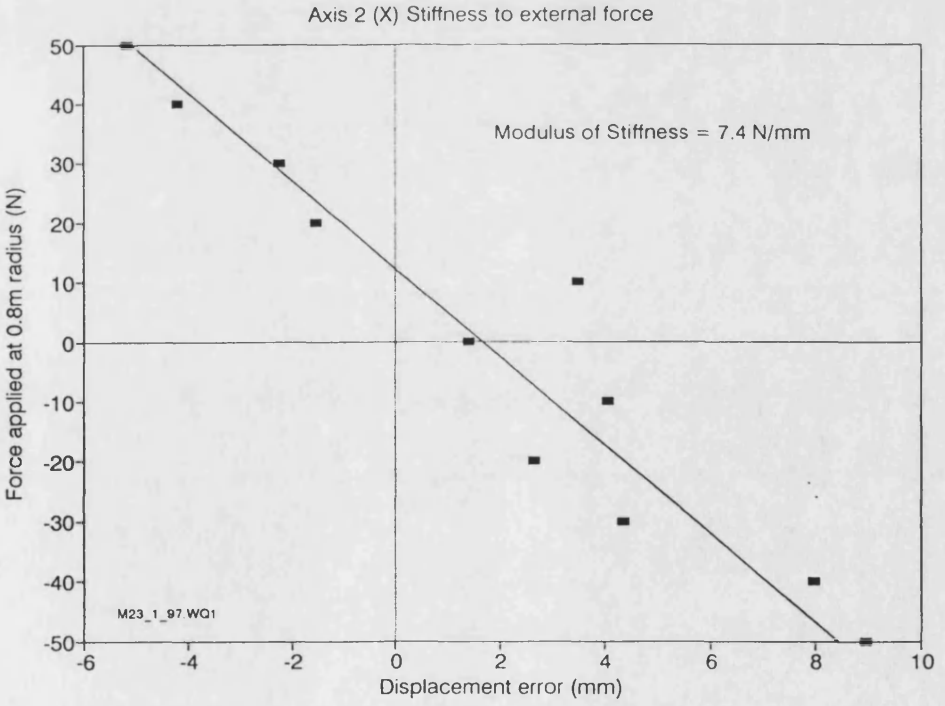

Figure A.6 Martonair Isoflex flow control valve static stiffness. $k_e = 32$, $k_v = 128$, $k_a = 531$, $U_{upper} = N + 350$, $U_{lower} = N - 350$.

A3.3 Festo M5 flow control valve

This valve is the smallest of a range of five valves. Advertised flow rates range from 100 l min^{-1} for the M5 valve tested here to 2000 l min^{-1} for the G⅜ version. In fact all but the largest valve in the range received some testing, though it quickly became clear that the M5 valve was the most suitable. The penalties of using an oversized valve were an increase in hysteresis as a percentage of working stroke and a slower response time.

Hysteresis was found to be ± 30 counts. The upper and lower limits used to achieve a maximum linear speed of 0.74 ms^{-1} were ± 600 counts from the null value. Thus hysteresis as a percentage of the working range was 5%. The closed-loop time response illustrated in Figure A.7 was well damped with a small but acceptable overshoot in some step movements. Steady state error was generally within ± 1.4 mm, though like the Martonair Isoflex valve there was a tendency for low frequency hunting about the set point. However, this occurred less often and only over a 6 mm stroke. A feature of this valve was excellent repeatability in dynamic performance. The modulus of stiffness measured from Figure A.8 was 7.6 N mm^{-1}.

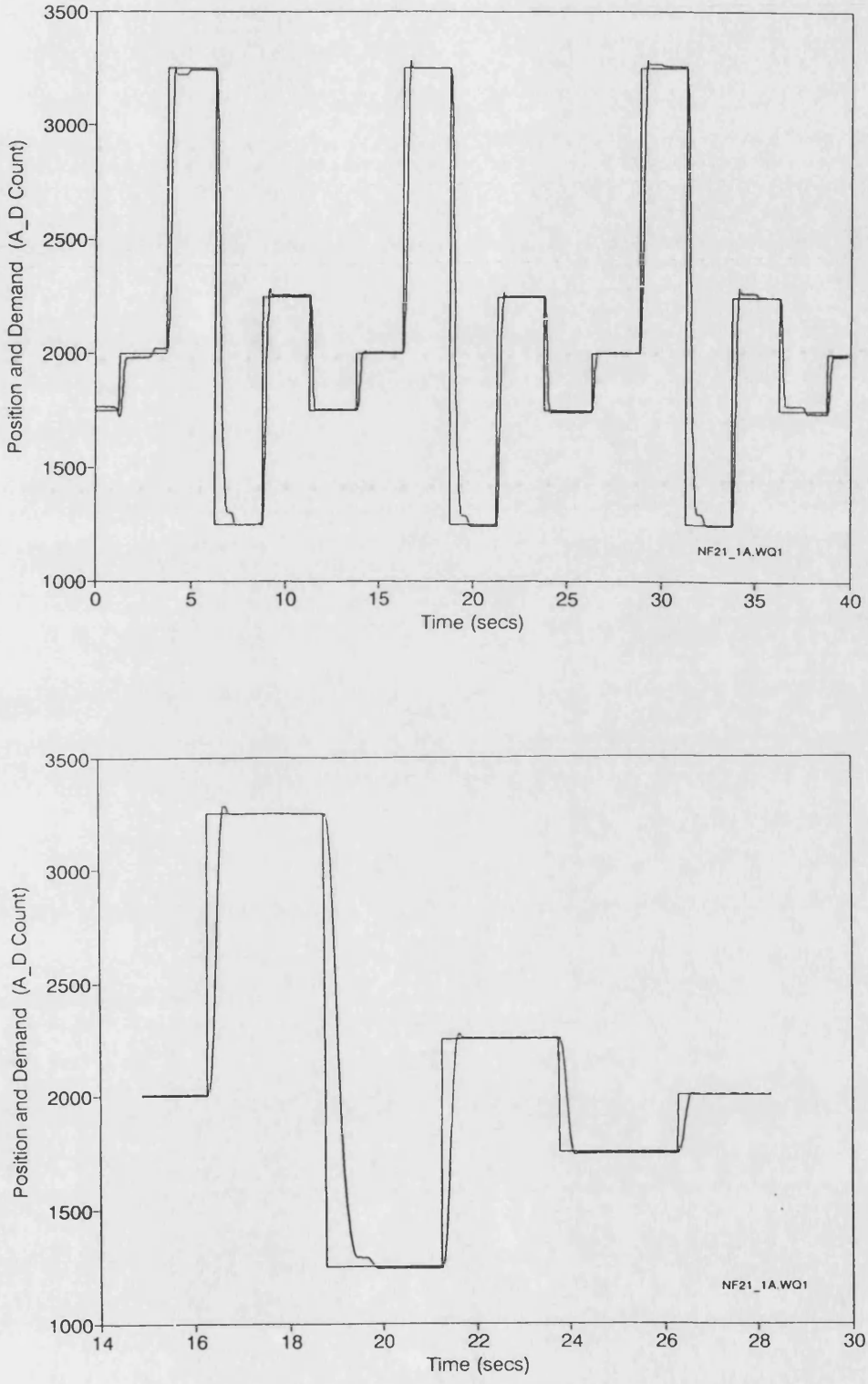

Figure A.7 Festo M5 flow control valve time response. $k_e = 21$, $k_v = 48$, $k_a = 403$, $U_{upper} = N + 600$, $U_{lower} = N - 600$.

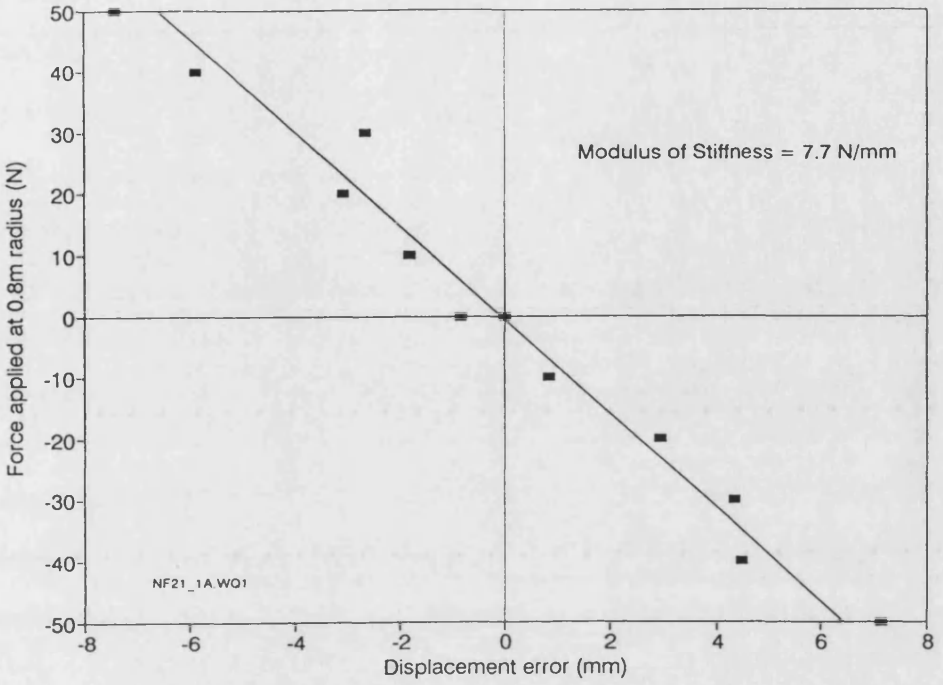

Figure A.8 Festo M5 flow control valve static stiffness. $k_e = 21$, $k_v = 48$, $k_a = 403$, $U_{upper} = N + 600$, $U_{lower} = N - 600$.

A3.4 SMC pressure regulating valve

For the purpose of these tests the manual regulator was adjusted to 2.9 290 kPa and the supply regulator to the proportional valve to 580 kPa. Hysteresis was found to be ± 70 counts, of the 12 bit (4096) output. The upper and lower limits on output used in position control tests were ± 200 counts[8]. Thus hysteresis as a percentage of working range was 35%. Hysteresis quoted in the data sheet is 2.5% of full scale (880 kPa) which is ± 11 kPa. This absolute pressure range of hysteresis probably remains constant regardless of supply pressure, though this was not tested.

[8] It should be noted that in this case the limits control maximum pressure and therefore acceleration rather than maximum velocity as in the case of flow control valves.

If the dynamics of the valve internal pressure control loop are fast in relation to system dynamics the system can be regarded as one consisting of an inertial load controlled by a force input (neglecting cylinder friction). An appropriate controller for such a linear system would be based on a proportional to error and velocity feedback with no acceleration term. Indeed the experimental results illustrated in Figure A.9 indicate that this was largely true. However, the characteristics of the real system cause actual performance to fall short of the ideal. In particular the system had a tendency to oscillate at about 6 Hz. Relatively poor stability at this frequency was thought to be due to an accumulation in system lags. These were from the servo-controlled regulator (30 ms), signal processing (10 ms) and other factors such as pneumatic delay in pipes. The response time of the manually adjusted regulator was not known. As an illustration, a 40 ms delay at 6 Hz would cause an 85° phase lag, which would go some way towards accounting for these results.

A further area in which the actual performance fell short of the ideal was in steady state error. In most cases error was very low typically less than ± 1 mm, though in certain parts of cylinder stroke this was consistently increased to as much as 8.4 mm. The difference has been attributed to varying external loads with position. In particular the method by which the output arm is suspended from the vertical axis cylinder (of fixed length for these experiments) results in a tendency for the arm to centralize. The system was sensitive to external loads including friction since, unlike systems using flow control valves there is no integrating effect. At the steady state the restoring force is proportional to error only and will not increase with time. The solution would be to introduce an integrator into the control algorithm. Sensitivity to offset loads is also illustrated in Figure A.10 from which a modulus of stiffness of 2.7 N mm^{-1} has been calculated.

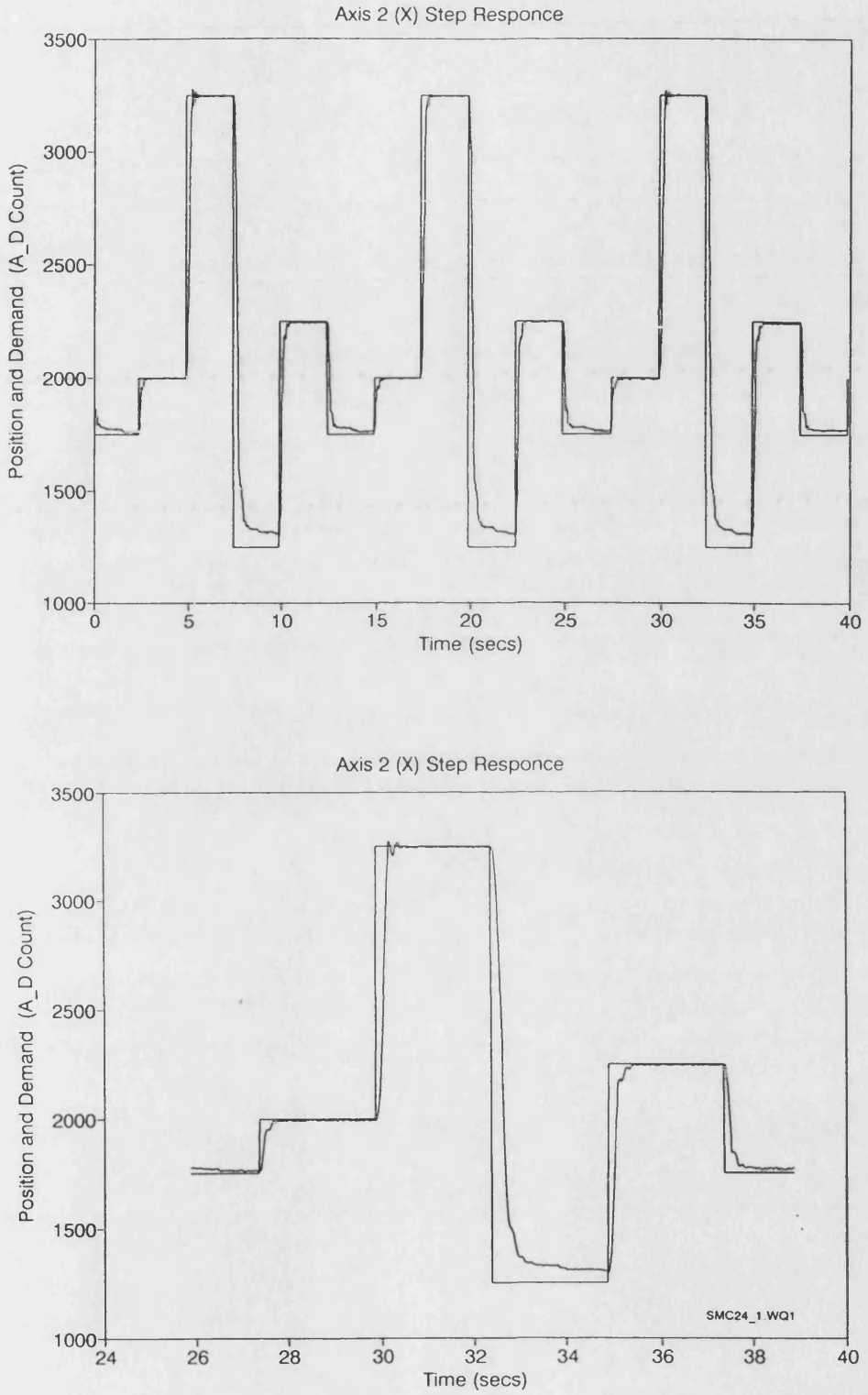

Figure A.9 SMC pressure control valve time response. $k_e = 34$, $k_v = 160$, $k_a = 0$, $U_{upper} = N + 200$, $U_{lower} = N - 200$.

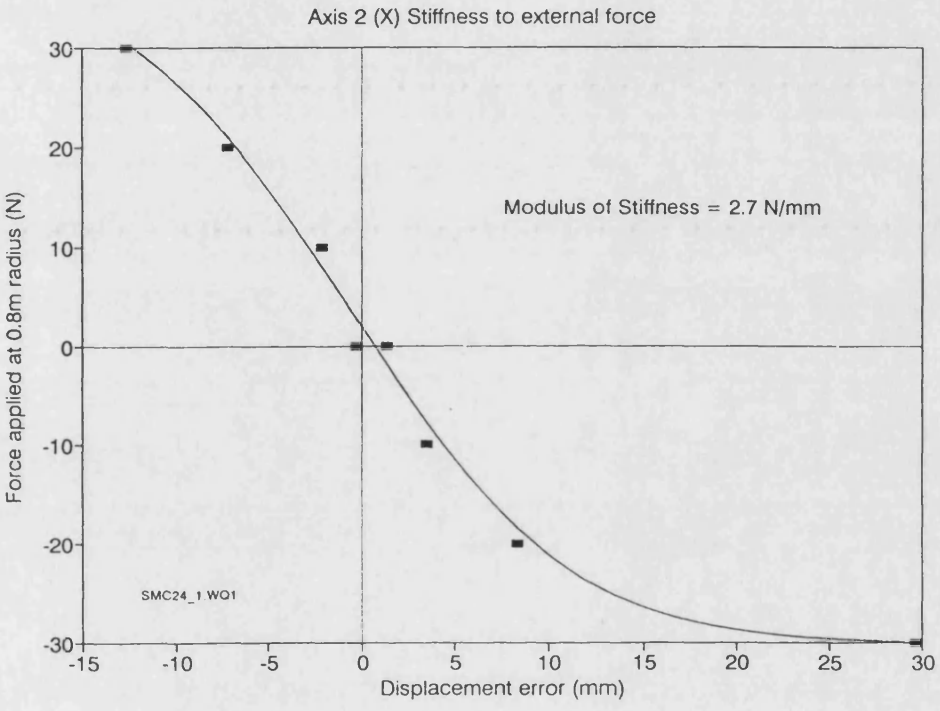

Figure A.10 SMC pressure control valve static stiffness. $k_e = 34$, $k_v = 160$, $k_a = 0$, $U_{upper} = N + 200$, $U_{lower} = N - 200$.

Characteristic	Prototype Martonair	Martonair Isoflex	Festo M5	SMC
Operating mode	Flow control via open-loop control of spool, solenoid vs. spring	Flow control via open-loop control of spool, solenoid vs. spring	Flow control via closed-loop control of spool position using a solenoid	Pressure control via pilot control of a regulator incorporating two poppet valves
% of valve working range used	15% of flow	17% of flow	30% of flow	30% of pressure
Hysteresis as a % of working range	8%	5%	5%	35%
Steady state error (mm)	± 2.1	± 2.2 with some hunting of ± 6	± 1.4 with occasional hunting of ± 3	Variable but repeatable from 1 to 8 depending on position
Time to settle within steady state error(s)	1	1	1	1
Modulus of stiffness (N mm^{-1})	1.8	7.4	7.6	2.7
Filtration (μm)	20	5	5	5
Lubrication	Normal	Fog	None	None
External driver required	Yes	Yes	No	No
Cost: valve regulator	Not available Not required	150 Not required	350 Not required	

Table A.1 Summary of Valve Characteristics

A4 Discussion

It is important to remember when considering the results above that they were intended to show relative performance. The simple control algorithm used was unlikely to result in the best possible performance for any of the valves. In many ways the performances achieved were very encouraging, indicating that probably all of the valves tested could be made to perform adequately well, given sufficient controller development. It would not be practical however to develop a system in which any of the valves could be used interchangeably as service replacements due to their different hardware and software requirements. From inspection of the time responses alone, one might be tempted to conclude that the Martonair prototype valve would be the best choice. Unfortunately it is out of production and its very high leakage air consumption at the steady state would make it expensive to run. It also produced the least stiff system, though the fact that it has been used successfully in the early experimental systems may indicate that stiffness is adequate.

The performance of the SMC valve would seem to be the least satisfactory due largely to its relatively slow response rate. The principle of incorporating a pressure feedback element to the controller would however be possible in conjunction with one of the flow control valves. The authors experience of pressure feedback and transient pressure feedback in other servo-pneumatic positioning systems suggest that this may be worth pursuing. An advantage of using a pressure term as an alternative to the second differential of position is that output noise is much reduced. This may have advantages in controllability and in improving valve life.

The repeatability of dynamic performance achieved with the Festo and SMC valves which incorporated internal feedback may provide opportunities to simplify and improve controller design. However, the relatively crude driver used to supply the Martonair valve may have contributed to variability, particularly in neutral value. The use of non-linear control strategies will improve performance over that achieved in these tests. The type of non-linear control, gain-scheduling, sliding mode, fuzzy logic

etc. are all worthy of further investigation, though the best choice may be dependent on valve characteristics.

All the valves tested were being operated at a small part of their available flow range. Consequently, hysteresis and sensitivity is larger than that which is technically achievable. An estimate of the required flow rate can be made by multiplying piston area by piston speed. For the geometry of the apparatus used in these tests, to achieve 1 ms^{-1} at the tip of the arm required a 0.21 ms^{-1} piston speed. The 40 mm diameter piston moving at this speed gives a peak flow rate of 0.27 l/s or 16 l/min. The data sheet for the M5 Festo valve states its maximum flow rate as 100 l/min which is reasonably consistent with the use of only 30% of its range in the experiments when one takes into account back pressures. It might be worthwhile consulting the manufacturers to investigate the feasibility of producing modified valves with reduced flow rates. This is most easily achieved by reducing the orifice at the spool/sleeve interface and need not require an extensive re-design of the valve (see Appendix B).

It is clear that the relatively high friction of the cylinder seals is contributing to the problem of hunting. Inspection of Figure A.5 shows that the maximum range of differential pressure for no movement was 180 A-D counts, corresponding to 50 kPa. For the 40 mm diameter piston and 15 mm diameter rod this would have produced a force of 54 N. On this basis the frictional forces are thought to be approximately ± 27 N which is ± 6% of maximum output. Manufacturers of cylinders are known to offer a range of alternative seals each with different friction characteristics. The contribution of cylinder friction to the stability of the system is however another factor which may mean that zero friction is not the optimum solution. This is an area which may be worthy of further investigation, which would have to be done in conjunction with controller design.

A5 Conclusions

- All the valves tested could, with some development, produce adequate performance for low accuracy point to point positioning systems.

- Flow control valves are probably the most appropriate for a position control system.

- Whilst the cost of the Festo valve incorporating spool feedback is higher than the Martonair Isoflex, it does have some convenience and performance advantages, particularly with respect to repeatability.

- To evaluate the potential benefits of the Festo valve vs. the Martonair Isoflex it should be tested with a more sophisticated controller.

- All of the valves tested are oversized for this application. There are potential performance benefits from using modified or new valves of an appropriate capacity.

- None of the valves have been evaluated for long term reliability in a working environment.

- There are a number of factors which combine with valve choice to influence dynamic performance and may benefit from further investigation. These include:

  - Cylinder selection, size and seal type.
  - Alternative feedback terms, pressure and transient pressure.
  - Alternative control strategies.

APPENDIX B - Effect of Restrictions on Flow Rate

The importance of ensuring that the greatest restriction in the air path between valve and actuator occurs at the valve spool sleeve interface is best explained by considering flows in the two situations depicted in Figure B.1. In both diagrams the spool orifices are represented by linked variable restrictions with flow coefficients KV_1 and KV_2. The annular volume around the spool between the input ports 1 and 2 has pressure P_3. This connects directly to the output port in one case and connects via a third restriction KV_3 in the other. The input ports would normally be the exhaust, which is open to atmosphere and the supply. The output is connected to one element of an actuator. Neglecting the compressibility of air, and to illustrate the point, using the rather simplified relationship where Q is the volumetric flow rate:

$$Q = KV\sqrt{\delta P} \tag{B.1}$$

For the first case represented in Figure B.1 (i):

$$Q_{out} = Q_1 + Q_2 \tag{B.2}$$

$$Q_1 = KV_1\sqrt{(P_1 - P_{out})} \tag{B.3}$$

$$Q_2 = KV_2\sqrt{(P_2 - P_{out})} \tag{B.4}$$

$$Q_{out} = KV_1\sqrt{P_1 - P_{out}} \quad + \quad KV_2\sqrt{P_2 - P_{out}} \tag{B.5}$$

For given input and output pressures the flow Q_{out} will be approximately linearly related to the linked flow coefficients KV_1 and KV_2. For the case represented in Figure B.1(ii):

$$Q_{out}=KV_1\sqrt{(P_1-P_3)}+KV_2\sqrt{(P_2-P_3)} \tag{B.6}$$

$$Q_{out}=KV_3\sqrt{(P_3-P_{out})} \tag{B.7}$$

$$P_3=(\frac{Q_{out}}{KV_3})^2+P_{out} \tag{B.8}$$

The flow Q_{out} is no longer simply related in this way. At large values of KV_3 in relation to the valve flow coefficients differences will be small, with P_3 almost equal to P_{out}, but at other values the effect will be marked. Given that air is in fact compressible if choked flow is induced at the third restriction then the valve will cease to provide variable flow control.

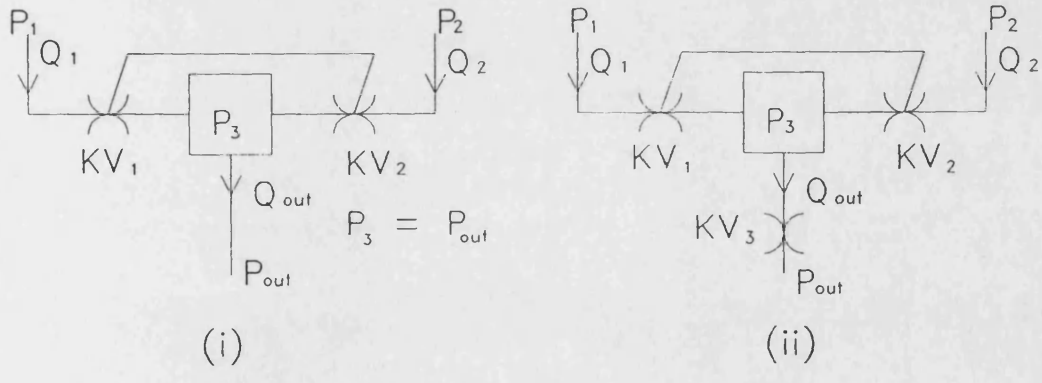

Figure B.1 Diagrammatic spool valve.

APPENDIX C - Measurement of Linearized Valve Coefficients

The analysis below was used to derive expressions for the linearized valve coefficients C_1 and C_2 in terms of the rate of charge and discharge of pressure vessels. It is followed by a description of the procedure used to determine these coefficients experimentally.

For conservation of energy:

$$C_p \dot{m}_a T_s - p_a \frac{dv_a}{dt} + \frac{dq}{dt} = \frac{d\,(C_v \rho_a V_a T_a)}{dt} \qquad (C.1)$$

where: C_p = constant pressure specific heat

C_v = constant volume specific heat

$C_p \dot{m}_a T_s$ = energy flow in

$p_a \frac{dV_a}{dt}$ = external work

$\frac{dq}{dt}$ = heat transfer

$\frac{d}{dt} (C_v \rho_a V_a T_a)$ = change in internal energy .

for adiabatic change discharging into a fixed volume V_a Equation C.1 simplifies to:

$$C_p \dot{m}_a T_s = \frac{d}{dt} (C_v \rho_a V_a T_a) . \qquad (C.2)$$

Assuming an ideal gas

$$\rho_a = \frac{P_a}{R T_a} \quad . \tag{C.3}$$

Combining Equations. C.2 and C.3:

$$\dot{m}_a T_s = \frac{V_a}{\gamma R} \frac{dP_a}{dt} \quad . \tag{C.4}$$

The linearized model of the spool valve from equations (7.4) and (7.5) is:

$$\dot{m}_a = C_1 x - C_2 (P_a - P_q) \tag{C.5}$$

where: P_q = quiescent pressure at steady-state, X = valve spool displacement and lower case indicates a change from initial conditions.

Combining Eqns. C.4 and C.5:

$$C_1 x - C_2 (P_a - P_q) = \frac{V_a}{\gamma R T_s} \frac{dP_a}{dt} \quad . \tag{C.6}$$

Thus when $(P_a - P_q) \approx 0$ and a step value of ΔX from the zero position is applied C_1 can be obtained from the gradient of a P vs. t plot.

$$C_1 = \frac{V_a}{\gamma R T_s \Delta X} \cdot \frac{dP_a}{dt} \tag{C.7}$$

Similarly when x = 0 C_2 can be obtained from the gradient of a P vs. t plot :

$$C_2 = \frac{V_a}{\gamma R T_s} \frac{1}{(P_a - P_q)} \frac{dP_a}{dt} . \tag{C.8}$$

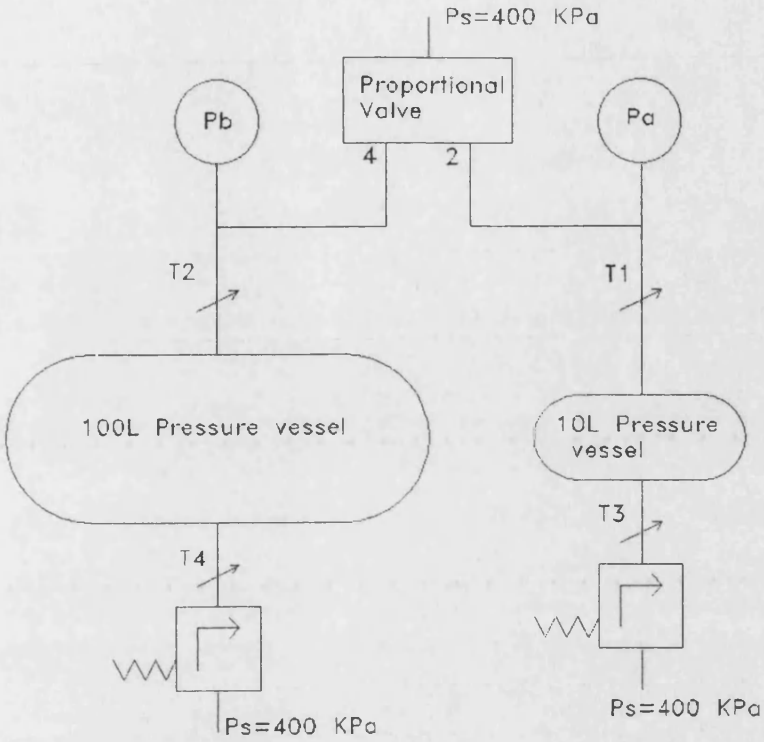

Figure C.1 Experimental apparatus to measure linearized valve coefficients

In order to evaluate C_1 an apparatus was constructed as depicted in Figure C.1. With taps T1 and T2 open and T3 and T4 closed pressure in the two vessels was allowed to reach equilibrium before a step change was made in spool position. Pressure was logged over time and the initial rate of change of pressure evaluated graphically, from which the mass flow rate was deduced. This was repeated five times for each step change value so that an average mass flow rate could be calculated. A typical result for a step change of +0.5V (nominally 0.075 mm spool movement) is given in Figure C.2. The procedure repeated for eight different step change values and plotted against mass flow as shown in Figure C.3. The gradient of this line represents an average value for C_1 of 1.5 $kgs^{-1}\ m^{-1}$.

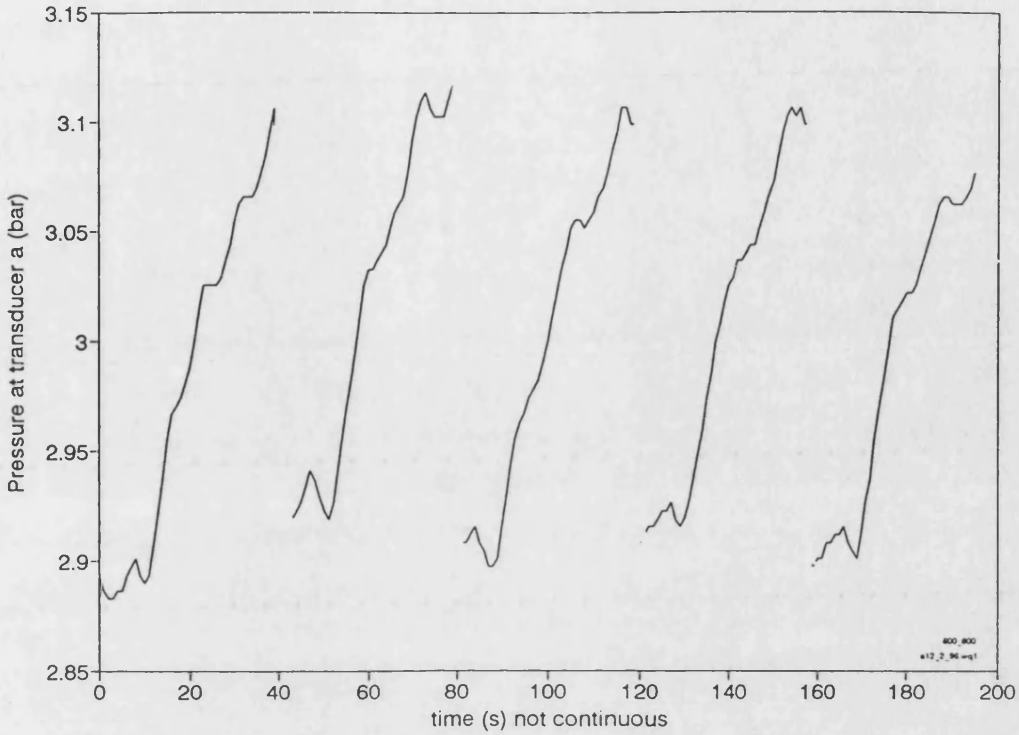

Figure C.2 Typical record of rate of change of pressure in a fixed volume vessel for the evaluation of valve mass flow rate with varying spool displacement

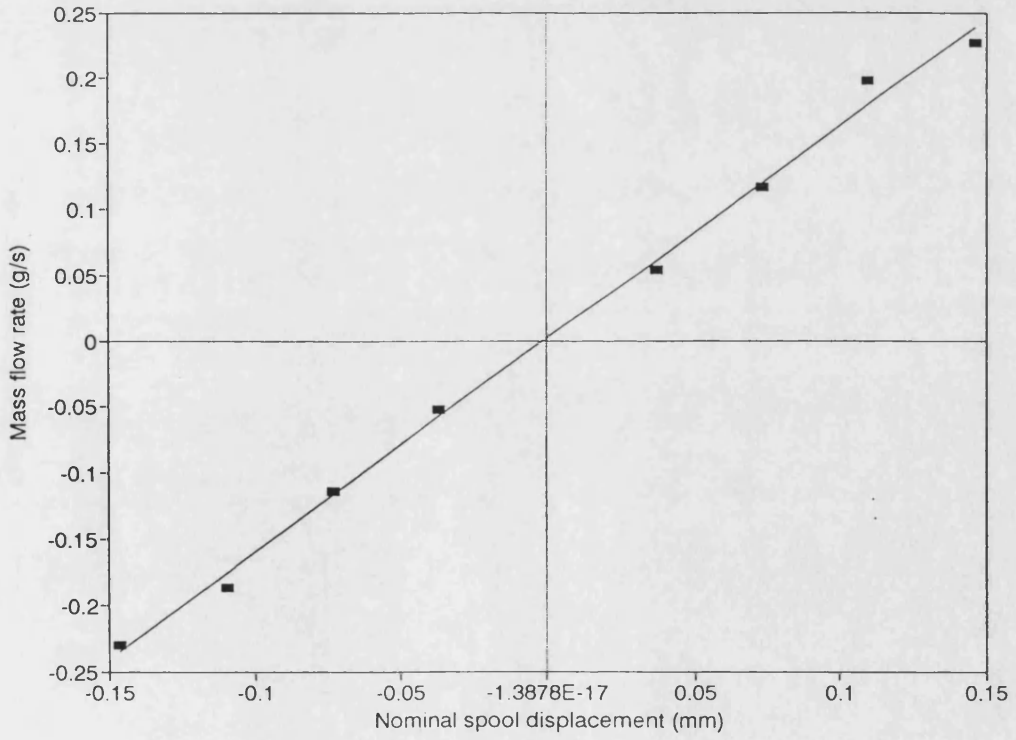

Figure C.3 Plot of mass flow rate against spool displacement as a means of calculating valve coefficient C_1

A similar apparatus and procedure was adopted to evaluate C_2. The valve input signal was maintained constant at the nominal neutral position and equilibrium was reached with the tap to the smaller reservoir T1 closed. The pressure in this smaller vessel was adjusted by opening tap T3 and using a regulator to adjust pressure relative to the quiescent value. Tap T3 was then closed and T1 opened whilst pressure was logged. Tap T2 remained open and tap T4 closed during this procedure. Typical results as given in Figure C.4 were presented as a plot of pressure against time. The gradient was used to calculate mass flow rate and divided by the pressure differential to yield the coefficient C_2. However, it is clear from Figure C.4 that flow was choked whilst the ratio of vessel pressure to supply pressure was less than 0.528, ie whilst $P_a < 210$ kPa. To obtain a mean value for C_2 the gradient was taken at the transition pressure and at a value corresponding to approximately half that differential pressure which overall gave the result $C_2 = 0.4.\ 10^{-8}$ ms.

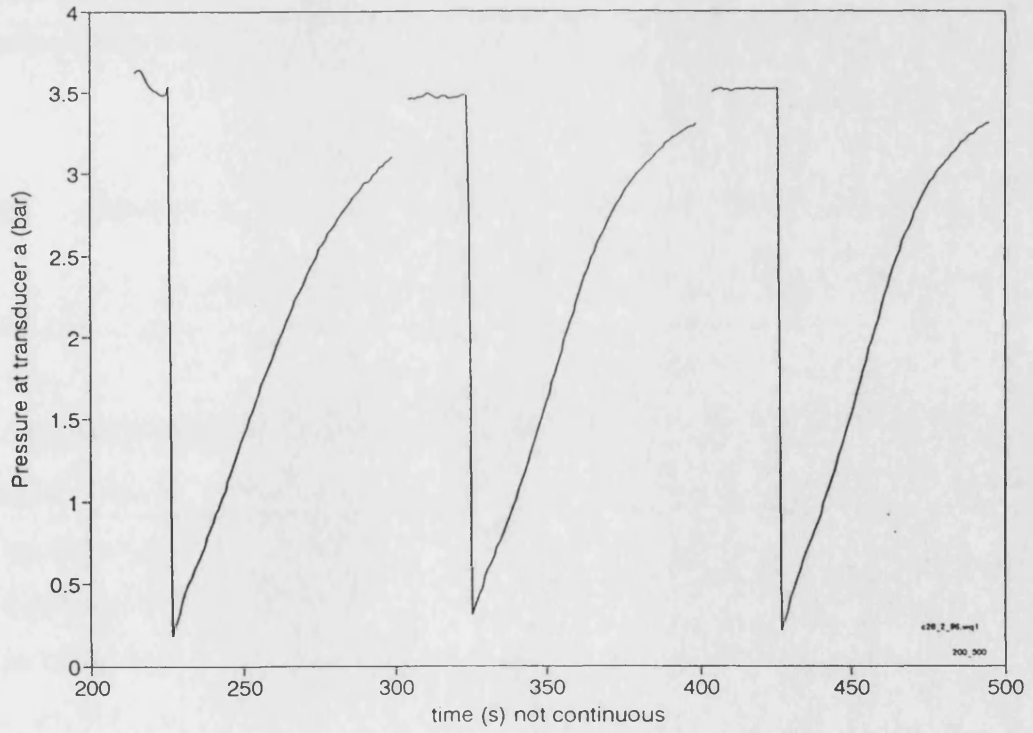

Figure C.4 Typical record of rate of change of pressure in a fixed volume vessel for the evaluation of valve mass flow rate at varying differential pressures

APPENDIX D - Transient Pressure Feedback Experimental Implementation

D1 Introduction

The purpose of the work described in this Appendix was to experimentally evaluate the potential for using transient pressure feedback as a practical alternative, or addition to, either differential pressure or acceleration. For discussion of the theoretical relative merits of these feedback terms the reader is referred to Chapters 6.1, 7.3.2 and 7.4.1.

The results reported here are only preliminary ones. No attempt was made to optimise filter parameters other than by manual tuning. The experimental system used in this trial was the pneumatic cylinder based single axis rig introduced in Appendix A. The principles are similar to those for the flexible actuator onto which the equipment could be transferred at a future date.

D2 Filter design

In order to obtain the transient element of the differential pressure, the signal was passed through a high pass filter so as to remove low frequency and DC terms which contribute to steady state errors. In order to eliminate noise problems in this filter the signal is first passed through a low pass filter to eliminate the frequencies higher than those of interest in control terms. The resulting bandpass filter has been implemented as a first order RC filter for simplicity and in order to minimise the phase shift problems associated with higher order filters. An op-amp buffer was used between the two filters to bring their behaviour closer to the idealised model of zero impedance driving an infinite load. An output amplifier was also provided. The circuit diagram is given in Figure D.1 and includes the pressure transducer which had its own output amplifier.

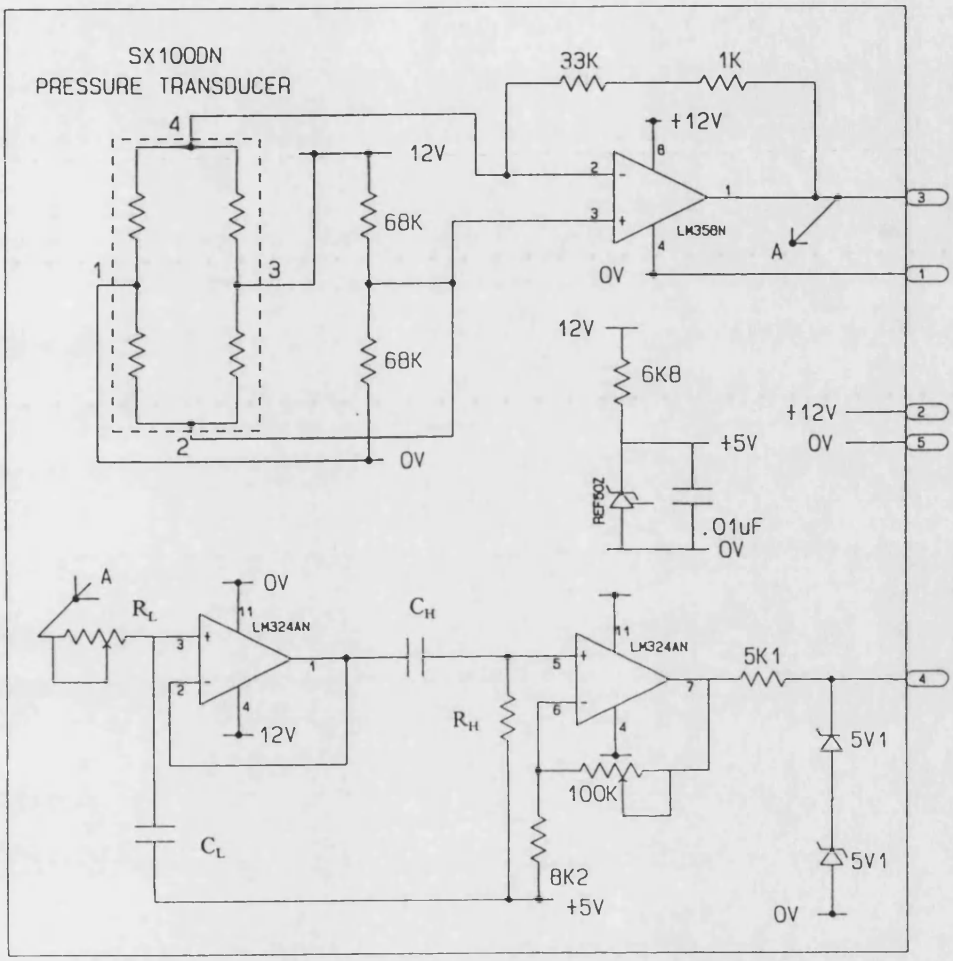

D.1 Bandpass filter and pressure transducer circuit diagram.

In order to select appropriate component values it is necessary to determine the overall gain and phase response, for which the transfer function is required.

The transfer function of the low pass filter is:

$$TF_{LP} = \frac{1}{1 + j\omega R_L C_L} \qquad (D.1)$$

The equivalent for the high pass filter is:

$$TF_{HP} = \frac{j\omega R_H C_H}{1 + j\omega R_H C_H} \qquad (D.2)$$

where ω is the frequency, R and C are resistor and capacitor values and L and H denote low pass and high pass stages respectively.

In this case the responses of the two filters could be evaluated separately and combined, though for the analysis presented here an overall transfer function (TF_{BP}) was derived.

$$\frac{V_{out}}{V_{in}} = TF_{BP} = TF_{LP} \cdot TF_{HP}$$

$$= \frac{j\omega R_H C_H}{1 + j\omega (R_H C_H + R_L C_L) - \omega^2 R_L R_H C_L C_H}$$

$$= \frac{j\omega R_H C_H \left[(1 - \omega^2 R_L R_H C_L C_H) - j\omega (R_H C_H + R_L C_L)\right]}{(1 - \omega^2 R_L R_H C_L C_H)^2 + \omega^2 (R_L C_L + R_H C_H)^2} \qquad (D.3)$$

The phase response is determined by the ratio of the real to the imaginary part.

$$\tan \phi = \text{imaginary} / \text{real}$$

so

$$\phi = \tan^{-1} \left(\frac{1 - \omega^2 R_L R_H C_L C_H}{\omega (R_L C_L + R_H C_H} \right) \qquad \text{(D.4)}$$

The amplitude response is a function of the real part only, so the imaginary part can be eliminated using the relationship,

$$V_{out} = (V_{out} \cdot V_{out}^{*})^{½}$$

where V_{out}^{*} is the complex conjugate.

This leads to:

$$\left| \frac{V_{out}}{V_{in}} \right| = \frac{\omega R_H C_H}{\left((1 - \omega^2 R_L R_H C_L C_H)^2 + \omega^2 (R_L C_L + R_H C_H)^2 \right)^{½}} \qquad \text{(D.5)}$$

Equations (D.4) and (D.5) have been entered into a spreadsheet so the gain and phase responses can be visualised over a range of component valves (Figures D.2a and D.2b). The valves used in this trial were $R_L = 3.2\ k\Omega$, $R_H = 390\ k\Omega$ and $C_L = C_H = 1\mu F$. They were chosen after brief experimentation and in the light of the simulation results of Chapter 7 relating to the flexible actuator.

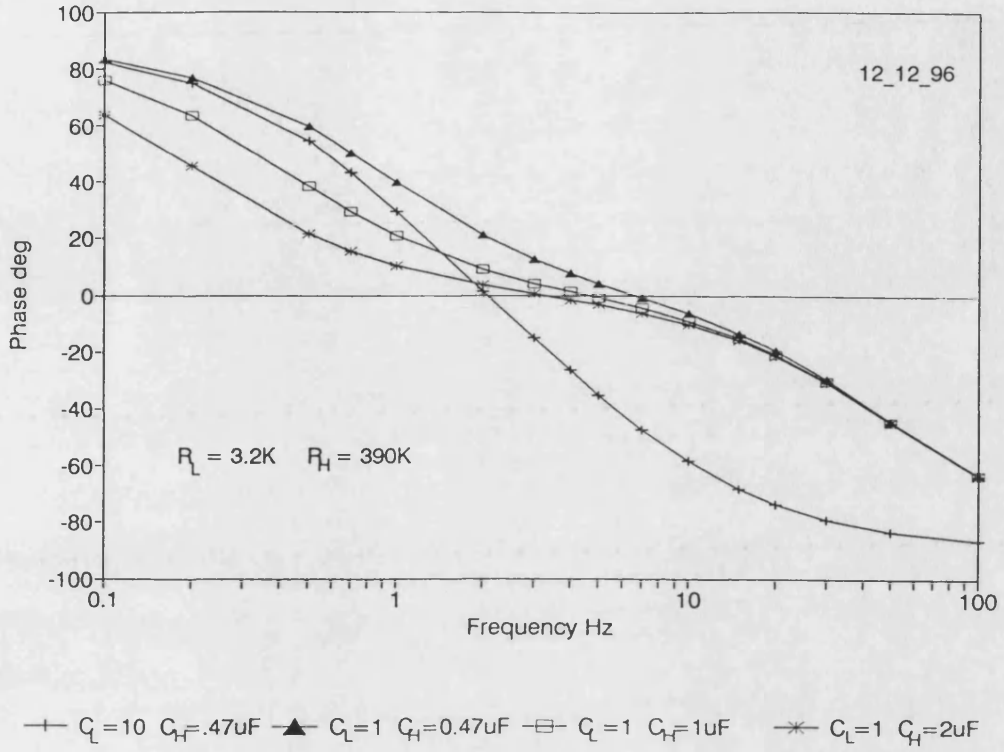

D.2a Bandpass filter phase response.

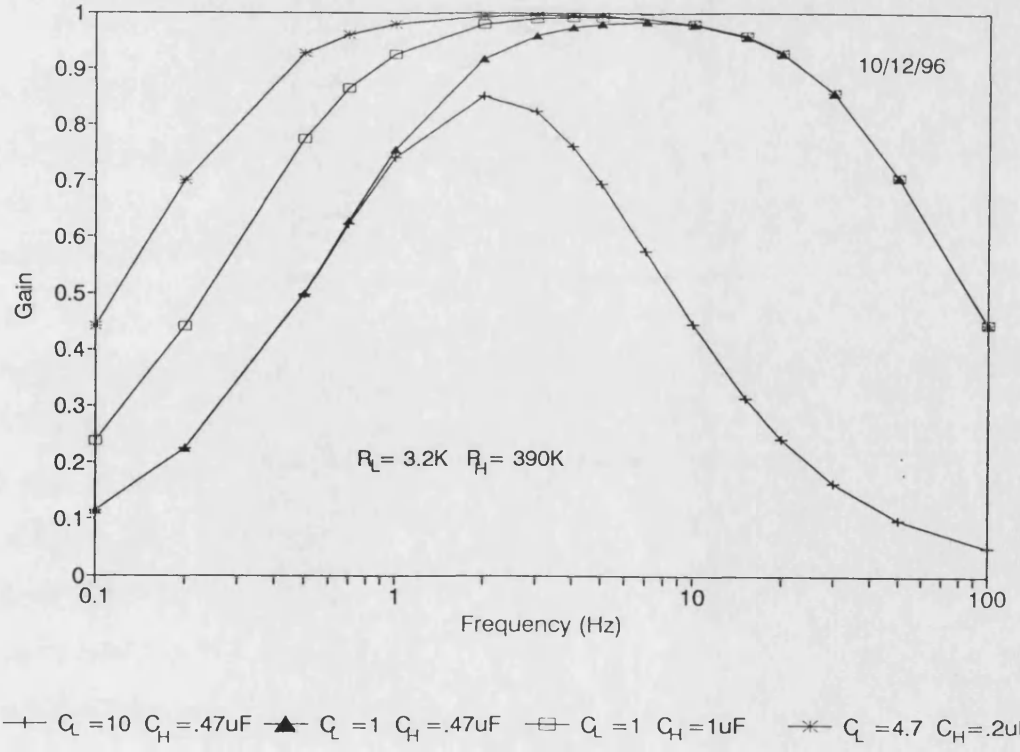

D.2b Bandpass filter gain response.

D3 Experimental procedure

The apparatus was identical to that used to obtain the results given in Appendix A, except for the addition of the filter. The Festo flow control valve introduced in Appendix A was used throughout. The controller was extended to include differential pressure and transient pressure feedback terms, so that Equation A.1 was replaced by:

$$V_{out} = k_e(\theta_o - \theta_d) - k_v\dot{\theta}_o - k_a\theta_o - k_p(P_a - P_b) - k_{tp}\left[TF_{BP}(P_a - P_b)\right] + N \qquad (D.6)$$

For purposes of comparison the proportional and velocity gains, output limits and the step wave input were the same as those used to obtain Figure A.7. The acceleration gain however was set to zero.

D4 Results and conclusions

In Figure D.3a the response using transient pressure feedback is presented. The value of transient pressure feedback gain (k_{tp}) was chosen after manual tuning in which all other parameters were kept constant. The result, which is noticeably inferior to that achieved in Figure A.7 with acceleration feedback, does however exhibit a reasonably low steady state error when compared to Figure D.4 in which transient pressure feedback has been replaced by differential pressure. Close inspection of Figure D.3b, which presents both the direct pressure and transient signals, shows that the filter is indeed removing much of the DC element which has caused the large steady state errors of Figure D.4. The dynamic characteristics evident in Figure D.3a are, however, not as good as that achieved with the direct unfiltered signal (Figure D.4). This suggests that more time needs to be spent in tuning the filter to pass a more desirable part of the signal frequency range. However, it is clear that some of the problems are due to the effects of friction. For example, the steady build up of pressure whilst the piston is static but with a significant steady state error, causes a constant offset in the filter

output. Once pressure builds up to the point that friction is overcome there is a jump in output position leading to the phenomenon of hunting discussed in Appendix A.

The filter is functioning as intended and the overall effects are reasonably good given the stage of development. Further work is required to optimise the filter component valves, though system parameters such as friction may influence optima.

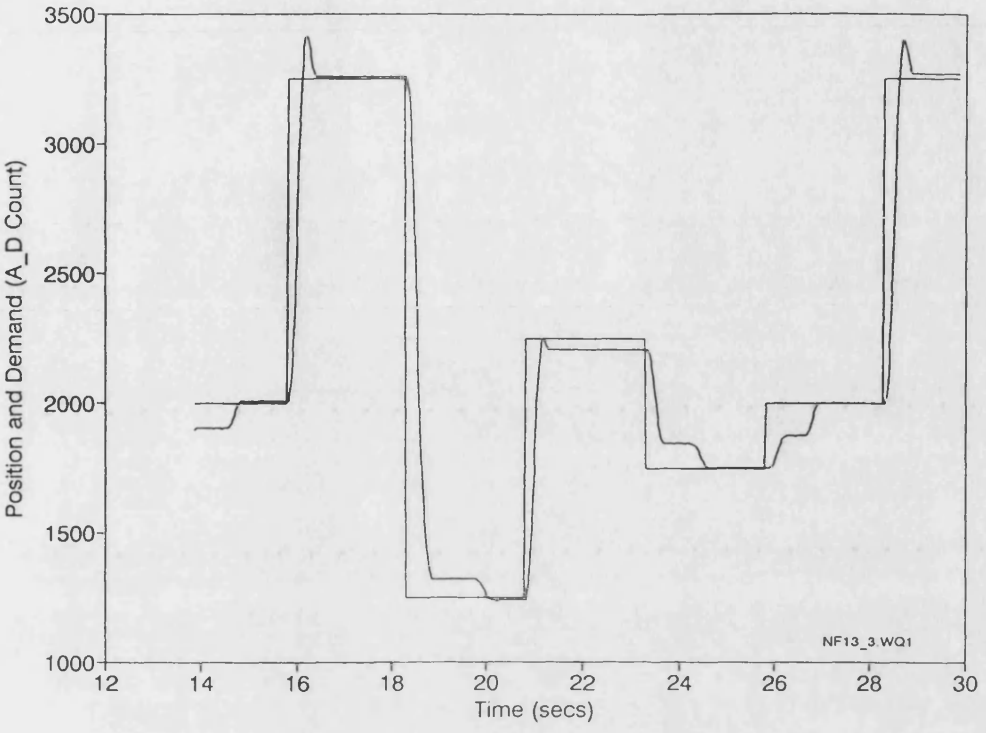

D.3a Time response using transient pressure feedback. $k_e = 21$, $k_v = 48$, $k_a = 0$, $k_p = 0$, $k_{tp} = 36$, $V_{upper} = N + 600$, $V_{lower} = N - 600$.

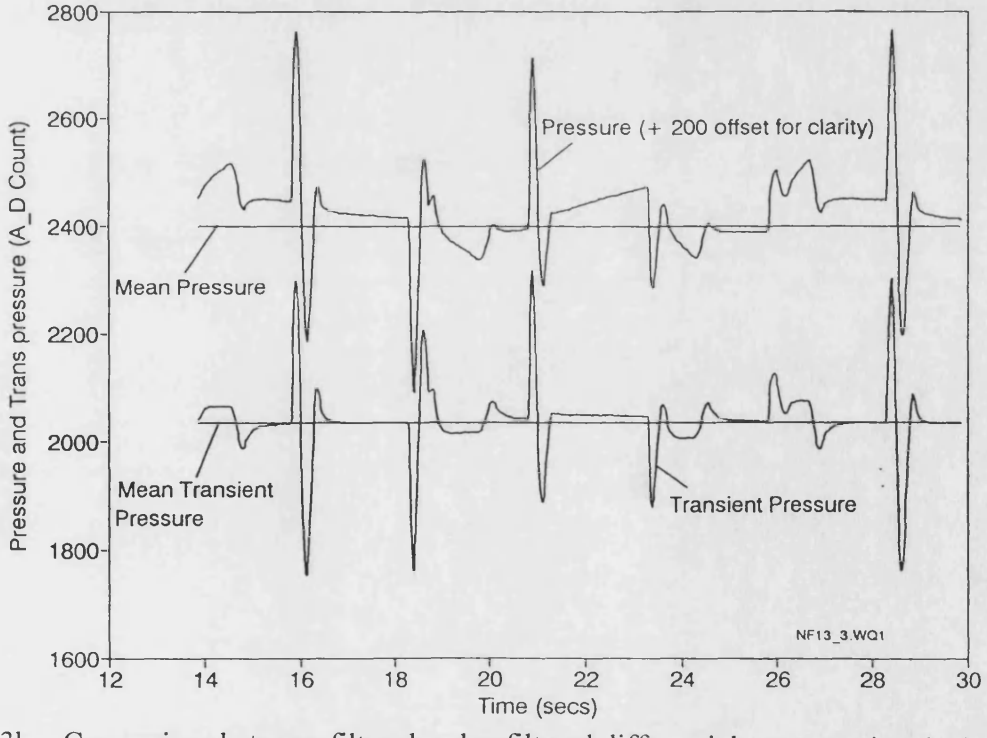

D.3b Comparison between filtered and unfiltered differential pressure signals during the run presented in Figure D.3a.

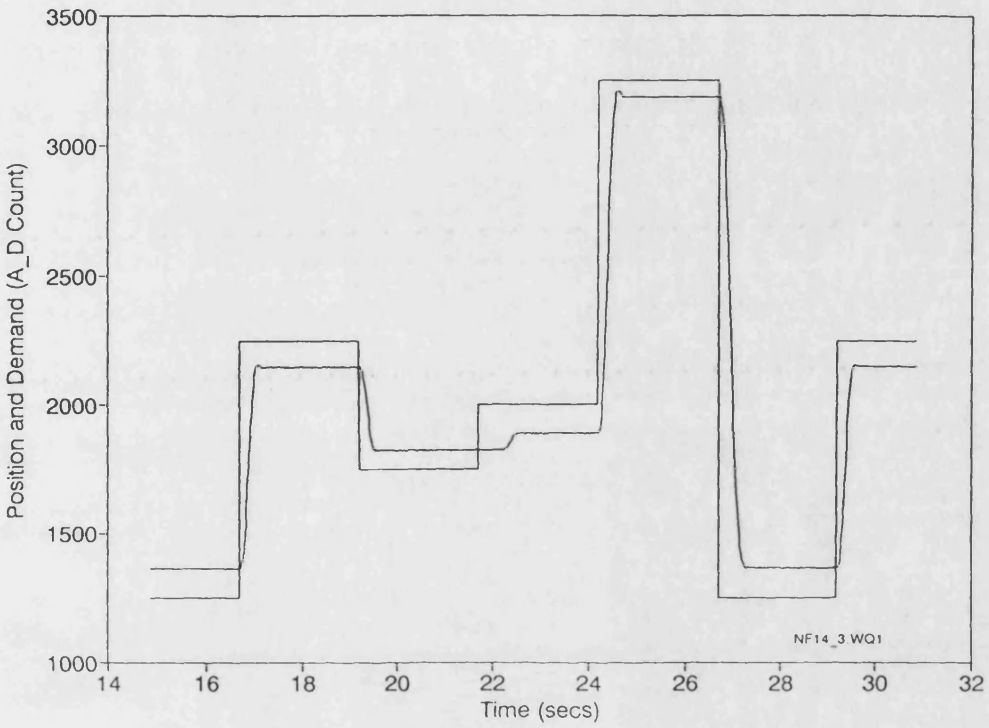

D.4 Time response using direct differential pressure feedback. $k_e = 21$, $k_v = 48$, $k_a = 0$, $k_p = 35$, $V_{upper} = N + 600$, $V_{lower} = N - 600$.

APPENDIX E - Manipulator Coordinate Transformation

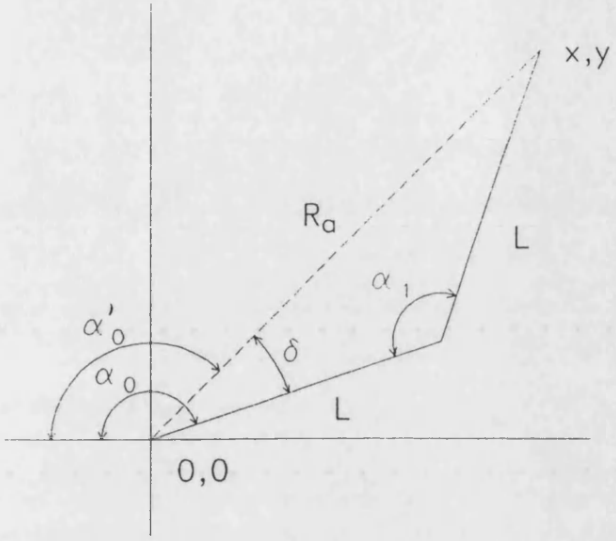

Figure E.1 Geometry for coordinate transformations

Referring to the geometry depicted in Figure E.1 to convert from Cartesian to joint coordinates:

$$R_a = \sqrt{(x^2 + y^2)} \tag{E.1}$$

$$\alpha_1 = 2.\sin^{-1}(R_a/2L) \tag{E.2}$$

$$\delta = \cos^{-1}(R_a/2L) \tag{E.3}$$

where α_0 and α_1 are joint output angles, δ is the angle between link 0 and the radius, L is the arm link length and R_a is the arm radius.

For -ve x and +ve y:

$$\alpha_o' = \tan^{-1}\left|\frac{y}{x}\right| \tag{E.4}$$

$$\alpha_o = \alpha_o' + \delta \tag{E.5}$$

so

$$\alpha_o = \tan^{-1}\left|\frac{y}{x}\right| + \cos^{-1}\left(\frac{R_a}{2L}\right) \tag{E.6}$$

For +ve x and +ve y:

$$\alpha_o' = 90 + \tan^{-1}\left|\frac{y}{x}\right| \tag{E.7}$$

so

$$\alpha_o = 90 + \tan^{-1}\left|\frac{y}{x}\right| + \cos^{-1}\left(\frac{R_a}{2L}\right) \tag{E.8}$$

To convert from joint to Cartesian coordinates:

Rearranging (E.2):

$$R_a = 2L \sin\left(\frac{\alpha_1}{2}\right) \tag{E.9}$$

Since both links have the same length:

$$\delta = 90 - \sin\left(\frac{\alpha_1}{2}\right) \tag{E.10}$$

From (E.5) and (E.10):

$$\alpha_o' = \alpha_o - 90 + \frac{\alpha_1}{2} \qquad \text{(E.11)}$$

If $\alpha_o' < 90$:

$$y = R_a \sin(\alpha_o') \qquad \text{(E.12)}$$

$$x = R_a \cos(\alpha_o') \qquad \text{(E.13)}$$

If $\alpha_o' > 90$:

$$x = R_a \sin(\alpha_o' - 90) \qquad \text{(E.14)}$$

$$y = R_a \cos(\alpha_o' - 90) \qquad \text{(E.15)}$$